CHEMICAL COMPOSITION AND CLOUD NUCLEATION ABILITY OF MARINE AEROSOL

A Dissertation

by

CHUNHUA DENG

Submitted to the Office of Graduate and Professional Studies of
Texas A&M University
in partial fulfillment of the requirements for the degree of

DOCTOR OF PHILOSOPHY

Chair of Committee,	Sarah Brooks
Committee Members,	Don Collins
	Qi Ying
	Russ Schumacher
Head of Department,	Ping Yang

December 2013

Major Subject: Atmospheric Sciences

ABSTRACT

This study is focused on the chemical composition and cloud nucleation ability of marine aerosol based on two cruise researches over Pacific Ocean and North Atlantic Ocean respectively. Implications of CLAW hypothesis and the factors influencing its validity are analyzed for the contemporary era with ever-increasing pollution.

The pacific cruise started from Punta Arenas, Chile and ended in Seattle, WA during March-April of 2010. Raman microspectroscopy (RMS) was employed to identify the chemical composition and mixing conditions of single particles collected. By analyzing multiple particles in a collected ensemble, the degree of external/internal mixing of particles was also determined. Atmospheric aerosol concentration, cloud condensation nuclei (CCN) concentration, and chlorophyll *a* concentration in the underlying water (a metric for phytoplankton biomass in the ocean), were also measured. Our results indicate that long chain organic molecules were prevalent in the marine aerosol samples throughout the cruise. Long chain organic compounds tended to stay mixed with other organic and inorganic components. The influence of marine organic aerosols on cloud nucleation ability is analyzed.

The North Atlantic cruise started from Woods Hole, MA and returned back to the same location during June-July 2011. The cruise passed through a wide range of conditions, including areas of high phytoplankton biomasses and extremely high DMS levels (over 1800 pptv). Aerosol concentration, cloud condensation nuclei (CCN) concentration, particle size distribution, as well as surface seawater and atmospheric DMS concentrations were performed simultaneously during the cruise. HYSPLIT back trajectories were used to classify air mass origins. Even though continental sources increased the total aerosol population, it depressed the

effective CCN concentrations possibly due to the competition in particle growth. Continuous high CCN and elevated DMS concentrations over the open ocean occur concurrently, which can be explained by enhanced nucleation and condensational growth of aerosols in marine boundary layer (MBL) resulting from the DMS oxidation or primary aerosols from the sea surface. Our data also indicated that uncertainties remain in sea spray aerosol production flux function, especially for particles with dry diameter smaller than 200 nm.

DEDICATION

I dedicate this dissertation to my family and friends. My most gratitude goes to my wife Xinghua Wang. Without her understanding and support, I would not have been able to finish this work. I cannot thank my parents enough for their willingness to keep me in school even when they have to work extremely hard to do so.

I also want to dedicate this work to many of my friends who have given me help during my studies. My friends Bo Yang and Fang Li kept encouraging me when I encountered difficulties. The help from my friends Guanglin Tang and Tao Wang in Matlab programming made it possible for me to learn to program efficiently and effectively. The companionship of my roommate Chao Liu when coming to the school during nights and weekends prevented me from feeling alone. Without listing all their names, I also owe gratitude to many other fellow students for their companionship during my studies at Texas A&M University.

ACKNOWLEDGEMENTS

It would have been impossible to finish my dissertation without the patient guidance of my advisor, Dr. Sarah Brooks. I want to express my deepest gratitude to her. The same gratitude goes to Dr. Dan Thornton for bringing me into the field of marine aerosol science. Without his cooperation with Dr. Brooks, I would not have the opportunity to carry out research on this hot topic. I also want to thank my committee members, Dr. Don Collins, Dr. Qi Ying, and Dr. Russ Schumacher for their sage suggestions and comments.

I would like to thank Dr. Shari Yvon-Lewis and Dr. Scott Miller, the chief scientists of the 2010 Pacific cruise and the 2011 North Atlantic cruise, respectively. Without their help, I would not have had the chance to get involved in marine aerosol research. I also want to thank the fellow scientists and crew members of the two cruises for their help and companionship.

Special thanks go to Dr. Eric Saltzman for letting me access their DMS data while I was analyzing the aerosol data. Another particular thank you goes to Dr. Peter Liss for his help and guidance when discussing the DMS and CCN analysis with me. Thanks also go to Dr. Yina Liu for helping me downloading the satellite data of chlorophyll *a* concentrations.

I also owe many thanks to my fellow group members. My advisor, Dr. Sarah Brooks, and postdoc researcher, Dr. German Vidaurre, carried out the sampling and field measurements during the 2010 cruise. Dr. German Vidaurre also travelled to the port in Woods Hole, MA, to help me install and unload the sampling system for the 2011 cruise. Without their involvement, I would not have the data to do all the analyses. My fellow PhD candidate Andy Glen also helped me a great deal in preparing for the field and lab measurements. My officemate Katie Jeziorski also helped me a great deal with the research.

TABLE OF CONTENTS

Page

LIST OF FIGURES

Page

LIST OF TABLES

1. INTRODUCTION AND LITERATURE REVIEW

1.1 Basic concepts and definition

Aerosol, a term which officially means liquid or solid particles suspended in an air (Poschl 2005), is used interchangeably with particle in this manuscript. Aerosol can be generated in an experimental system or present in the ambient air. The ambient aerosol is a focus of environmental and climate researches. Ambient aerosols can be distinguished by the original locations of their sources, including marine aerosols, urban aerosols, rural continental aerosols, remote continental aerosols, free troposphere aerosols, polar aerosols, desert aerosols, and so on (Seinfeld and Pandis, 2006). This dissertation is primarily concerned with marine aerosols. Aerosol can also be classified by their chemical composition, such as sulfate aerosol, nitrate aerosol, ammonium aerosol, organic aerosol, sea salt aerosol, and so forth (Seinfeld and Pandis, 2006). Aerosols can also be identified by their mixing state, i.e., internally mixed or externally mixed, which will be discussed further in this chapter. When using the singular form "aerosol" it denotes a general type of aerosol; when using the plurals form "aerosols" it represent many particles or a subgroup of aerosol types based on other categorization method in the primary group. For example, there are sea salt aerosol, sulfate aerosol, organic aerosol and other types of aerosol in marine aerosols.

With the possible exception of chemical composition, aerosol size is the most important characteristic in understanding their influence in direct and indirect radiative effects (Dusek et al., 2006; Twohy and Anderson, 2008). Different "modes" are used to describe marine aerosol sizes, including nucleation mode, Aitken mode, accumulation mode, ultrafine mode, fine mode, and coarse mode (Seinfeld and Pandis, 2006). Based on the distribution functions of aerosol

population, different modes were defined. However, there are various distinctions about the ranges of these modes. Table 1.1 summarized a few of these classifications.

Table 1.1 Different definitions of size ranges of aerosol modes.

Sources	Modes			
Junge 1956			Small SSA: 0.1μm ≤r_{80}≤1 μm	Giant SSA: r_{80}≥1 μm
Whitby 1978			Fine particles: r<1 μm	Coarse particles: r>1 μm
Lewis and Schwartz, 2004			Small SSA: r_{80}≤1 μm	Medium SSA: 1 μm ≤r_{80}≤25 μm Giant SSA: r_{80}≥25 μm
Kulmala et al., 2004b	Nucleation: 3-20nm	Aitken: 20-90nm	Accumulation: 90-1000nm	Coarse: >1000nm
Seinfeld and Pandis, 2006	Nucleation: < 10nm	Aitken: 10-~100nm Ultrafine: <100nm	Accumulation: ~ 0.1 - ~2μm Fine: < 2.5 μm	Coarse: 2.5 - ~50μm
Leck and Bigg, 2007	Nucleation: < 10nm Ultrafine: 10-25nm	Aitken: 25-80nm	Accumulation: ~ 80nm-1μm	Coarse: >1μm

All sizes unspecified are referred to as aerodynamic diameter; r represent radius; r_{80} represent radius at 80% RH.

1.2 Marine aerosol sources and composition

Marine aerosol is one of the most important groups of aerosols since more than 70% of the earth surface is covered by ocean. Marine aerosol is composed of sea salt or sea spray aerosols (de Leeuw et al., 2011), non-sea-salt (nss) sulfate aerosol (Charlson et al., 1987), secondary organic aerosols (Meskhidze and Nenes, 2006), and iodine-mediated coastal particles (McFiggans et al., 2010), as well as species from continental sources and anthropogenic

activities (Mochida et al., 2007). An overview of the sources and categories of marine aerosol is summarized by the author of this dissertation in Figure 1.1.

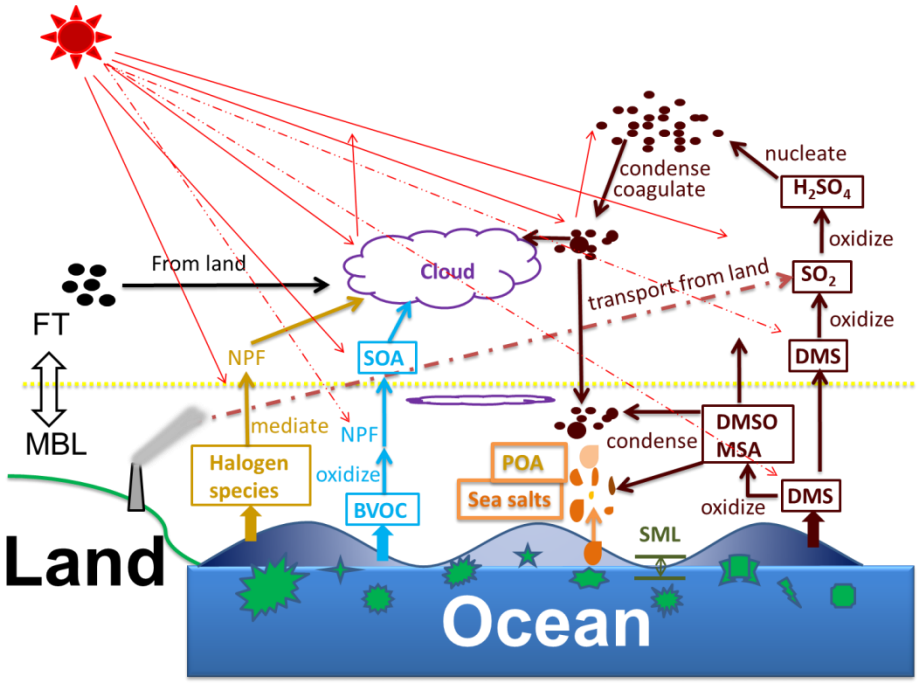

Figure 1.1 Diagram summarizing marine aerosol formation and transportation. DMS, DMSO, MSA, BVOC, POA, SOA, NPF, MBL, FT, SML stand for dimethyl sulfide, dimethyl sulfoxide, methanesulphonic acid, biogenic volatile organic carbon, primary organic aerosol, secondary organic aerosol, new particle formation, marine boundary layer, free troposphere, and sea surface microlayer, respectively.

Sea salt or sea spray aerosol is the primary aerosol produced during the air-sea interactions. Sea salt aerosol is composed of inorganic particles produced through bubble bursting processes (Blanchard 1963). Organic species were reported more and more frequently in primary marine aerosol over the past decade (Gantt and Meskhidze, 2013). Sea spray aerosol

(SSA) is the term used to represent the combinations of sea salt and primary organic aerosols (or simply primary marine aerosols), mixed either internally or externally (de Leeuw et al., 2011). "SSA" will be used equivalently with "sea spray aerosol" in the remaining part of this manuscript, even though it is also often used as the acronym of sea salt aerosol in the literature before the importance of organics was realized. SSA constitutes the majority of marine aerosol mass production flux and is comparable in mass load to continental dust aerosol (Andreae and Rosenfeld, 2008).

Non-sea-salt sulfate aerosol in marine aerosols refers to the portion of sulfate in excess of that present in seawater. Nss-sulfate over the oceans is mainly emitted from phytoplankton synthesized dimethylsulfoniopropionate (DMSP), a precursor to dimethyl sulfide (DMS), especially over remote marine regions (Charlson et al., 1987). DMS can be oxidized by a number of oxidants in marine atmosphere into sulfur dioxide (SO_2) and further into gaseous phase sulfuric acid (H_2SO_4) which can trigger nucleation of new particles (Andreae et al., 1995). In addition, SO_2 emitted from anthropogenic activities and volcanic eruptions can also be transported over the ocean and lead to nss-sulfate. In additional to gaseous phase oxidation, DMS can be oxidized in aqueous phase and contribute to the growth of the newly formed particles and other pre-existing particles (Barnes et al., 2006). The scattering and reflection effects of these DMS-evolved aerosols as well as their ability to serve as cloud condensation nuclei (CCN) were hypothesized to be enhanced with the increase of phytoplankton biomass. Surface water chlorophyll *a* concentration is one metric for phytoplankton biomass. The biomass itself is enhanced by increased temperature and sunlight, in the seminal paper prosed by Charlson, Lovelock, Andreae, and Warren in 1987. This phytoplankton-DMS-aerosol-cloud climate feedback was recognized as a negative feedback and was then commonly referred to as "CLAW hypothesis" (Ayers and Cainey, 2007). Although there have been investigations

showing no strong feedback mechanisms and doubting the validity of CLAW (Woodhouse et al., 2010; Quinn and Bates, 2011), there also have been many studies supporting the original biosphere-mediated climate feedback and indicating the necessity of further researches (Cropp et al., 2005, 2007; Liss and Lovelock, 2007; Ayers and Cainey, 2007; Vallina and Simo, 2007).

Secondary organic aerosol (SOA) in the marine atmosphere is formed through new particle formation (NPF) from biogenic volatile organic compounds (BVOC) and their oxidation products (Rinaldi et al., 2010). BVOCs and their oxidation products can also be the condensable vapors to condense onto the preexisting aerosols and contribute to particle growth (Rinaldi et al., 2010). Examples of VOCs include isoprene (Meskhidze and Nenes, 2006), amines (Facchini et al., 2008a), dicarboxylic acid (Kawamura and Sakaguchi, 1999), etc. Methanesulfonic acid (MSA), an oxidation product of DMS, is also an important type of SOA (Facchini et al., 2008a).

An additional mechanism, iodine-mediated coastal particle formation has been found in multiple locations (McFiggans et al., 2010). Reactive halogen species (RHS) such as iodine monoxide (IO) and atomic iodine (I) derived from macroalgae can react with oxidants (e.g. O_3, HO_2, and NO_2) to form condensable products which are able to form new particles and facilitate particle growth (McFiggans et al., 2010). All the above discussed marine aerosol types could be present over the world oceans, independently or synergistically, mixing internally or externally.

1.3 Direct and indirect effect of marine aerosol

Aerosols exert their influence on the earth mainly by deteriorating air quality and complicating climate change (Poschl 2005). Due to the maritime origin and the relatively smaller amounts transportable to populated areas, the adverse impact of marine aerosol on human health by deteriorating air quality is overshadowed by its terrestrial counterparts (Poschl 2005;

Darquenne 2012). Therefore, the main focus of current researches about marine aerosol is to unravel its function in climate change. Marine aerosol can influence global climate by interacting with incoming solar radiation and outgoing terrestrial radiation, defined as direct climate forcing, and by serving as CCN to modify cloud albedo and lifetime, referred to as indirect climate forcing (IPCC 2007). The direct radiative forcing (radiative forcing, or RF, is the difference on radiative balance at the top of the atmosphere due to the addition of an atmospheric component, e.g., aerosol) due to sea salt aerosol mass load was estimated to range from -0.5 W m^{-2} to -6.0 W m^{-2} (Satheesh and Moorthy, 2005), compared to the overall direct radiative forcing due to all aerosol types being 0.5 ± 0.4 W m^{-2} and that due to mineral dust being 0.1 ± 0.2 W m^{-2} (IPCC 2007: 204). The large range in the estimation of the direct RF due to sea salt is mainly resulted from its uncertainty in production flux, especially for large particles and at very high wind speeds (de Leeuw et al., 2011). The global average indirect RF due to sea salt aerosols was estimated to be -2.9 W m^{-2} (within the range of -10 to 2 W m^{-2}), considering only particles with radii between 0.8 micron and 25 micron (at 80% relative humidity) (Ma et al., 2008). If the potential abundance of SSA particles smaller than 0.8 micron is considered, the indirect forcing due to marine aerosols is subjected to even larger uncertainty than what has been shown in Ma et al. (2008). This is because the indirect effect depends much more on particle number concentration than its mass concentration (Fan and Toon, 2011). Identification of the major sources of marine particles which are most important for indirect RF, i.e. those smaller than 200 nm, is currently a controversial topic (Prather et al., 2013). Bigg (2007) report that only a negligible amount of sea salt particles are present in marine aerosol at sizes smaller than 200 nm, while others reported that significant amounts of sea salts could be detected, either in laboratory or in field samples (O'Dowd and Smith, 1993; Martensson et al., 2003; Clarke et al., 2006). The uncertain sources of marine particles have undoubtedly complicated the evaluation of indirect

RF due to sea salt aerosol or marine aerosol. To reiterate, the aerosol direct and indirect RFs can both counteract the warming effects inflicted upon the earth by anthropogenic greenhouse gases (GHG), and both of them are still subjected to large uncertainties (IPCC 2007; Mahowald et al., 2011).

1.4 Emerging importance of primary organic aerosol in marine atmosphere

It has been known for several decades that organic matter is a component of primary marine aerosols, especially submicron SSA (Blanchard 1964). However, organic contributions to marine aerosol have only gained much attention during the past decade or so (Tervahattu et al., 2002; O'Dowd et al., 2004; Facchini et al., 2008b; Rinaldi et al., 2010; Ovadnevaite et al., 2011a, b; Gantt and Meskhidze, 2013). Primary organic aerosols (POA) are injected into lower marine atmosphere from the sea surface microlayer (SML) which is the topmost tens to hundreds of micron of the ocean surface and enriched with particulate matter, polysaccharides, proteins, surface active materials, bacteria and viruses, debris of phytoplankton, and so on (Sellegri et al., 2006; Cunliffe et al., 2013). The organic species present in SML can be further enriched in aerosols which are formed during the wave breaking and bubble bursting processes. The properties of POA detected in marine atmosphere depend on the locations of sample collection and observations. Fragments and debris of marine organisms, exopolymeric secretions (EPS) of bacteria and viruses, and gel-like substances of uncertain origin have been frequently detected in individual particles with sizes of tens to hundreds of nm in Arctic oceanic area (Leck and Bigg, 2005a, b, 2007; Bigg 2007; Bigg and Leck, 2008; Karl et al., 2012, 2013). It is likely that these microgels and nanogels are capable of serving as CCN, though rigorous measurements of their cloud nucleation abilities have not been performed to date (Leck and Bigg, 2008, 2010). Water insoluble organic compounds (WIOC), including organic colloids and aggregates, have been

found in marine aerosols generated over Northeastern Atlantic Ocean (Cavalli et al., 2004; Ceburnis et al., 2008; Facchini et al., 2008b; Ceburnis et al., 2011; Ovadnevaite et al., 2011a, b). Predicting the hygroscopicity of these insoluble organic materials can be complicated, in part because different growth potentials under different levels of water vapor saturation (Irwin et al., 2010; Ovadnevaite et al., 2011a). A prominent feature of these WIOC is their increasing organic mass fractions in aerosols with decreasing size (O'Dowd et al., 2004; Cavalli et al., 2004; Keene et al., 2007; Facchini et al., 2008b; Vignati et al., 2010; Ault et al., 2013). Water soluble organic carbon (WSOC), including aliphatic substances, humic like substances, and surface active materials, were also detected in marine aerosols as a component of POA (O'Dowd et al., 2004; Decesari et al., 2007; Yoon et al., 2007; Miyazaki et al., 2010; Facchini et al., 2008a; Ceburnis et al., 2008, 2011;). However, it needs to be noted that these detected WSOC also include SOA, which could be dominant sometimes (Decesari et al., 2007; Yoon et al., 2007; Ceburnis et al., 2008; Miyazaki et al., 2010; Rinaldi et al., 2010). Organic compounds (WSOC and WIOC) have been found to be enriched in biologically active regions and seasons (Cavalli et al., 2004; Yoon et al., 2007; Miyazaki et al., 2010). The combined effects of the presence of both WSOC and WIOC on cloud nucleation ability of aerosols could be a dichotomy since some of the surface active organics will reduce the surface tension of the particle but some insoluble organics may hinder the adsorption of water onto the particle (Wex et al., 2010a, b; Westervelt et al., 2012; Cunliffe et al., 2013). For the time being, the overall enhancement effect of the primary organic aerosol on cloud nucleation ability has found to be small (Westervelt et al., 2012; Prather et al., 2013).

1.5 Secondary aerosol formation by photochemical oxidation and nucleation

The most important secondary aerosol in marine atmosphere is nss-sulfate. Nss-sulfate aerosol forms through the oxidation of DMS, followed by new particle formation processes (Andreae and Rosenfeld, 2008). DMS can be oxidized in both gaseous phase and aqueous phase in the atmosphere (Barnes et al., 2006). It is oxidized by OH, NO_3 and halogen radicals into series of compounds in gaseous phase in both MBL and upper troposphere (Barnes et al., 2006; Stark et al., 2007). The oxidation mechanism of DMS oxidation in gaseous phase in summarized in Figure 1.2.

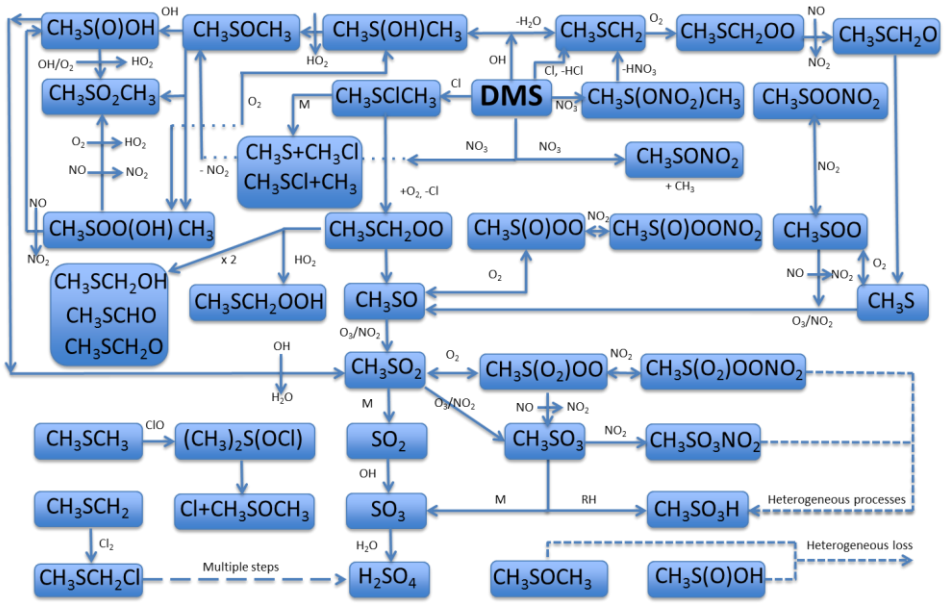

Figure 1.2 Schematic of DMS oxidation mechanism in the gaseous phase (Revised from Barnes et al., 2006 and Stark et al., 2007).

As shown in Figure 1.2, DMS is mainly oxidized by the three oxidants through two mechanisms, H-abstraction and OH-addition. These oxidation reactions result in a sequence of products which can play their parts during the new particle formation and particle growth (Andreae et al., 1999). A distinct feature of the oxidation mechanism is that, the closest step leading to sulfuric acid (SA) involves hydroxyl radical so that SA can only be produced with the presence of OH. It has been taken that OH production in the atmosphere is predominantly initiated by photolyzing O_3 (Stark et al., 2007). However, field measurements have detected both gaseous (Eisele and Tanner, 1993; Zheng et al., 2011) H_2SO_4 and OH radical during nighttime when sunlight is obviously unavailable (Khan et al., 2008), indicating either a missing OH source or a different DMS oxidation mechanism or both. Other products resulting from DMS oxidation, such as dimethyl sulfoxide ($CH_3S(O)CH_3$, DMSO), dimethyl sulfone ($CH_3S(O)_2CH_3$, $DMSO_2$), methanesulphonyl peroxynitrate ($CH_3S(O)_2OONO_2$, MSPN), methanesulphinic acid ($CH_3S(O)OH$, MSIA), and methanesulphonic acid ($CH_3S(O)_2OH$, MSA), can be involved in the condensational growth of particles (Kulmala et al., 2004b; Arsene et al., 2005a).

In addition to gaseous phase oxidation, significant concentrations of DMS can be oxidized by O_3 in the aqueous phase (Gershenzon et al., 2001; Barnes et al., 2006). In contrast, oxidation by O_3 in gaseous phase is six orders of magnitude slower than in aqueous phase (Du et al., 2007). As a consequence, the oxidation of DMS by ozone in the aqueous phase leads to DMSO at an efficiency of unity (Barnes et al., 2006). In addition to oxidation by ozone, DMS can also be oxidized by hydrogen peroxide (H_2O_2) in aqueous phase and result in DMSO. Aqueous phase oxidation rates are dependent on pH (Barnes et al., 2006). Furthermore, the intermediate oxidation products, including DMSO, $DMSO_2$, MSI^- (methanesulphonic ion), MS^- (methanesulphonic ion), can also be oxidized by OH, H_2O_2, Cl, and other oxidants in aqueous phase (Barnes et al., 2006). The oxidation of DMS and its intermediate oxidation products will

contribute to particle growth and should be treated as important additional steps in the overall formation of secondary particles.

Other types of secondary aerosols include those containing WSOC which has been oxidized from emissions of marine biota and anthropogenic VOCs (O'Dowd et al., 2004; Cavalli et al., 2004; Decessari et al., 2007). These WSOC contain aliphatic and aromatic substances, saturated and unsaturated hydrocarbons, oxygenated and nonoxygenated groups, and hydroxyl group (Cavalli et al., 2004; Yoon et al., 2007; Miyazaki et al., 2010). Specific compounds of WSOC include aliphatic alcohols, ethers, esters, oxalic acid, levoglucosan, succinic acid, adipic acid, pinonic acid, glutaric acid, nonanoic acid, diacids, and azelaic acid (Cavalli et al., 2004; Decessari et al, 2007; Miyazaki et al., 2010).

1.6 Uncertainty in primary marine aerosol production flux

SSA particles, which include inorganic sea salt and primary organics, are generated by bubble bursting due to breaking waves which are shown as whitecaps in the sea surface (Blanchard 1963, 1983), and by directly tearing wave crests when wind is strong (Monahan 1983). Two types of drops, film drops and jet drops, can be produced by bubble busting. Submicron SSA particles generated by bubble bursting are usually film drops and supermicron SSA ones are jet drops, with the former dominating in numbers. Large bubbles produce film drops by disintegrating their caps or films (Spiel 1998), while small bubbles produce jet drops by forming a vertically cylindrical jet at the space left by the bubble (Blanchard and Woodcock, 1957). A bubble can generate up to 1000 film drops dominating submicrometer SSA (size ranging from 10 nm to hundreds of micrometer possible), while only up to 10 jet drops can be formed through a jet with their size roughly 1/10 of their parent bubbles (Martensson et al., 2003; Lewis and Schwartz, 2004; de Leeuw et al., 2011).

The production flux of SSA is usually parameterized by wind speed at 10 meters above sea surface, in a power law or exponential form (Lewis and Schwartz, 2004). Most of the production fluxes are parameterized from a scheme between whitecap coverage and wind speed and an assumed production rate per whitecap area and there is an inherent cutoff of sizes smaller than 0.5 micron (Monahan et al., 1986; de Leeuw et al., 2011). SSA mass production flux would suffer only small uncertainty from the size cutoff at the lower side since larger particles dominate aerosol mass. However, SSA number flux is subject to large uncertainty from the size cutoff since Aitken mode particles and accumulation mode particles (<0.5 micron) dominate SSA number concentration (Geever et al., 2005). Parameterizing SSA source functions in the small size end correctly is vital for characterizing marine aerosol properly in global climate models.

The key of the problem in estimating number source function is to find out if the majority of particles smaller than 200 nm are nss-sulfate resulting from DMS or SSA particles produced during the sea-air interactions (Prather et al., 2013). Many investigations have observed SSA particles down to tens of nm in both laboratory and field measurements (O'Dowd and Smith, 1993; Nilsson et al., 2001; Martensson et al., 2003; Clarke et al., 2006; O'Dowd et al., 2008). However, others have detected no sea salt component during their sampling in several years (Bigg 2007; Bigg and Leck, 2008). It is unequivocal that POAs are present in this size range. However, whether or not POA production can be parameterized by the same way as inorganic sea salt particles production is unknown. In addition, even though SSA can be parameterized similarly as inorganic sea salt particles, it is hard to distinguish the relative abundance of small SSA and nss-sulfate aerosol or other secondary aerosols since the latter ones are also present in this size range. Due to the difficulty of unraveling the chemical composition and mixing states of single particles smaller than 200 nm, the understanding of marine particles

in this range needs significant efforts. Recent lab studies simulating wave processes have produced particles <200nm with NaCl cores (Ault et al., 2013; Prather et al., 2013), which is a significant progress toward understanding these particles better.

1.7 Mixing states of marine aerosol

Mixing state of aerosols is vital for understanding direct and indirect radiative effects due to its influence on optical property and hygroscopicity (Lohmann et al., 2007; Khan et al., 2008; Swietlicki et al, 2008; Ghan et al., 2012). Two simplified mixing states are used to describe aerosols, i.e., externally mixed and internally mixed. For an aerosol population to be externally mixed, every particle in the population has to be pure and uniform in chemical composition, even though composition may differ among particles. On the other hand, for an aerosol population to be internally mixed, individual particles must have multiple components. Aerosol populations containing internally mixed particles may or may not have the same number of components and do not have to be uniform within the particle (Lewis and Schwartz, 2004; Seinfeld and Pandis, 2006). The idealized case in which every particle in a population has the same number of chemical components and relative abundances is termed as "fully internally mixed". In a fully internal mixture, the mixing in each particle of the same number of species could be either homogeneous or nonhomogeneous in the molecular level, even though it is more realistic to be homogeneous since it requires equal relative abundance in each particle. On the other extreme side, an aerosol population composed of particles formed by one single pure species is a pure aerosol. The actual state of mixing of the majority of ambient aerosols is between fully internally mixed and pure aerosol. However, both of these scenarios possibly happen in some special conditions and certainly in experimental systems. Recently a mixing index χ with a scale from 0 to 1 was proposed to express the mixing state of ambient aerosol,

with the fully internally mixed particles to be 1 and the totally externally mixed particles (every particle being a pure species) to be 0 (Riemer and West, 2013). The intent of this mixing index is to express the mixing state of an actual ambient aerosol. However, implementation of the index may only be feasible in models and impossible to be obtained based on experimental results for the time being.

To summarize, marine aerosols can be internally mixed, externally mixed, or both (Lewis and Schwartz, 2004; de Leeuw et al., 2011; Prather et al., 2013). Large supermicrometer marine aerosols are usually dominated by sea salt particles, with soluble organic matter a possible coating layer (O'Dowd and de Leeuw, 2007). Small submicrometer marine aerosols (actually SSA) were found to be enriched in WIOC (O'Dowd et al., 2004; Cavalli et al., 2004; Facchini et al., 2008b) and WSOC (Keene et al., 2007; Rinaldi et al., 2010).

1.8 The scope of the dissertation

This study is purported to understand the chemical and physical properties of marine aerosol in all possible respects, including its organic component, cloud formation potential and influence on global climate, its source function parameterized by wind speed, as well as its role played in CLAW hypothesis.

The dissertation will discuss organic components measured by Raman microspectroscopy, most probably with primary origins, for samples collected during a 10,000 km cruise across the Pacific Ocean from Punta Arenas, Chile to Seattle, WA. It will also analyze the mixing state of individual particles sampled during the cruise as well as the mixing tendency of organic species.

The dissertation will discuss about the cloud nucleation ability as well as the CCN concentration of aerosols measured during a cruise in pursuit of phytoplankton blooms over the North Atlantic Ocean. The oxidation of DMS by different oxidants is also analyzed in this study. Nucleation and condensational growth of particles resulting from the oxidation of DMS is also discussed. Therefore, validity of CLAW hypothesis in an increasingly polluted environment is evaluated.

Last but not least, SSA production mechanism is also discussed based on the relationships between the concentration of particles at varying sizes and the wind speed.

2. USING RAMAN MICROSPECTROSCOPY TO DETERMINE CHEMICAL COMPOSITION AND MIXING STATE OF AIRBORNE MARINE AEROSOLS OVER THE PACIFIC OCEAN*

2.1 Introduction

Airborne particles play an important role in climate both directly, by scattering and absorbing solar radiation, and indirectly by serving as cloud condensation nuclei (CCN) on which clouds form (Poschl 2005). The combined effects of aerosols on climate have been identified by the Intergovernmental Panel on Climate Change (IPCC) as the greatest uncertainty in evaluating overall radiative forcing (IPCC 2007). To understand aerosol effects, the major components of the aerosol, including sea salts, sulfates, and organics must be known (Menon et al., 2002; Kirkevag et al., 2008; and Ghan et al., 2012). In addition, the magnitude of direct radiative forcing is uncertain in part due to uncertainties in the mixing state of various components within aerosol particles (Ocko et al., 2012).

The ocean covers 71% of the Earth's surface and it is an important source of aerosol. However, marine sources of aerosol are poorly understood compared with sources of terrestrial origin. The marine biosphere has long been considered a source of aerosol, primarily because phytoplankton emits dimethyl sulfide (DMS), which is oxidized in the atmosphere, forming sulfate aerosol (Charlson et al., 1987). This process is the basis of the CLAW hypothesis, named after scientists Charlson, Lovelock, Andreae, and Warren (Charlson et al., 1987). According to the CLAW hypothesis, DMS-derived sulfate comprises the majority of aerosols acting as CCN

* Reprinted with permission from "Using Raman Microspectroscopy to Determine Chemical Composition and Mixing State of Airborne Marine Aerosols over the Pacific Ocean" by Deng et al., 2014. Aerosol Science and Technology, in press, DOI: 10.1080/02786826.2013.867297

in the pristine marine boundary layer. However, in light of more recent information regarding composition and sources of marine aerosols, changes ranging from modification to outright rejection of the CLAW hypothesis have been proposed (Leck and Bigg 2005b, 2007; Quinn and Bates, 2011). It has been hypothesized that CCN production may be connected to marine biota through pathways other than the products of DMS oxidation, including direct injection of organic particulate matter from the ocean surface into the atmosphere (Leck and Bigg, 2007). Consistent with this hypothesis, high concentrations of organic compounds have been observed in marine aerosols (O'Dowd et al., 2004; Russell et al., 2010). In fact, organic microgels have recently been observed in aerosols and cloud droplets over the Arctic Ocean, an indication that they are potentially a source of CCN (Orellana et al., 2011). Assuming that these organics activate as cloud condensation nuclei at relatively low humidity, they may represent a significant and overlooked global contribution to cloud formation and climate change.

Organic matter found in marine aerosols may be emitted directly from the ocean through the bubble bursting mechanism (Verdugo et al., 2004; Verdugo 2012). Most organic carbon in the ocean is in the form of dissolved organic carbon, which has an estimated inventory of 662 Pg C in the global ocean (Hansell et al., 2009). Organic matter is generally concentrated in the sea surface microlayer (SML) relative to the bulk seawater and further concentrated in atmospheric aerosols generated during bubble bursting (Blanchard and Syzdek 1970, 1982; Aller et al., 2005). However, the ocean biota of the SML is highly complex and the relationship between ocean biology and atmospheric aerosols is currently poorly understood (Prather et al., 2013). The SML contains whole organisms, high molecular weight surfactants and colloids, such as proteins and transparent exopolymer particles (TEP), and smaller organic molecules (Aller et al., 2005; Wurl and Holmes, 2008; Cunliffe et al., 2009, 2010). Organic particles of marine origin as large as one micrometer or more in diameter have been observed in atmospheric samples in several locations

(Leck and Bigg 2005a, 2010; Bigg 2007; Orellana et al., 2011). The majority of gelatinous organic particles found in cloud water in the Arctic were fairly large, with diameters in the range of 200 to 700 nm (Orellana et al., 2011).

Field studies have shown that surface-active organic compounds may be found in atmospheric aerosols from marine (Mochida et al., 2003) and continental sources (Zappoli et al., 1999; Facchini et al., 2000). Laboratory measurements report reduced surface tension of solutions containing atmospherically relevant organic compounds relative to pure water (Svenningsson et al., 2006; Hyvarinen et al., 2006; Brooks et al., 2009). Traditional Köhler theory predicts that reduction in surface tension causes a reduction in the critical supersaturation required for cloud droplet activation (Facchini et al., 2000). CCN measurements confirm that for simple two-component systems, the addition of the surface-active component does indeed reduce the critical supersaturation as predicted in many, but not all cases (Abbatt et al., 2005; Svenningsson et al., 2006). In other studies, only minor reductions in critical supersaturation were observed (Wex et al., 2010a; King et al., 2009; Asa-Awuku et al., 2010). Since surface tension of tiny droplets is inferred, not measured in CCN experiments, the optimal theoretical treatment of the data, including constraints on surface partitioning and kinetic effects, is debatable (Prisle 2010; Ruehl et al., 2012). Calculations show that the CCN activities of surface-active organics are overestimated unless surface partitioning is taken into account (Li 1998; Sorjamaa et al., 2004; Prisle 2010). Differences in both experimental results and modeling approaches may arise from the fact that surface tension reduction does in deed occur, but only when there is enough surface active material to form a thick layer on the droplet (Abbatt et al., 2005; Ruehl et al., 2012). Hence, increased CCN activity in ambient populations may only be observed when the mixing ratios of surface active materials are high.

Recent studies have highlighted the importance of mixing state in assessing the impacts of marine aerosols on climate (Wex et al., 2010b; Gaston et al., 2011; Meskhidze et al., 2011; Gantt et al., 2012). Gaston et al. (2011) observed that large marine organic aerosol (0.5 to 2.5 μm in diameter) measured over Indian Ocean were often found in external mixtures with sea salt aerosols. Assuming all emitted organic material is internally mixed with sea salts could result in an underestimation of the marine CCN concentration at supersaturation of 0.2% by up to 20% (Meskhidze et al., 2011). Treating all marine CCN as internally mixed with hygroscopicity assigned the value of their most hygroscopic component could result in an overestimation of activated CCN concentration by as much as 100% (Wex et al., 2010b). Since modeling studies typically constrain mixing state based on assumptions rather than measurements, estimations of aerosol-cloud interactions and their role in climate may be inaccurate.

Bulk measurements of aerosol composition provide no information on mixing state and to date, direct measurements of individual marine airborne particles are few (Hawkins and Russell, 2010; Gaston 2011; Sobanska et al., 2012). Hawkins and Russell (2010) used Near-Edge Absorption X-ray Fine Structure (NEXAFS) spectroscopy to identify polysaccharides, proteins, and fragments of phytoplankton in marine aerosol. While NEXFAS offers the highest resolution spectral information available at this time, it is also extremely labor and resource intensive. In that study, only 28 particles were analyzed, and the statistical representativeness of these particles is debatable. Single particle mass spectroscopy measurements collected at three marine locations have shown that particles of organic carbon in mixtures with Mg^{2+}, Ca^{2+} and K^{+} were observed in marine environments during periods of elevated chlorophyll *a* (Chl-a) concentration. Interestingly, sea salt was not observed in these mixed particles (Gaston et al., 2011). In a separate study, particles collected at M'Bour (Senegal) included mineral dust

particles coated with marine compounds (Deboudt et al., 2010). Additional measurements of marine aerosol mixing state are clearly needed.

The Raman microspectroscopy (RMS) is a technique developed to probe single particles collected in the field and identify the components of individual particles including multiple components in internal mixtures (Ivleva et al., 2007; Deboudt et al., 2010; Hiranuma et al., 2011; Baustian et al., 2012; Sobanska et al., 2012). As in other Raman applications, an excitation laser is used to excite molecular transitions. While the majority of electrons excited to higher energy levels return to the ground state by Rayleigh (elastic) scattering, a fraction of the excited molecules instead undergo inelastic scattering, emitting radiation with an energy offset from the Rayleigh scattering by the difference between the first vibrational energy level of the ground state and the original ground state (Raman 1929). The associated frequency shift, referred to as Raman shift, corresponds to a specific transition within molecules and thus can be used to identify the compounds in which they occur. RMS has advantages over other techniques. First, it is non-destructive, provided that low excitation energy is employed (Nakamoto 2009; Barletta 2012). Second, since spectra of single aerosol particles can be collected, RMS can be used to assess the mixing state of individual particles found in ensembles of atmospheric particles (Hiranuma et al., 2011). Raman spectroscopy is sensitive to key components present in atmospheric aerosols including organic compounds, inorganic aerosol components such as $(NH_4)_2SO_4$ and NH_4NO_3, and soot and humic-like substances (HULIS) (Sadezky et al., 2005; Ivleva et al., 2007; Hiranuma et al., 2011; Baustian et al., 2012; Avzianova and Brooks 2013). Sadezky et al., (2005) and Ivleva et al., (2007) reported that laboratory-generated soot particles can be differentiated from HULIS using RMS. However, Moon showed additional varieties of HULIS and reported that the spectra of certain varieties of HULIS are indiscernible from those of soot (Moon 2011). Using RMS in combination with SEM-EDX, Deboudt et al. (2010) found

that marine aerosol particles sampled at M'Bour, Senegal, were predominantly internally mixed with dust or carbonaceous materials. In another study, traditional Raman spectroscopy was combined with electron probe X-ray microanalysis (EPMA) to categorize chemical composition and mixing state of aerosols collected in a coastal site in Korea (Sobanska et al., 2012). Results indicated that more than half of the particles were internally mixed species and that humic-like substances were mixed with sea salt in the particles. In cases when more than one peak with a Raman intensity of 20 cps or greater was present (and the peaks were not multiple features of the same molecule), the particle was classified as multicomponent or internally mixed aerosol. Here we illustrate the utility of Raman microspectroscopy in determining variations in chemical composition and mixing state of marine aerosols sampled along an 11,000 km cruise track in the Pacific Ocean during the Halocarbon Air Sea Transect – Pacific (HaloCAST) cruise.

2.2 Experimental section

2.2.1 Field measurements

During HaloCAST, all *in-situ* aerosol instrumentation was located in a lab van situated on the upper front deck of the research vessel R/V *Thomas G. Thompson*. Continuous aerosol sampling was conducted during the transit from Punta Arenas, Chile (53°17'S, 70°54'W) to Seattle, WA (47°36'N, 122°19'W) from March 30 to April 27, 2010. Sample air was drawn through conductive tubing of three meter length and 1/2 inch inner diameter, extending above the top of the lab van. The sampling inlet was equipped with a rotating cone-shaped nozzle and a weather vane to direct the inlet into the relative wind. The sample flow passed through a heater and a desiccant dryer to maintain relative humidity (RH) below 50% throughout the project, and to the suite of instruments shown in Figure 2.1. The ship's exhaust stack was located behind the laboratory van and our sampling inlet. Therefore, all data collected when the relative wind was

blowing from the back of the laboratory sampling van (90° to 270° relative to the bow of the ship) were eliminated to preclude potential contamination from the ship stack (Shank et al., 2012).

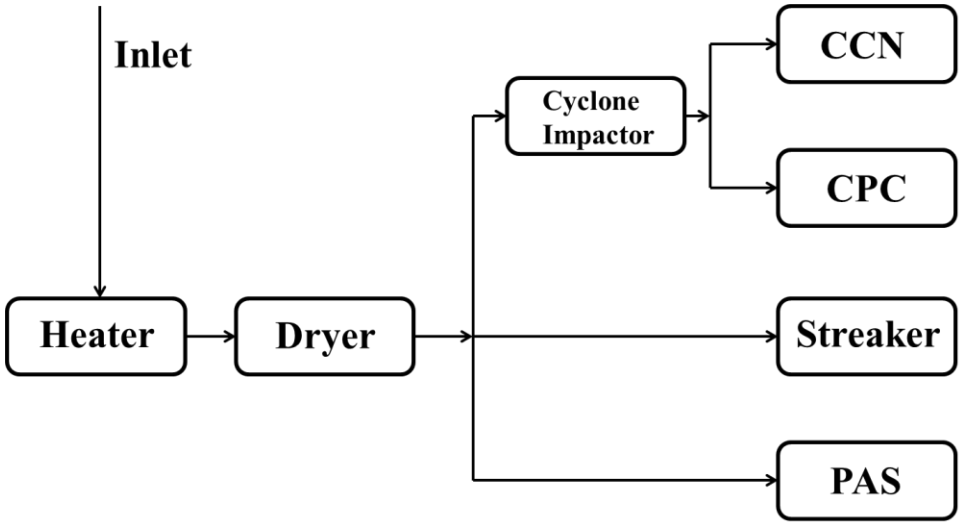

Figure 2.1 Schematic of instrumentation for measurements and sample collection. CCN represents cloud condensation nuclei counter; CPC is condensation particle counter (CN counter); Streaker is the sampler for particle collection; PAS stands for portable aerosol spectrometer which is used to make particle size distribution scanning for particles between 0.3 and 20 μm in diameter.

Aerosol collection for Raman microspectroscopy analysis was conducted using a PIXE Streaker sampler. Aluminum foil was chosen as the impaction substrate since it causes no interference in the Raman spectra (Ivleva et al., 2007). Prior to sampling, the foil was cleaned by rinsing first with acetone (Sigma Aldrich, ≥99.5% purity) and then with ultrapure water (≥18.2 MΩ·cm) and dried at room temperature in a clean container covered by plastic wrap. The PIXE Streaker was operated with an air flow of 1 L min^{-1}. The Streaker was advanced (rotated

by eight degrees) every 4 hours, which results in an intentionally low coverage of particles in each distinct sample area or "streak" on the 82 mm aluminum foil which is ideally suited for the single particle RMS analysis. Samples were replaced by a new filter daily, stored in a freezer at -20 °C, and transported in a refrigerated cooler to Texas A&M University and stored frozen until Raman spectral analysis could be completed. While nominal size range of the Streaker sampler is 2.5 to 10 μm in aerodynamic diameter (Kavouras and Koutrakis, 2001), we observed some particles on the filters out of the specified size range, as we have previously observed in other projects (Hiranuma et al., 2011). Several factors including turbulence, inconsistent flow rate, and irregular shape and density of particles may have contributed to the lack of a distinct size cut-off point in the sampling.

Supporting atmospheric measurements include the concentration of aerosols (0.0045 to 3 μm diameter) by a condensation particle counter (CPC) Model 5.400 from GRIMM Technologies, concentration and size distribution of large aerosols by a GRIMM Model 1.1.08 Portable Aerosol Spectrometer (PAS), and concentration of activated cloud condensation nuclei (CCN) by a Droplet Measurement Technologies CCN counter (DMT CCN). The PAS is an optical particle counter with fifteen bin sizes between 0.3 and 20 μm. Here we use the PAS to determine the total number of aerosols in these bins, and the super-micron aerosol concentration obtained by summing the concentrations in the larger bins. The CCN instrument was stepped through five sequential water vapor supersaturation levels (1.2, 0.9, 0.5, 0.25, and 0.15%) repeatedly, such that an average critical supersaturation can be calculated for every 27 minute segment of the cruise track.

In addition, chlorophyll *a* (Chl-*a*) concentrations along the cruise track were retrieved from the Sea-viewing Wide Field-of-view Sensor (SeaWiFS) satellite. Oceanic surface Chl-*a*

concentration is used as a proxy for marine phytoplankton biomass (Ohde and Siegel 2010; Fauchereau et al., 2011). SeaWiFS data with a resolution of 9 km was downloaded from Giovanni data system (http://daac.gsfc.nasa.gov) developed and maintained by the NASA GES–DISC (Goddard Earth Sciences Data and Information Services Center). The data contains Chl-*a* concentration obtained from an ocean color empirical algorithm OC4V4 by taking the ratio of blue light to green light signals (Dierssen 2010).

2.2.2 Raman microspectroscopy

The Thermo Scientific DXR Raman Spectrometer was equipped with an Olympus BX 20 microscope and a charge-coupled device (CCD) camera. A frequency doubled Neodymium-doped Yttrium orthovanadate ($Nd:YVO_4$) diode pumped solid state laser was used for excitation at a wavelength of 532 nm. For this work, an excitation laser power of 4 mW (variable from 1 to 10 mW), a sample collection time of 5 s, a 50× magnification objective, and a 25 μm confocal aperture were chosen for all measurements. Spectra of the marine aerosol samples were recorded over the range of 50 to 3500 cm^{-1}. The Raman apparatus also featured a motorized stage that moved automatically across the Streaker sample to map out composition in 2-dimensional area in the horizontal plane.

For RMS analysis, the daily Streaker samples were sectioned so that each 4 hour "streak" could be analyzed independently. Samples collected during potential contamination conditions (i.e. when the wind direction was between 90° to 270° relative to the bow of the ship) were removed. All other samples collected along the ship track were analyzed by RMS. The standard operating procedure employed in this work was to use RMS to automatically advance in 5 μm step increments, taking a spectrum at each step. A single map was collected over a 45 × 45 μm area (10 points × 10 points). Three to six maps were collected for each impactor stage

depending on the particle coverage on the sample. Most spectra signify a single independent particle, while occasionally some agglomerates could generate multiple spectra. In addition to the standard mapping procedure, additional spectra were occasionally collected using a smaller step size to manually survey variability within aggregates of particles. Due to the fairly low coverage of particles on the filter, approximately two thirds of the spectra (~77,000 out of a total of 108,000) contained no peaks. It was assumed that these spectra were taken between particles on the stage, and hence they were discarded. A summary of the results of single particle composition are presented below.

2.3 Results and discussion

2.3.1 Selection of marine segments according to chlorophyll *a* concentration in the ocean

Raman analysis was conducted on samples collected along the HaloCAST transect shown on the map in Figure 2.2. The color scale in the figure indicates the Chl-*a* concentration along the track as retrieved from SeaWiFS observations. It is well known that elevated Chl-*a* levels often occur near the coasts, due to coastal upwelling which brings nutrients from deep waters to the sunlit surface waters, as well as nutrients carried by runoff from the land (Thornton 2012). In addition, upwelling in the equatorial regions also increases biological activity. Since observations of Chl-*a* concentration are often used as a proxy for phytoplankton biomass (Ohde and Siegel 2010; Fauchereau et al., 2011; Thornton 2012), we used observed variations in Chl-*a* concentrations to identify the transition points between segments passing through different regions along the ship track, including Southern Coast, Southern Open Ocean, Tropical Open Ocean, Northern Open Ocean and Northern Coast segments as shown on Figure 2.2. Comparisons of aerosol properties were made between the different segments. Sampling

throughout the full HaloCAST transect provided the opportunity to investigate how differences in season, hemisphere, and coastal/open ocean scenarios may modulate air-sea interactions.

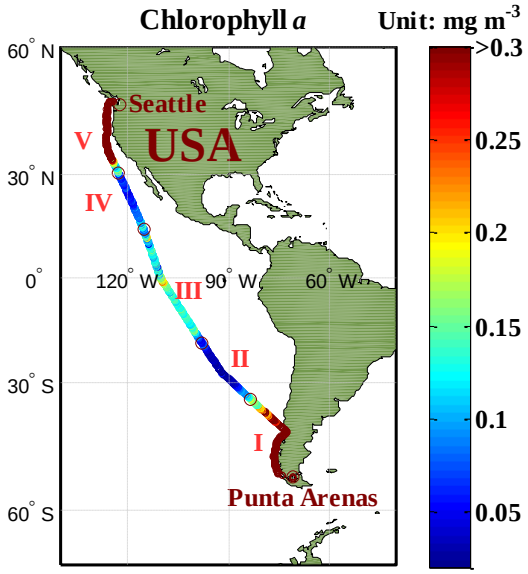

Figure 2.2 Variation of SeaWiFS retrieved chlorophyll *a* (Chl-*a*) concentration along the cruise track. The values are capped with a value of 0.3 mg m^{-3} to better display variation in the open ocean. Roman numerals are the segments divided based on Chl-*a* levels. Centers of open circles are the positions to divide segments.

In the Southern and Northern Coast segments, i.e. Segments I and V, we observed average Chl-*a* concentrations of 0.55 and 0.93 mg m^{-3} respectively, compared to the average open ocean concentration of 0.11 mg m^{-3}. To a lesser extent, biological activity was also enhanced in the equatorial region, which we attribute to upwelling. We observed that the average Chl-*a* concentration in the Tropical Open Ocean segment (Segment III) was 0.12 mg m^{-3},

significantly higher than in either the Southern (Segment II) or Northern Open Ocean (Segments IV) segments.

2.3.2 Classification of aerosol composition

Raman spectra were used to determine the chemical composition of individual particles in the collected samples. Each individual spectrum was placed into one of the main composition categories based on peak assignment of the highest peak in the spectra and any secondary peaks of an intensity of 20 cps or higher, based on the instrumental signal to noise ratio. Figure 2.3 shows examples of spectra from each of the main categories observed in the samples.

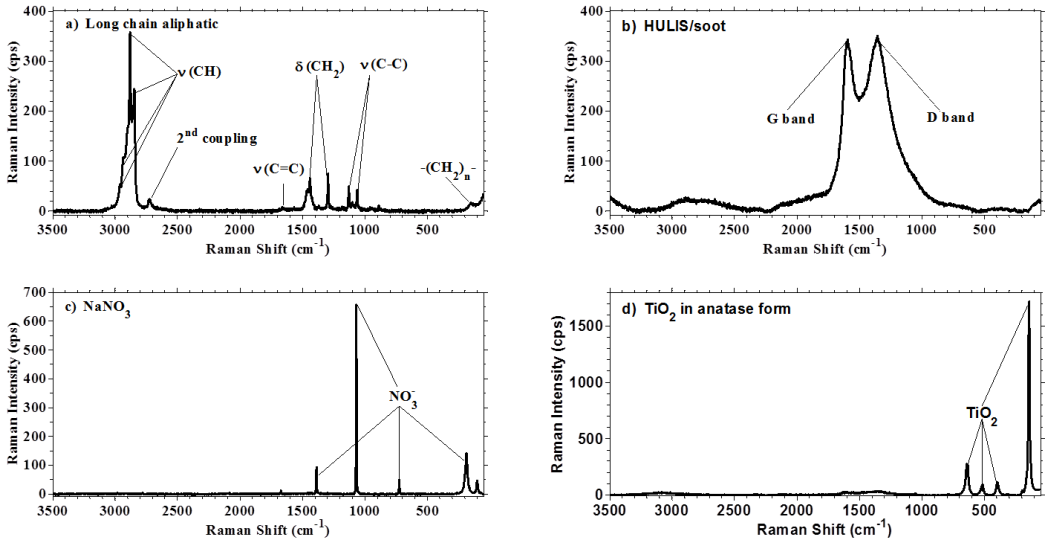

Figure 2.3 Representative spectra of the main chemical composition categories: (a) Long chain organic compounds; (b) Humic-like substances (HULIS) and/or soot identified by the graphitic and irregular/graphic defect peaks; (c) $NaNO_3$, a member of the water soluble inorganics category; (d) TiO_2 in anatase form, a member of the "Unclassified" category. The ν symbol signifies a stretching mode and δ signifies a bending mode. 2nd coupling indicates an overtone of a primary tone or a sum tone of primary overtones. G band and D band represents ideal graphitic lattice stretching mode and disordered graphitic lattices, respectively.

The first category of compounds identified through Raman spectroscopy was pure long chain organics (Figure 2.3a). All spectra of long chain organic compounds have a prominent doublet with peaks positioned at ~2880 and ~2850 cm^{-1} arising from C-H stretching modes. Presence of this doublet at an intensity greater than other peaks (and greater that the nominal baseline value, 20 cps) was the criteria for placing a spectra in the long chain organic class (Snyder and Schachtschneider, 1963; Sebek et al., 2011; Schumacher et al., 2011). The spectrum in Figure 2.3a closely matches the standard spectrum of octadecanoic acid in the Omnic Spectral Reference Library, which contains $-(CH_2)_{16}-$ as its skeleton chain. In addition, the spectrum in 3a contains a small peak at low wavenumber, 150 cm^{-1}. Interestingly, there is a simple approximate relationship between the length of saturated hydrocarbon chains and Raman peak position, as shown:

$$x = 2400/N_c \quad (2.1)$$

where x is the band position (in cm^{-1}), and N_c is the methylene group number in the chain (Schaufel and Shimanouch 1967; Hasegawa 2004). According to this formula, the compound shown in Figure 2.3a contains a $-(CH_2)_{16}-$ structural backbone. While the value of N_c may vary for unsaturated hydrocarbon chains and branched structures, it provides further indication of the presence of long hydrocarbon chains of some type. The small peak at 150 cm^{-1} was common in many of the spectra classified as long chain organics in this study (Miyazaki et al., 2010).

Additional features frequently observed in the long chain hydrocarbons spectra include $-CH_2-$ scissoring, $-CH_2-$ twisting, C-C symmetric stretching, and C-C asymmetric stretching at 1440 and 1458, 1295, 1128, 1062 cm^{-1}, respectively (Snyder and Schachtschneider 1963; Snyder et al., 1982). Many long chain organic spectra contained a peak at 1650 cm^{-1} indicative of a C=C stretching mode in straight chain aliphatic acids. These are consistent with alkenones and

alkenoic acids identified by NEXFAS spectra of marine aerosol collected off the coast of Chile (Hawkins and Russell, 2010). In addition, some of the spectra identified as long chain organic species contained hydroxyl groups. In general, our results imply that that the samples we collected contain a combination of multiple chemical species, with a common trait of a long chain aliphatic molecular framework.

Interestingly, aromatic rings characterized by C-H stretch modes in the range of 3200-3000 cm^{-1} and a C=C sharp double peak at 1580 to 1600 cm^{-1} (signatures of carbonaceous urban pollutant particles) were notably absent from nearly all samples, with the exception of a few collected near the coast (Mayo et al., 2003). While long chain organic molecules have been reported by others (O'Dowd et al., 2004; Russell et al., 2010, 2011), our study is the first to illustrate the vast geographic area and a wide range of conditions over which high concentrations of long chain organics are present in marine aerosol.

Figure 2.3b shows representative spectra in the second category, identified as HULIS and/or soot species. Spectra in this group were identified by an apparent doublet at about 1350 cm^{-1} and 1580 cm^{-1}. While this feature looks like two broad peaks, it has been modeled as a combination of five graphitic peaks present in both humic acids and soot spectra (Ivleva et al., 2007). While it has been reported in the literature that at least one type of humic acid is discernible from soot (Ivleva et al., 2007), our own research group has found that when a broader range of humic acids were surveyed humic acids and soot could not be definitely distinguished from one another due to spectral variability depending on acid type and overlapping peaks (Moon 2011). Thus, HULIS and soot are combined into one class in this work.

The source of the HULIS in marine atmospheric particles is uncertain. These large acids are products of decomposition which may originate from marine organisms in seawater which

are transferred to the atmosphere by bubble busting (Krivacsy et al., 2008). Alternatively humic-like substances may form in the atmosphere through chemical reactions through oxidation of smaller gas phase organic molecules (Krivacsy et al., 2008; Limbeck et al., 2003). HULIS has been observed by others in both submicron and supermicron mode particles (Cavalli et al., 2004; O'Dowd et al., 2004). Finally, the possibility that some of these spectra contain soot cannot be ruled out. The ship stack was a potential source of soot. However, since we have employed a strict filter; removing all samples collected when the wind direction was from the back to the laboratory van as described above, we assume that all potential contamination from the stack has been removed. From this point forward, we denote the group of HULIS/soot simply as HULIS.

The third spectral group, as shown in Figure 2.3c, is water soluble inorganic species (WSIO), including typical inorganic species of atmospheric aerosols such as $NaNO_3$ (identified in Figure 2.3c by the primary sharp peak at 1067 cm^{-1}) and Na_2SO_4 (sharp peak at 995 cm^{-1}) or carbonate salts (1086 cm^{-1}). Unfortunately, NaCl, a major component of sea spray (Mamane and Gottlieb 1992; Krueger et al., 2003; Ciuraru et al., 2011), is not Raman active and will be undercounted by Raman analysis (Oliveira et al., 1981; Sobanska et al., 2012). The inorganic species in this category may contain various cations such as Na^+, K^+, Ca^{2+}, and Mg^{2+}, though the Raman cannot be used to determine which cations are present. Figure 2.3d shows the spectra of titanium dioxide (TiO_2) in anatase form, observed in less than 1% of the aerosol particles. Spectra containing TiO_2 in either anatase or rutile form, silicon species, and spectra of unknown composition were placed in the "Unclassified" category.

Spectra of an additional type (not shown) that were characterized by a sharp peak at about 520 cm^{-1} were occasionally observed (~10% of the spectra). This peak matches that of crystalline silicon. A possible source of the silicon component in marine aerosol is diatom cell

wall fragments (Lara and Thomas 1995). Mineral dusts contain silicon oxide (Gallavardin et al., 2008). However, silicon dioxide has unique and different spectral features, which were not detected in any of our samples (Popovic et al., 2011). Reports about tiny silicon/silicon dioxide particles in ambient aerosol samples are not widespread but have been reported from field measurements in the urban Houston area (Phares et al., 2003; Glagolenko and Phares 2004). Silicon species were believed to be the oxidation product of industrial gas compound silane, which is widely used in the electronic industry for silicon oxide film production (Azatyan et al., 1980). In our own samples, a fraction of spectra may be placed in this category due to background noise arising from the aluminum foil substrate, which contains trace amounts of silicon. Al foil is the preferred substrate because in the vast majority of spectra it produces no signal interferences. However, less than 2 percent of the spectra collected on clean aluminum foil produced a peak at around 520 cm^{-1}. Thus, a small fraction of sample spectra in this category may arise due to background.

2.3.3 Observations of mixing state: internally mixed aerosols

An advantage of Raman microspectroscopy is that it provides spectra of single particles and thus information on aerosol mixing state. Examples of observed multicomponent aerosol particles are shown in Figure 2.4. In the majority of multicomponent spectra, two or three components were identified. For example, Figure 2.4a shows a spectrum of particles containing long chain organic and HULIS, as well as a soluble inorganic species Na_2SO_4. A large number of spectra contained a combination of long chain organics and HULIS and soluble inorganic species such as Na_2SO_4 and $NaNO_3$, as exemplified by Figure 2.4a. Figure 2.4b shows a spectrum of particles containing HULIS and long chain organic species. Figure 2.4c shows an example of a mixture of $CaSO_4$, long chain organic species, HULIS and $CaCO_3$. The most

frequently observed combination was mixtures of the two predominant species, long chain organic species and HULIS, as shown in Figure 2.4b. On rare occasions, as many as five components were identified in a single spectrum, as exemplified by Figure 2.4d. Figure 2.4d shows an example of mixture of long chain organic species, HULIS, $CaCO_3$, silicon and the rare observation of rutile TiO_2. Since RMS is unusually sensitive to TiO_2 due to its large Raman cross-section, our measurements suggest the occasional presence of a low concentration of this compound (Sobanska et al., 2012).

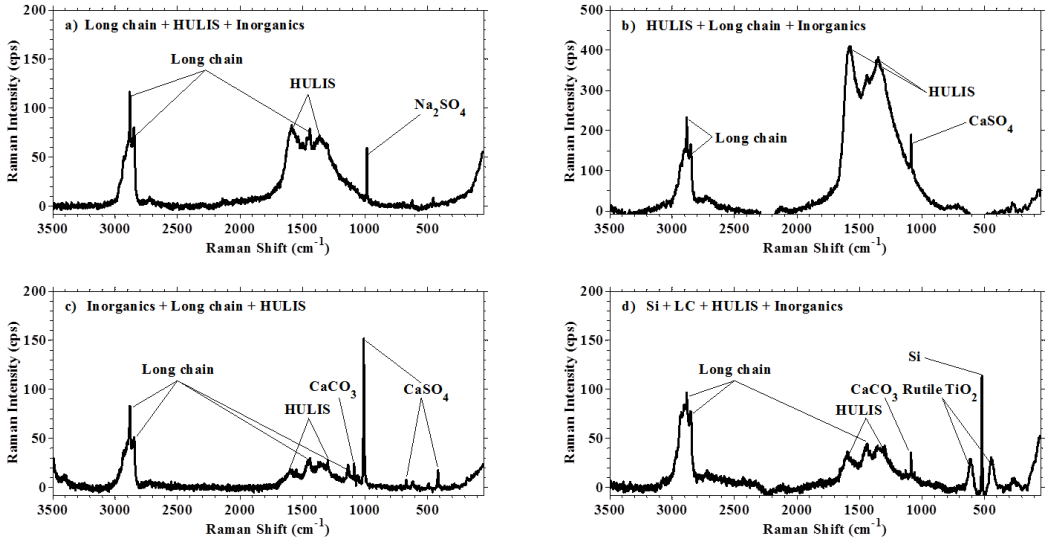

Figure 2.4 Examples of collected spectra of multi-component aerosols: (a) Long chain organics, HULIS, and inorganic species; (b) HULIS, long chain organics, and inorganic species; (c) Inorganic species, long chain organic species, and HULIS; (d) Si crystal, long chain organic species, HULIS, inorganic species, and a form (rutile) of rare species TiO_2.

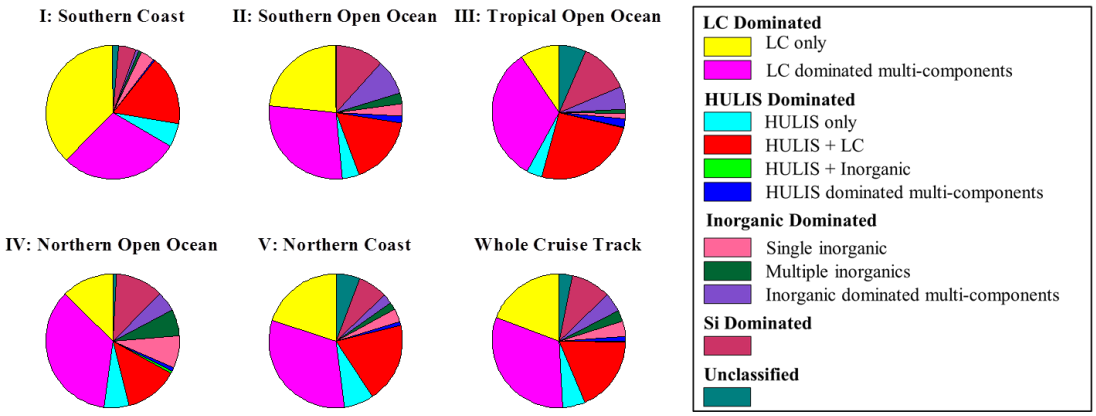

Figure 2.5 Particle composition pie charts representing the occurrence of peaks identifying the given components in the Raman spectra. Each pie chart shows the average information of a specific segment. Abbreviations: "HULIS" -- Humic-like substances; LC -- Long Chain Organics; "Unclassified" -- All other species not categorized, including TiO_2.

Beyond classification according to primary component, spectra were further categorized based on secondary components they contain in lesser quantities (Figure 2.5). We include in this analysis only secondary peaks with intensities of 20 Raman cps or greater. Multicomponent aerosol classified as "long chain organic dominated" in Figure 2.5 may also contain HULIS, water soluble inorganics, metallic or silicon components, or any combination of them. Further categorization of the long chain organic dominated group is not possible due to the overlapping spectral regions between multiple minor peaks of primary species and major peaks of secondary species which may be present. HULIS dominated spectra were subdivided into those containing long chain organics, soluble inorganics, or both. Water soluble inorganics-dominated spectra include those containing a single soluble inorganic species (labeled Single Inorganic in Figure 2.5), species containing two or more different soluble inorganic species (labeled Multiple Inorganics in the figure), and others dominated by inorganics but containing other species, i.e.,

long chain organics, HULIS, or TiO_2 (labeled Inorganic dominated multi-components). Finally, the "Unclassified" category includes all spectral types which do not fit in the categories above, including TiO_2 spectra and some other species which have not been identified.

2.3.4 Aerosol composition throughout the Pacific Ocean

In looking for variations in aerosol composition under different oceanic conditions, the RMS data was divided into five segments of the cruise transect based on location and changes in surface seawater Chl-*a* concentrations, as shown in Figure 2.2. In Figure 2.5, the percentages of particles classified into each category are reported for each of the five segments. Samples were collected continuously. However, persistent winds from the rear of the ship made it necessary to remove significant sections of data along the coast of South America and the Tropical Open Ocean to eliminate potentially contaminated samples.

As can be seen in Figure 2.5, the purely long chain organic species and those dominated by long chain organics comprised a significant fraction of spectra during the entire cruise. The highest percentage of purely long chain organic aerosols, 37%, was detected in the Southern Coast segment. Combining these pure organic aerosols with those containing the long chain organics found in internal mixtures yields a total fraction of aerosol containing long chain organics aerosol fraction of 67% in the Southern Coast Segment. These organics are present in coastal waters and the open ocean, in the Southern and Northern Hemispheres, and in the autumn (Southern Hemisphere) and in the spring (Northern Hemisphere). Throughout the entire cruise track, more than 50% of the sampled particles contained long chain organics.

Our initial hypothesis was that if biological activity in the ocean was the primary source of long chain organic aerosol in the atmosphere, then increased concentrations of organic

aerosols would be observed over regions of elevated Chl-*a*. Unlike Chl-*a* concentration, which was highest along both coasts, the fraction of pure long chain organic particles was highest near the coast of South America, but lower near the North American coast than in all other segments except in the tropical open ocean. Since coastal samples may be influenced by continental sources of organic compounds, we draw no conclusions based on the lack of relationship between Chl-*a* and long chain organics in coastal samples. Among the open ocean segments, Chl-*a* was highest in the Tropical Open Ocean segment, but the fraction of pure long chain organics was lowest. The fraction of pure long chain organics was not correlated with Chl-*a*, even in open ocean segments under little or no influence of continental aerosol. There are several possible reasons for the lack of correlation. Organics in the SML may become internally mixed prior to arrival in the atmosphere. This is possible, although no correlation between either the combined pure and internally mixed organic fractions or the organic mixtures and Chl-*a* concentration was observed. In addition, no significant correlation between wind speed and long chain organic fraction was found in the study. Sea state, boundary layer height or other undetermined variables may exert strong influences over the concentration of marine aerosol in the lower atmosphere as well. Finally, observed variations in Chl-*a* in the open ocean were 0.04 to 0.27 mg m^{-3}. It is possible that the long chain organic fraction in atmospheric aerosol is not sensitive to changes of this magnitude.

HULIS-containing aerosols also occupied a significant fraction of all aerosols. For the open-ocean segments, the percentage of spectra classified as long chain organics, HULIS, or both were higher in the Southern and Tropical Open Ocean Segments than in the Northern Open Ocean. While our results corroborate the surprising recent reports of high concentrations of organic materials observed in both the Atlantic and Pacific Oceans (Mochida et al., 2003; Cavalli et al., 2004; O'Dowd et al., 2004; Russell et al., 2011, 2010), these data are significant since they

show the consistent prevalence of long chain organics across broad sampling conditions in the Pacific Ocean.

Considering homogeneous and internally mixed particles together, inorganic compounds were only observed in an average of 7 to 19% of the Raman spectra during the entire cruise track. A few exceptions to the low inorganic fraction were observed in episodes (4 hr samples) throughout the cruise track. During these episodes, the percentage of spectra classified in inorganic spectra spiked to greater than 50%. Silicon species were present in as many as 12% of the spectra in a sample in the middle of the Tropical Open Ocean segment. The silicon species were a more common occurrence in samples collected in the northern hemisphere than in the southern hemisphere. One possible explanation is the elevated industrial activity involving with silicon production in northern hemisphere (Azatyan et al., 1980; Phares et al., 2003).

Overall, less that 7% of the particles were categorized as "Unclassified". One brief exceptional episode to this occurred in the middle of the Tropical Open Ocean Segment. In the 4 hour filter sample collected during the episode, 27% of the spectra were identified as rutile type TiO_2. TiO_2 is a common component of paint. It is possible that the occasional detection of TiO_2 was due to shipboard contamination occurring times when HaloCAST crew painted the aging wood on the deck during the cruise.

2.3.5 Marine aerosol mixing state and cloud formation

According to a recent modeling study, variations in mixing state cause larger changes in cloud activation potential than any other marine aerosol property, including composition and hygroscopicity (Gantt et al., 2011). Because the presence of long chain organic particles will have effects on both the optical properties and cloud formation properties of aerosols depending

on whether they exist as pure single component particles or as internal mixtures, we are particularly interested in the mixing state of marine long chain organic molecules (Meskhidze et al., 2011; Baustian et al., 2012). According to a recent modeling study, the influence of marine primary organic aerosols on near-surface concentrations of CCN depends on mixing state, with the highest increases in CCN concentration, up to 20%, occurring when primary organics were assumed to be externally mixed with sea salt (Meskhidze et al., 2011).

By analyzing multiple particles of a collected ensemble with RMS, the degree of external mixing of particles of different composition can also be assessed. During no segment of the cruise did the aerosol population contain only one type of single component aerosol exclusively. We classified those spectra in which peaks arising from multiple components as internally mixed. Single particle spectra containing a single component were either externally mixed or pure aerosol, depending on the composition of other aerosols in a sampled ensemble. In Figure 2.6, the degree of internal mixing (reported here as the percentage of spectra which contained peaks arising from multiple components) is summarized. Since some components of aerosol (including sodium chloride) were either Raman inactive or simply not identified in our analysis, the degree of internal mixing of organic species reported here should be considered a lower limit. Shown in Figure 2.6 are the percentages of all aerosol spectra in a sampling segment containing: 1. a pure long chain organic species, 2. those containing mixtures dominated by long chain organic species, 3. mixtures containing long chain organic and at least one more species in any proportions, and 4. the internally mixed species containing many components.

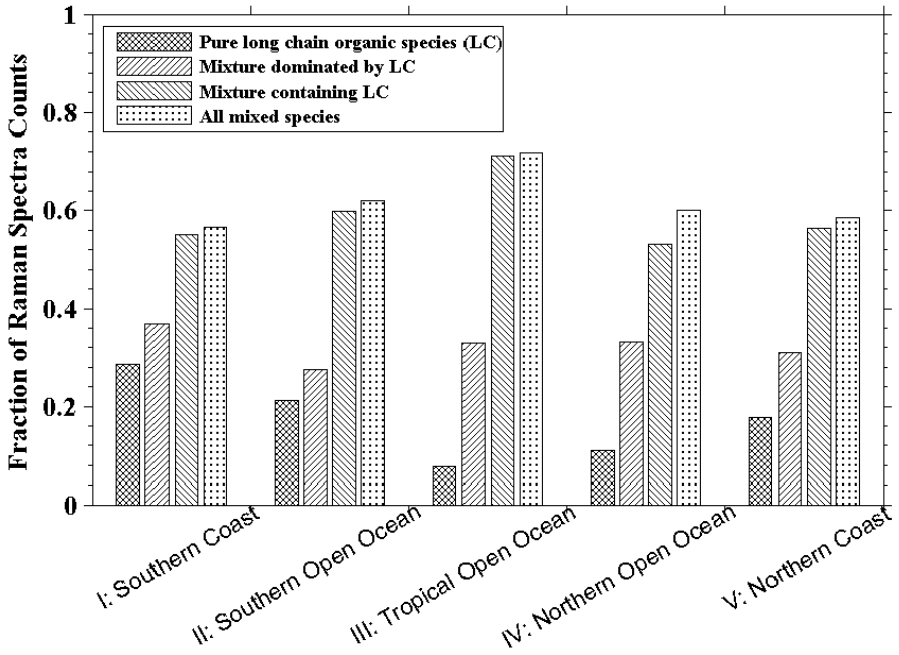

Figure 2.6 Mixing state of sampled marine particles according to Raman analysis. The fractions of analyzed particles identified as pure long chain organics, internally mixed particles in which long chain organics are the dominant species, mixtures in which long chain organics are present in lesser proportions than other compounds, and the overall fraction of particles which are multi-component mixtures, are shown in cross hatched, right-slanted, left-slanted, and dotted pattern, respectively.

Assuming only one spectrum was collected for each particle, the majority of particles collected throughout the entire project were internal mixtures. Based on Figure 2.6, long chain organics were present as single component aerosol 19% of the time on average (ranging from 8% to 29% during different segments). Since not all compounds present may be identified by RMS, we consider the degree of internal mixing reported here to be a lower limit on the actual percent of particles containing long chain organics mixed with other compounds. The percent of particles dominated by long chain organics is 32% on average (ranging from 28% to 37% during various segments). The long chain organics were most often found in internally mixed particles,

with percentage of long chain organics in internally mixed particles ranging from highest (71%) in the Tropical Open Ocean Segment to lowest (53%) in the North Coast segment. Total internal mixing was also high, which percentages of internal mixtures in all particles ranging from 57 to 72% for all segments. Like the trend for organics, the highest overall mixing occurred in the Tropical Open Ocean. A high degree of mixing is plausible given the lack of local pollutant sources near the Equator. This is consistent with a population of aerosol components which have had time to mix either within the SML prior to ejection or through atmosphere aging processes. From the entire ship track, only three daily samples did not contain a majority of internally mixed particles.

While our observations suggest that at least 60% of marine aerosol particles in the Pacific Ocean are internally mixed, aerosol composition and mixing state vary spatially and temporally. Spatial variations may in part explain why these results are not in agreement with a previous study which reported that large marine organic aerosol (0.5 to 2.5 μm) measured in Indian Ocean were often found in external mixtures with sea salt aerosols (Gaston et al., 2011). It has been reported that internal mixing can either increase or decrease aerosols' ability to act as CCN, depending on the competing effects of increased mass and reduced hygroscopicity at the location of interest. For regions of high marine biological activity, CCN concentrations are underestimated, according to that study (Meskhidze et al., 2011). Thus, for the most accurate modeling of aerosol-cloud interactions, the observed mixing state must be included.

2.4 Supporting measurements: concentration of aerosols and CCN

2.4.1 Particle concentration

Consistent with the Raman sampling, all aerosol data collected when the relative wind was blowing from the back of the laboratory sampling van (90° to 270° relative to the bow of the ship) were removed from the data set to avoid over-counting of particles due to ship contamination. The average aerosol concentrations observed during each sampling segment are summarized in Table 2.1. In general, particle concentrations were higher in Northern Open Ocean than in Southern Open Ocean segment in the size ranges sampled by the CPC (0.0045 μm to 3 μm diameter), the total PAS (0.3 μm to 20 μm diameter) and the supermicron aerosols (determined by summing the concentrations of the largest 10 size bins of the PAS data were summed together.

Table 2.1 Average aerosol number concentrations, Chl-*a* concentrations, and CCN critical supersaturations in different segments along the cruise track (numbers in parenthesis are 1δ standard deviation).

Segments / Parameters	Southern Coast (I)	Southern Open Ocean (II)	Tropical Open Ocean (III)	Northern Open Ocean (IV)	Northern Coast (V)
CPC (0.0045 to 3.0 μm) concentration (cm^{-3})	573 (1146)	147 (29)	227 (100)	274 (181)	455 (652)
PAS (0.3 to 20 μm) concentration (cm^{-3})	17.4 (27.3)	2.6 (3.8)	17.8 (24.6)	14.2 (5.2)	24.0 (16.0)
Super-micron particle (> 1 μm) conc. (cm^{-3})	1.05 (1.70)	0.09 (0.06)	0.65 (0.52)	0.50 (0.32)	1.19 (0.63)
Chl-*a* ($mg\ m^{-3}$)	0.93 (0.03)	0.05 (0.03)	0.12 (0.04)	0.07 (0.02)	0.55 (0.35)
CCN (1.2%) (cm^{-3})	175 (90)	115 (42)	214 (69)	173 (95)	189 (74)
CCN (0.15%) (cm^{-3})	63 (49)	45 (48)	150 (46)	119 (72)	114 (74)
S_{crit} (%)	1.4 (1.2)	0.7 (0.3)	0.1 (0.3)	1.2 (0.8)	0.2 (1.1)

Aerosol number concentration determined by the CPC was measured in the range from below 200 cm^{-3} in the southern hemisphere to ~10^3 cm^{-3} in the northern hemisphere. Average aerosol concentration measured by the CPC along the entire cruise track is shown in Figure 2.7A. (For direct comparison with the CCN data included in Figure 2.7B-D below, the CPC data included in these average concentrations was filtered to include only data collected during time which coincide with stable CCN data collection.) The concentration dropped by a factor of 3 or more times as the ship traveled from the southern coast waters to the southern open ocean. In the Southern Pacific Ocean, changes in concentrations were gradual, with the exception of a region between 14.5 to 10.5°S latitude. During the 8-hour period when the ship remained in this region, aerosol concentrations of 400 cm^{-3} and higher were observed. Elevated concentrations occurred during part of the ship track through the region of equatorial upwelling, as indicated its position (Tropical Open Ocean Segment III) and by increased Chl-*a* concentration relative to the open ocean.

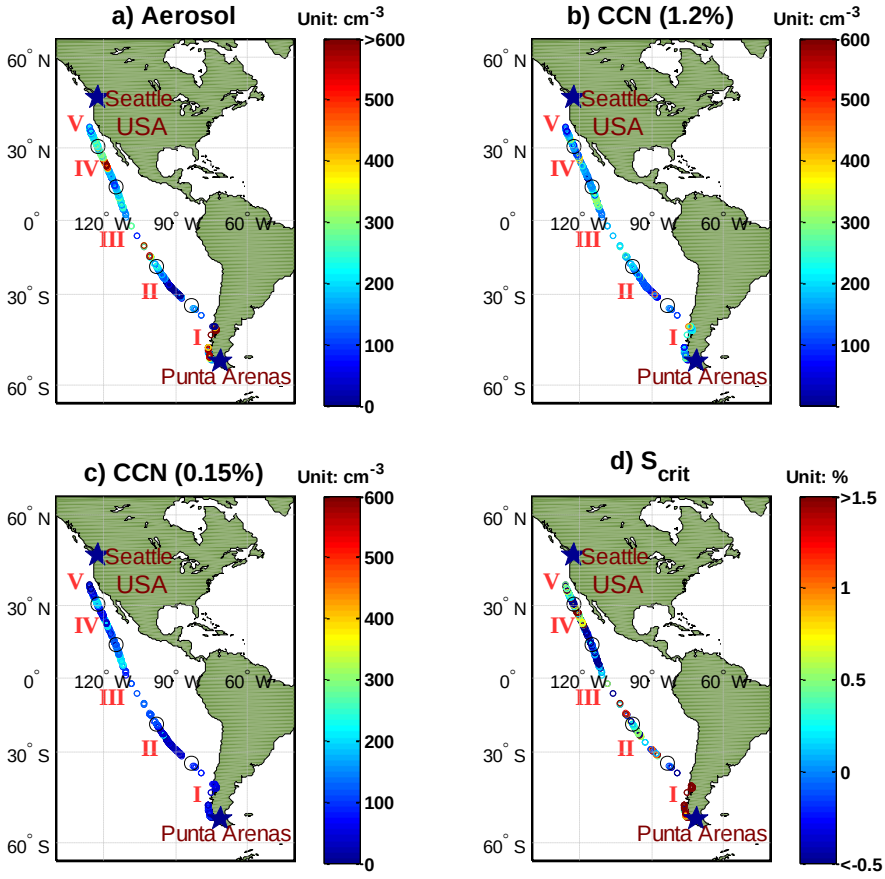

Figure 2.7 Average concentrations (27-minute averages) of aerosol concentration measured by the CPC, the concentration of aerosols activated at 1.2% SS, the concentration of aerosols activated at 0.15%, and the critical supersaturation determined by the CCN instrument are shown in (a-d), respectively.

Once the ship crossed into the Northern Hemisphere, spikes in concentration by up to 10 times were observed, with concentrations between 500 and 2000 cm^{-3} observed for a few miles. Despite the spikes, average concentrations remained rather low during all three open ocean segments. The spikes coincide with greater ship traffic was encountered in the northern hemisphere. In the absence of traffic, the open ocean aerosol concentrations in the northern hemisphere are very similar to those in the southern hemisphere. This suggests that any

influence of marine biology as indicated by changes in Chl-*a* did not produce dramatic variations in aerosols comparable to anthropogenic contributions. Aerosol concentration increased by a factor of two when the ship entered the Northern Coast Segment. Aerosol loadings above 4000 cm^{-3} were measured close to the North American coast. The northern hemisphere is subject to larger aerosol emissions and variability in aerosol concentration due to greater landmass, higher population, and more commercial shipping routes than in the Southern hemisphere. These facts can likely explain the measured high aerosol loads and variability.

The concentration of supermicron aerosol particles measured by PAS in Tropical Open Ocean was slightly higher than in Northern Open Ocean, probably due to enhanced primary aerosol generation in equatorial regions (Ohde and Siegel 2010). As for the coastal segments, we observed a higher number concentration for small particles (CPC measurement) in Southern Coast than in Northern Coast, which is most probably due to the closer sampling location to the continent in the southern segment. However, we observed a slightly higher particle number concentration from PAS measurement in the Northern Coast than in the Southern Coast segment. Overall, the average number concentrations in these segments varied increasingly in this order: Segment II (Southern Open Ocean Segment) < Segment III (Tropical Open Ocean Segment) < Segment IV (Northern Open Ocean Segment) < Segment V (Northern Coast Segment) < Segment I (Southern Coast Segment).

2.4.2 CCN concentration

Each CCN cycle included measurement of the concentration of aerosols activated as CCN at five set points, 1.2%, 0.9%, 0.5%, 0.25%, and 0.15% supersaturation with respect to water. In each 27 min cycle, instrumental conditions were held at each supersaturation level for five minutes, with the exception of the starting level, 1.2%, which was maintained an additional

two minutes to ensure stabilization after the larger change in supersaturation. The CPC measurements were carried out in parallel with CCN measurements. For each supersaturation level, only the last two minutes of data collected at each set point was used in analysis. CCN data collected at the highest (1.2%) and lowest (0.15%) set points throughout the duration of the ship track are included in Figure 2.7B and C, respectively.

The CCN data collected at all five set points can also be used to determine a single parameter, the critical supersaturation, S_{crit}, the supersaturation required for 50% of the particles in a population to activate. While useful for comparing the cloud-nucleating ability of aerosols in different locations, one caveat of examining critical supersaturation is that changes may occur due to changes in either aerosol size or composition. While observed reductions in S_{crit} may result from the high aerosol concentrations of surface-active components, the cause of variations in S_{crit} cannot be determined for certain.

To determine the critical supersaturation, the CCN concentrations were divided by their simultaneous aerosol concentration determined by the Grimm CPC (usually regarded as total condensation nuclei or CN concentrations) to produce a CCN/CN ratio spectrum every 27 minutes. Following the method of Rose et al. (2008), each CCN/CN ratio spectrum was fitted with a cumulative Gaussian (normal) by a distribution function using a non-linear least-squares fitting routine:

$$f_{CCN/CN} = a\left(1 + erf\left(\frac{SS - S_{crit}}{\sigma\sqrt{2}}\right)\right) \tag{2.2}$$

where *erf* is the error function (also called Gauss error function), a is the half maximum value of $f_{CCN/CN}$, S_{crit} is the supersaturation when $f_{CCN/CN}$ is equal to the half maximum value (a), and σ is

the standard deviation of the cumulative Gaussian distribution function. The operational critical supersaturation (S_{crit}) is defined as the supersaturation (SS) at which $f_{CCN/CN}$ equals 0.5, i.e., 50% particle activation. Values of S_{crit} obtained once every 27 minute CCN cycle are reported in Figure 2.7D. The average critical supersaturations of droplet activation for each segment of the ship track are shown in Table 2.1.

Spikes in aerosol concentrations along the ship track resulted in weaker increases in the concentrations of aerosols activated at 1.2% and very little increase in the concentration activated at 0.15%. This is consistent with an injection of aerosols characterized by poor or no CCN activation. Possible sources include soot particles emitted during incomplete combustion from passing ships and other anthropogenic activities which have low CCN activities (Tritscher et al., 2011). Short-term variability in concentrations is less significant in the segment-averaged concentrations. Higher concentrations of CCN activating at 1.2% or less are observed in the Tropical and Northern Open Ocean Segments than in the Southern Open Ocean. Concentrations of more effective CCN (activating at 0.15% or less) were also higher in the northern section of the Open Ocean. Interestingly, while the concentration of CCN active at 1.2% in the Southern Coast segment was 93% of the North Coast Concentration, the concentration of more effective CCN (active at 0.15%) in the Southern Coast segment was only 55%.

As seen in the table, the lowest average S_{crit}, 0.1 ± 0.3%, was observed during the Tropical Open Ocean Segment. The lowest critical supersaturation corresponds to aerosols, which require the least water vapor to activate as cloud droplets, and thus have the greatest propensity to facilitate cloud formation. The segment with the next lowest average $S_{crit,}$ 0.2 ± 1.0% was the Northern Coast Segment. While the Northern and Southern Coast Segments have comparable high aerosol concentrations, the S_{crit} observed in the Southern Coast, 1.4 ± 1.2% is

much higher. Reason for difference in observed cloud activation potential among the segments is not clear. Many factors can influence the cloud nucleation ability of aerosols even in the open ocean segments away from anthropogenic influences. In the northern hemisphere, values of S_{crit} (aerosols with reduced CCN ability) tended to increase in parallel to increased values in total aerosol concentration, an additional indication that injections of fresh aerosol which were not efficient CCN. In contrast, high S_{crit} values occur for a period of sampling centered at 30 °S, during a period of relatively low aerosol concentration. In general, most observed deviations from average conditions involved increased aerosol concentrations and higher values of S_{crit}, rather than reduced S_{crit} values which could potentially indicative of surface active species. Temporally, variations in CCN concentrations coincide with brief spikes in aerosol concentration, not with changes on the time scale of the ship's traverse through segments of differing Chl-*a*. Overall, no correlation between the presence of long chain organics and the cloud activation potential was observed in this study. This may be due in part to the fact that Raman analysis was performed primarily on particles in the larger end of the size range of those expected to activate as CCN. Given that aerosol composition may vary with aerosol size, the aerosol compositions measured here may not represent those available to act as CCN.

2.5 Conclusions and atmospheric implications

Here we successfully employed Raman microspectroscopy to determine that long chain organic compounds were consistently a major component in Pacific marine aerosol. Analysis of aerosol composition on the ~11,000 km HaloCAST cruise indicated that long chain organic species were the most common aerosol composition observed. This result corroborates previous reports of high concentrations of organics in marine aerosol, and extends previous knowledge in several significant ways. Our data include the aerosol composition, concentration and CCN-

ability in the marine boundary layer over understudied areas in the Pacific Ocean. While most previous reports have focused on organics found in submicron aerosols, our collection technique included coarse mode aerosol (>1.0 μm diameter). The percentage of particles containing pure and predominately long chain organics were 8% or more and 28% or more for all conditions in both the Northern and Southern Hemispheres. The prevalence of organics observed in samples far removed from continental anthropogenic effects strongly suggests a marine source. Also, these organic components were detected in autumn (in the Southern Hemisphere) and in spring (in the Northern hemisphere), suggesting that organics may be present throughout much of the annual cycle. While marine biological activity has commonly been considered as a source of large hydrocarbons in the atmosphere (Russell et al., 2010, O'Dowd et al., 2004), elevated levels of organics observed along the cruise track did not always occur with elevated concentrations of Chl-*a*. This lack of correlation may be due to the fact that variation in Chl-*a* was fairly subtle, and overall aerosol composition may only be sensitive to major changes in Chl-*a*. Also, transported air masses may have modified the locally generated aerosol substantially. Alternatively, the long chain organics observed may come from another source.

Water soluble inorganic species such as sulfate and nitrate were observed in higher frequency in the northern segments of the open ocean cruise track, possibly suggesting a stronger influence from anthropogenic activity in the northern hemisphere.

Despite the insensitivity of Raman to some compounds, the majority of particles collect in this Pacific cruise were classified as internally mixed. Long chain organics were found in mixtures with other compounds 57 to 72% of the time. Based on our observations, long chain organic species tended to be mixed most often with HULIS, and frequently with other organic and inorganic species.

Both the consistent prevalence of long chain organic species throughout the wide range of conditions and locations sampled during this cruise indicate that organics must be considered in modeling studies of marine aerosol. Furthermore, the variable composition and mixing states observed here suggest a need to treat marine organic aerosol in a more detailed manner for accurate modeling of the role of marine aerosols in cloud formation and climate. The complex marine aerosol composition and prevalence of organic aerosols must be considered in assessments of marine aerosol direct and indirect effects on climate.

3. CLOUD CONDENSATION NUCLEI AND AEROSOL CONCENTRATIONS UNDER EXTREMELY HIGH DMS LEVELS OVER THE NORTH ATLANTIC OCEAN

3.1 Introduction

According to the CLAW hypothesis (named after Charlson, Lovelock, Andreae, and Warren), dimethyl sulfide (DMS)-derived sulfate comprises the majority of aerosols acting as CCN in the pristine marine boundary layer (Charlson et al., 1987). Phytoplankton blooms lead to or enhance marine clouds through the emission of dimethyl sulfide (CH_3SCH_3, DMS) followed by the nucleation of new particles and their condensational growth by its oxidation products, which will serve as cloud condensation nuclei (CCN) (Liss and Lovelock, 2007). However, the extent to which algal growth and its DMS emission contribute to marine cloud formation is still under discussion, especially in light of increasing anthropogenic activities (Ayers and Cainey, 2007; Quinn and Bates, 2011). Further, marine biology may contribute to CCN production through pathways other than DMS oxidation, including direct injection of organic particulate matter from the ocean surface into the atmosphere (Leck and Bigg, 2005a, 2007).

Most studies aimed at unraveling the relationship between DMS and CCN were carried out in the Southern Oceans, where the atmosphere is less influenced by anthropogenic activities and continental sources than in the Northern Oceans (Cropp et al., 2005; Deng et al., 2013a). Air masses from continental regions differ from those stayed over the open ocean for 120 hr in their composition and concentrations, as well as their cloud nucleation abilities (Dall'Osto et al., 2010). The conversion of DMS to sulfate aerosol is influenced by anthropogenic air masses,

which provide OH and NO_x and oxidizing agents to the marine atmosphere (Stark et al., 2007). Therefore, field measurements over the Northern Oceans are needed to evaluate the combined influences of DMS and anthropogenic emissions on CCN.

Attempts to find correlations between Chl-*a* and CCN, and between DMS and CCN have led to mixed results in different oceanic regions even in the seasonally averaged data (Hegg et al., 1991; Putaud et al., 1993; Andreae et al., 1995; Vallina et al., 2006; Vallina and Simo 2007; Lana et al., 2012). Under some conditions, e.g., in the Sargasso Sea during summer, those correlations can even become significantly inversed, causing doubts about the validity of the original proposal of CLAW hypothesis (Simo and Pedros-Ali, 1999; Quinn and Bates, 2011).

DMS emitted into marine atmosphere can be oxidized to form sulfur dioxide (SO_2), dimethyl sulfoxide (DMSO), dimethyl sulfone ($DMSO_2$) and methanesulphonyl peroxynitrate (MSPN) and further into sulfuric acid (H_2SO_4) and methanesulphonic acid (MSA) which contribute to CCN (Liss et al., 1997; Arsene et al., 2005b; Barnes et al., 2006). The major oxidants are OH, halogens (Cl and BrO), and nitrate (NO_3) radicals (Chin et al., 1996; Barnes et al., 2006; Stark et al., 2007). Though there have been few experiments on the topic, DMS oxidation by O_3 in the gaseous phase is thought to be unimportant (Martinez and Herron, 1978; Stark et al., 2007). Among the three important DMS oxidants in gaseous phase, nitrate is the sole important oxidant of DMS during nighttime, while OH and halogens are the dominant oxidants during the daytime. The reasons are following. First, NO_3 is formed in the oxidation of NO_2 by O_3 during nighttime and NO_x is mostly transported from continental sources due to anthropogenic activities (Stark et al., 2007; Osthoff et al., 2009). However, Nitrate radical is photolyzed by light between 420 and 630 nm in early morning before OH radical formation (Stark et al., 2007). Second, OH is formed by reaction of water vapor with $O(^1D)$ which is in turn

produced in the photolysis of O_3 by light between 290 and 330 nm (Seinfeld and Pandis, 2006). Third, halogen species are considered to have a similar diurnal pattern to OH radical (Sander et al., 2003). It is estimated by a model study that globally DMS oxidation by nitrate radical amounts to one third of that by OH radical when assuming OH as the single daytime oxidant (Chin et al., 1996). It is then of practical importance to evaluate the relative magnitude of nitrate (nighttime) and OH (daytime) oxidations of DMS when air masses are under various influences. This is an important approach to evaluating the impact of anthropogenic activities on marine atmosphere in the contemporary era.

Sulfuric acid, one of the most important oxidation products of DMS, and water vapor, are responsible for the new particle formation in marine atmosphere, with the presence of ammonia and organics being a facilitating factor (Kulmala et al., 2004a; Kulmala and Kerminen, 2008). The nucleation of sulfuric acid and condensation of other oxidation products of DMS was once considered as the predominant source of marine CCN (Charlson et al., 1987). However, the binary nucleation of sulfuric acid and water vapor is only considered as common and realistic in the upper troposphere (UT) where DMS are transported upwards, which in turn will be transported back to the underlying marine boundary layer (MBL) to serve as cloud condensation nuclei, being accompanied with condensational growth by sulfuric acid and other DMS oxidation products (Korhonen et al., 2008; Kulmala and Kerminen, 2008). For MBL nucleation to happen DMS level has to be over 400 pptv and the total aerosol surface (available condensational sites) has to be very small (Pirjola et al., 2000). Since nucleation tends to happen in marine UT, nanometer-sized particle (nucleation mode, 3-25 nm) number concentrations are significantly (orders of magnitude) higher there than in MBL (Clarke 1993; Raes 1995; Clarke et al., 1997). Therefore, entrainment of air masses from UT could be the predominant process governing the total particle concentration in MBL (Katoshevski et al., 1999). The net

entrainment from UT to MBL will signify a particle concentration enhancement in MBL, and vice versa. In brief, except the influence of different air masses with varying origins, meteorological parameters like pressure signifying the vertical transport of air masses are also significant in modification of the nucleation mode aerosol concentration.

In addition to sulfate aerosol derived from DMS, particles composed of sea salt and organics also need to be considered as the possible sources of CCN in marine boundary layer (Andreae and Crutzen, 1997; Leck and Bigg, 2008). Microgels originated from the sea surface microlayer (SML) may also be important primary source of marine aerosol and CCN (Ovadnevaite et al., 2011b; Orellana et al., 2011; Verdugo 2012; Cunliffe 2013). Alternatively, a new mechanism in which marine microgels arrive in the atmosphere from evaporating fog and cloud water is supported by recent observations in the polar marine boundary (Orellana et al., 2011; Karl et al., 2012, 2013).

This cruise aboard the R/V *Knorr* over the North Atlantic during June - July 2011 was intended to pursue phytoplankton blooms signified by elevated chlorophyll *a* (Chl-*a*) concentrations to evaluate the linkage between marine biota and CCN concentrations for pristine marine air and polluted conditions. The ship passed through a wide range of conditions, including areas of high phytoplankton biomasses and extremely high DMS levels (over 1800 pptv). To the best of our knowledge, in situ CCN measurements have never been collected in DMS conditions as high as these. Coincident aerosol, CCN and DMS data will used to evaluate the contributions of ocean biology, specifically DMS oxidation, on aerosol concentration and cloud nucleating ability in the present and absence of anthropogenic influence.

3.2 Experimental section

3.2.1 Observations

This study, referred to as "Bloomcruise", was a three-week cruise from June 23rd to July 17th, 2011 aboard the R/V *Knorr*. The ship track spanned the area of 40°N to 60°N and 70°W to 35°W, as shown in Figure 3.1. The general goal of Bloomcruise was to characterize surface water, and the marine boundary layer, and fluxes between them and in zones of phytoplankton blooms, typically defined by elevated Chl-*a* concentrations relative to their surrounding surface seawater. Chl-*a* concentrations measured by shipboard fluorometer are also plotted along the cruise track. The ship stopped every two days to collect 24 hours or more of data at a fixed station, and to carry out multiple CTD (conductivity, temperature and depth) measurements. The stations are marked in Figure 3.1. In addition to the long stations, numerous half-hour stops were allowed every several hours for a CTD measurement in each stop. CCN and DMS (seawater and atmospheric) concentration measurements were carried out simultaneously.

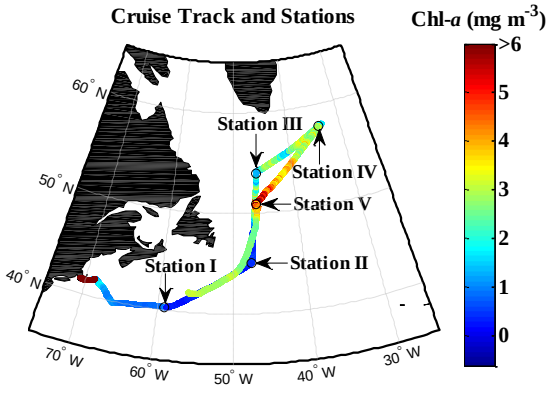

Figure 3.1 Cruise track of the Bloomcruise indicated by *in-situ* fluorometer-retrieved chlorophyll *a* concentration and long duration (≥ 1 day) stations. The truncation of data in the returning trip is due to the restriction of data publication.

A CCN counter (Droplet Measurement Technologies) was used to measure CCN concentration. A condensation particle counter (or CPC) from Grimm Technologies was used to count total particles between 4.5 nm and 3 μm, which we regard as CN (condensation nuclei) concentration. A portable aerosol spectrometer (PAS) from Grimm Technologies was used to measure particle size distribution from 0.3 μm to 20 μm. CCN and aerosol concentration measurement were carried out by sampling through an inlet (15 m above sea level) extending 3.5 meters over the lab van situated on the bow of the ship, constantly facing the incoming wind (Deng et al., 2013a). The sample flow passed through a heater and two dryers (a Nafion® dryer and a desiccant dryer) in order to maintain relative humidity (RH) below 50% throughout the project, to a suite of instruments shown in Figure 3.2. Beyond the desiccant dryer, the flow was distributed among samplings by the CCN counter, CPC and the PAS instruments. A cyclone impactor in front of the CCN and CN was installed to remove particles larger than 1.5 μm in aerodynamic diameter. The ship's exhaust stack was located behind the laboratory van and the sampling inlet. Therefore, all data collected when wind was from behind (the relative wind direction from 90° to 270°) were eliminated to preclude potential contamination from the ship stack (Deng et al, 2013a; Shank et al., 2012). CCN concentrations were measured at a series of five supersaturation levels. The five supersaturation (SS) levels of 1.2%, 0.9%, 0.5%, 0.25% and 0.15% were allowed 7min, 5min, 5min, 5min and 5min respectively in a single cycle, dividing the whole cruise as a series of 27-min cycles in terms of CCN measurements.

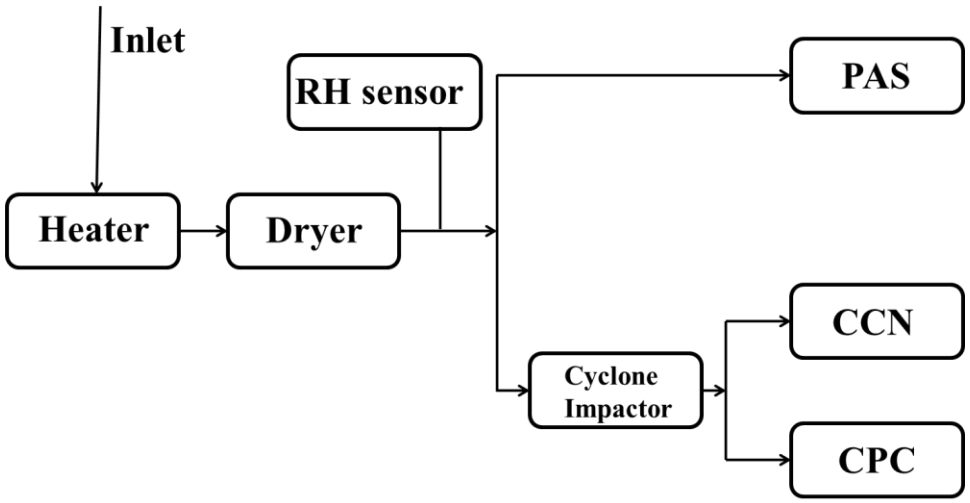

Figure 3.2 Schematic of particulate phase measurements.

Since the CCN counter takes a few minutes to stabilize after switching to a new SS level, only data collected in the last two minutes at each SS level were used to determine the average CCN concentration value at that level during a 27 min cycle. Aerosol concentrations reported for each cycle are the averages of the 10 min data, concurrent with the discontinuous CCN data at five SS levels. In each cycle, five CCN/CN ratios (also called CCN activation ratios) can then be calculated for five SS levels.

3.2.2 Critical supersaturation calibration

Calibration of CCN and CN instruments were performed both before and after the cruise research using 0.01% $(NH_4)_2SO_4$ (ammonium sulfate, or AS) solution (Baumgardner et al., 2001) to generate aerosol particles which will be size-selected by a dynamic mobility analyzer (DMA) to supply AS aerosol with mono-disperse size distribution. Experimental setup in calibration was similar to that shown in Figure 3.2 except that the inlet was connected to the aerosol generation apparatus and cyclone impactor is replaced by a DMA. Singly sized particles selected by DMA were directed to the CCN counter and CPC in parallel. CCN measurement was cycled in the five

SS levels and an activation spectrum (CCN/CN ratio) can be plotted against the SS levels for each dry particle size, as shown in Figure 3.3. The CCN activation data collected at all five SS points can also be used to determine a single parameter, the critical supersaturation, S_{crit}, the supersaturation required for 50% of the particles in a population to activate into CCN. Each activation spectrum can be fitted with an accumulated Gaussian curve based on the least-squares fitting principle. On each curve, the SS at which the activation ratio equals 0.5 is the critical SS required for particle population to activate and grow to cloud droplets. The critical SS (S_{crit}) values for each particle size were plotted against the corresponding dry sizes. The smaller the S_{crit} is, the more effective the aerosols are as cloud condensation nuclei.

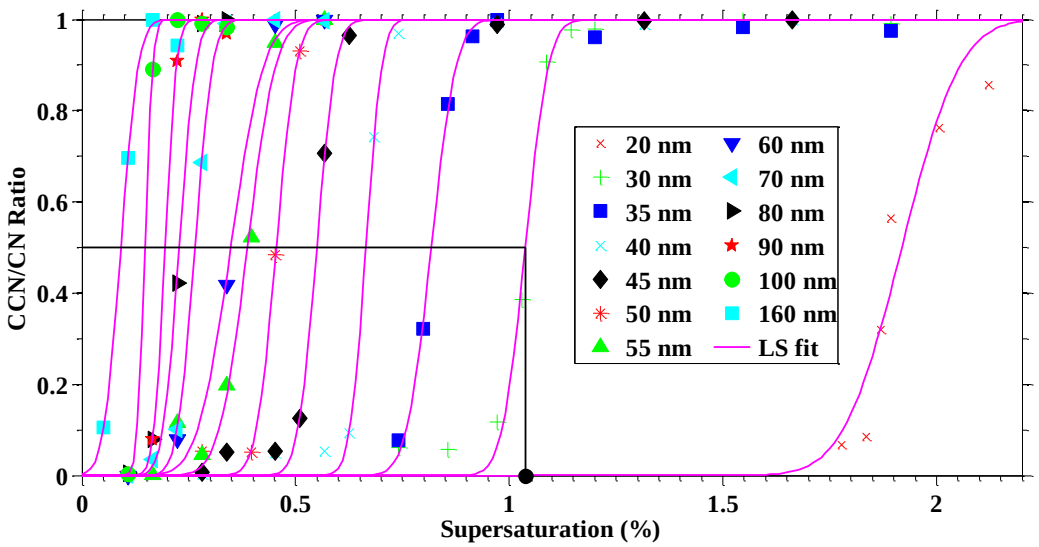

Figure 3.3 Calibration of CCN and CN instrument measurements using $(NH_4)_2SO_4$ with different dry particle sizes. Activation ratios of different sizes with varying supersaturation (SS) levels and their least-squares (LS) fitted activation spectrum are shown together. The black lines show an example of critical SS is determined. The critical SS for 30 nm aerosol is marked by the black dot.

For an activation spectrum of ambient air sample measured at five SS levels (1.2, 0.9, 0.5, 0.25, and 0.15%) the scattered points can be fitted similarly with an accumulated Gaussian curve. While useful for comparing the cloud nucleation ability of aerosols in different locations, one caveat of examining critical supersaturation of ambient particle populations is that changes may occur due to changes in either size or composition. While observed reductions in S_{crit} may result from the high aerosol concentrations of surface-active components, the cause of variations in S_{crit} cannot be determined for certain. For the data impossible to fit into an accumulated curve when there is a point of inflection in the curve, the S_{crit} is not pursued. Otherwise, one S_{crit} is obtainable for each 27 min CCN cycle unless the data is rejected due to ship stack contamination possibility. This operational S_{crit} differs from theoretical critical supersaturation (s_c) in that s_c describes the SS level required for a 50% activation of dry particles with a certain size, e.g. 50 nm dry ammonium sulfate aerosol with a s_c of about 0.65% based on Köhler theory (Seinfeld and Pandis, 2006). The operational S_{crit} is used to denote the cloud nucleation ability of mixed size particles measured during an interval (27 min for this research).

3.2.3 DMS measurement

Atmospheric pressure chemical ionization mass spectrometry (API-CIMS) was used to measure DMS concentrations, following the method of Marandino et al. (2007). Water samples were pumped from a depth of 5 m below sea surface and atmospheric samples are sucked from a few meters above sea surface DMS concentrations in the surface seawater and atmosphere were measured every 5 and 10 minutes, respectively. DMS data is included here to lend context to the aerosol and CCN measurements by providing a quantitative characterization of ocean biology during atmospheric measurements.

3.2.4 Supporting measurements

Shipboard measurement from meteorological sensors on different positions of the ships (main mast, forward mast port side and starboard side) were carried out continuously and data were recorded every minute. These parameters include air temperature (three sensors), barometric pressure (three sensors), shortwave irradiance (one sensor), rain intensity (two sensors) and rain accumulation (two sensors), wind speed and direction (three sensors). The values from different sensors were averaged for each meteorological parameter in the Bloomcuise cruise for use. The navigation direction and speed of the ship were also logged to derive the true wind direction and speed based on the measured relative wind direction and speed. Sea surface temperature (two sensors) and salinity (two sensors) of seawater were measured by sensors located in the bow chamber outboard of the surface water pump. A fluorometer sensor was aboard the research vessel. The reading was used to derive Chl-*a* concentration along the cruise track. However, the Chl-*a* concentration maps used to decide the navigation direction in the pursuit of phytoplankton blooms are retrieved form MODIS (or Moderate Resolution Imaging Spectroradiometer) satellite data, which were downloaded from Giovanni data system (http://daac.gsfc.nasa.gov) developed and maintained by the NASA GES–DISC (Goddard Earth Sciences Data and Information Services Center).

3.2.5 HYSPLIT back trajectories

Using the HYSPLIT back trajectory retrievals were carried out for every hour along the cruise track using (Draxler and Rolph, 2013). GDAS (global data assimilation system) data was used for meteorology input data. Vertical velocity was modeled based on meteorological data. 500m, 200m and 10m were chosen as the three starting point elevations. The total run time was set to be 48 hours for every back trajectory. The back trajectories were used to classify all air

mass origins into one of three scenarios: those had passed through continent in the previous 48 hours, those influenced by North American or Greenland coastal atmosphere in the preceding 48 hours, and those were completely in the open hour in the past 48 hours, as shown in Figure 3.4.

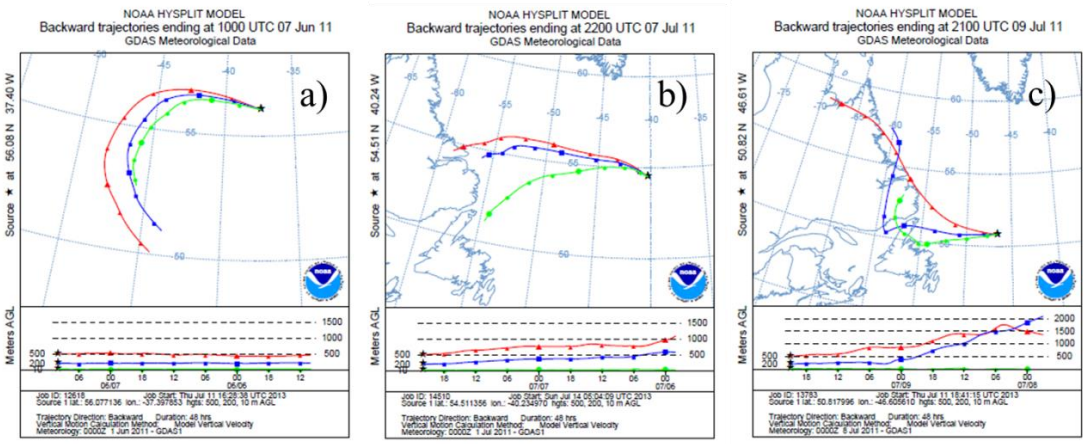

Figure 3.4 Examples of 48-hr back trajectories. Red, green and blue colors are for starting point at 500 m, 200 m and 10 m above sea level respectively. Panel a) shows an example of air masses completely over the open ocean in the previous 48 hours; panel b) shows an example of air masses ever influenced by coastal air in the past 48 hours; and panel c) shows an example for air masses passed through the continent in the preceding 48 hours.

3.3 Results and discussion

3.3.1 Overview of measurement results

The time series of aerosol (CN) concentration and CCN concentrations at each of the five supersaturation settings observed throughout the cruise are shown in Figure 3.5a. Particle size distribution (15 bins in 0.3 to 20 micron) was also recorded every 6 s during the cruise, as detailed in Deng et al. (2013b, in preparation). Among the five CCN concentrations, the ones at

0.15% and 0.25% have a practical importance because they are in the range of the SS levels most commonly achievable in marine stratocumulus clouds and stratiform clouds (Katoshevski et al., 1999; Russell et al., 1999). The highest SS of 1.2% exemplifies an upper limit of meaningful CCN at an achievable SS level in marine atmosphere while the other two (0.5% and 0.9%) are less frequent but achievable SS levels in marine atmosphere. The colored lines in the top of Figure 3.5a delineate the classification of the air mass sampled at that time, according to the HYSPLIT 48-hr back trajectories described above. To inspect the possible connection between aerosol concentration and cloud nucleation ability, DMS concentration in the atmosphere and in the surface ocean waters, and Chl-*a* are plotted in Figure 3.5B and 5C, respectively. For reference, periods during which the vessel was anchored at a station location for one day or longer are marked in 5B and atmospheric pressure is included in 5C.

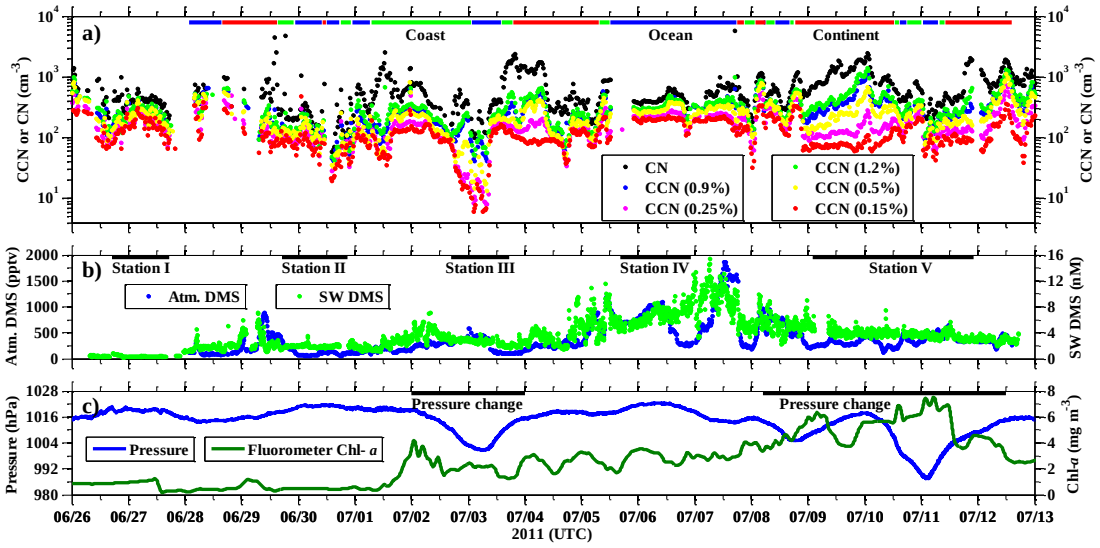

Figure 3.5 Time series presentation of measurements during the cruise research with time aligned with each other. Panel a) shows the variation of CN concentration and CCN concentration at five different supersaturation levels. Bold lines with blue, green and red colors in this panel show segments when their air masses passed through the open ocean, coast, and continent in the past 48 hours respectively. The three segments which are marked with "Ocean", "Coast", and "Continent" are three special cases with longest continuous duration for each category; Panel b) shows variation of DMS concentration in both atmosphere and seawater. Stations marked by bold black lines and marked with segment numbers are the periods with no spatial variation; Panel c) shows fluorometer measured chlorophyll a concentration ship-board barometric reading. The two segments delineated with bold black line and marked underneath with "Pressure change" are the phases with apparent sea surface pressure change.

The raw data in Figure 3.5 illustrates the combined and at times opposing influences of continental air mass, ocean biology, and meteorological conditions on aerosol concentration and characteristics. Each of these influences is discussed in greater detail in the sections that follow. We first discuss the general trends made clear by 5A. Air masses passed over continental regions had the highest aerosol concentrations, followed by coastal and open ocean segments. Secondly, the continental air mass produced aerosols with lower cloud nucleating ability. Under

continental influence, there is a wide spread in the CCN concentration depending on the supersaturation set point. In general, variations in concentration of aerosols and CCN at the three highest SS levels (0.5 to 1.2% SS) follow the trend of sea surface pressure for air masses under continental influence. However, concentrations of CCN at lower SS (0.15%) are on average 74% lower than those at 1.2% for continental air mass, while the CCN (0.15%) for coastal and open ocean air masses are only 57% and 48% lower than their CCN (1.2%), respectively. Although there are more aerosols present under continental conditions, if the ambient supersaturation is low, the number of aerosols activating as CCN may be even lower than those in unpolluted air masses. For example, in the "Ocean" segment, while the aerosol concentration is on average 40% lower than the average in the "Continental" segment prior to it, the concentration of those aerosols activating as CCN at 0.15% SS is 70% higher.

Within the "Ocean" segment, variations do occur, including two peaks at the middle between July 6th and July 7th and the middle between July 7th and July 8th in which aerosol concentration rose by 50% and 13 folds separately, and a trough just before July 7th in which aerosol concentration plummeted to 70% of the average. The CCN concentrations behaved similarly as aerosol concentration in this segment, with a variable enhancement factor of 64% to 84% at the first peak and 1.6 to 2.7 folds at the second peak, and a drop of 22% to 29% at the trough, for the five SS levels. A similar trend was observable in the variation of atmospheric DMS concentration, with the first peak of DMS (120% increases) a few hours earlier than the first peak of aerosol and CCN, but the second peak (220% increases) and the trough (45% decrease) happened at similar times. The observations suggest a possible link between aerosol concentration and atmospheric DMS. The peaks and troughs of seawater (SW) DMS concentration are less visible during this segment and therefore the link between aerosol and SW DMS is believed to be weaker. Overall, in the "Ocean" segment aerosol and CCN concentrations

are consistently high and less variable than any other segments (verifiable from the standard deviations in Table 3.1) when DMS concentration is significantly elevated, possibly due to the abundance of condensable vapors when DMS concentration is extremely high.

Table 3.1 Summary of CN and CCN concentrations influenced by three different scenarios of air masses. The concentrations during the special "Ocean" segment which is the longest continuous period of open ocean air mass are shown in the last column. The bottom row shows the approximate average sizes in each segment by assuming ammonium sulfate (AS) particles. All values are shown in arithmetic mean ± 1 δ (one standard deviation).

Time segments	Aerosol of all air masses	Aerosol of open ocean air mass	Aerosol of coastal air mass	Aerosol of continental air mass	"Ocean" segment
	CN, in unit of cm^{-3}, corresponding to AS particles with diameter > 4.5 nm				
Day and night	708±560	445±421	639±517	956±575	580±597
Night only	543±567	364±177	584±218	933±484	407±55
Day only	492±589	493±509	647±547	966±608	615±649
	CN (1.2%), in unit of cm^{-3}, corresponding to AS particles with diameter > 26 nm				
Day and night	329±208	269±130	263±122	422±262	356±92
Night only	221±166	224±108	281±87	440±262	305±26
Day only	232±238	297±135	261±127	414±263	370±99
	CN (0.9%), in unit of cm^{-3}, corresponding to AS particles with diameter > 32 nm				
Day and night	293±182	255±125	233±113	364±229	340±70
Night only	199±150	208±104	255±82	383±226	296±24
Day only	205±210	285±129	230±117	356±230	353±74
	CN (0.5%), in unit of cm^{-3}, corresponding to AS particles with diameter > 48 nm				
Day and night	231±145	216±110	189±111	273±178	290±53
Night only	159±126	180±108	199±78	296±179	261±15
Day only	161±167	238±105	188±115	263±177	297±56

Table 3.1 Continued

Time segments	Aerosol of all air masses	Aerosol of open ocean air mass	Aerosol of coastal air mass	Aerosol of continental air mass	"Ocean" segment
	CN (0.25%), in unit of cm^{-3}, corresponding to AS particles with diameter > 75 nm				
Day and night	163±97	166±87	145±82	173±111	221±36
Night only	116±92	139±91	155±72	174±102	215±14
Day only	115±114	182±81	143±84	172±115	222±39
	CN (0.15%), in unit of cm^{-3}, corresponding to AS particles with diameter > 105 nm				
Day and night	122±70	139±78	114±61	113±66	192±27
Night only	89±73	119±85	118±54	109±66	194±10
Day only	86±82	153±70	113±62	115±66	192±31
Avg. size	nm	nm	nm	nm	nm
Day and night	58±48	85±54	57±50	50±50	88±27
Night only	55±46	88±110	64±69	51±57	115±60
Day only	59±51	84±45	56±42	49±49	84±27

Note: Values are calculated based on various amounts of 27 min cycles. Calculation of average size is achieved by assuming all particles are composed of ammonium sulfate (AS). Particles with the differential concentrations of CN and CCN (1.2%), of CCN (1.2%) and CCN (0.9%), of CCN (0.9%) and CCN (0.5%), of CCN (0.5) and CCN (0.25%), as well as of CCN (0.25%) and CCN (0.15%) are assumed to have an average size of 15 nm, 30 nm, 40 nm, 60 nm, and 90 nm respectively. Particles detected as CCN (0.15%) are assumed to have an average size of 200 nm. Standard deviation of average sizes is calculated from the standard deviation of differential concentrations.

It should be noted that changes in aerosol concentration and cloud nucleating abilities coincide with variations in DMS emission, rather than changes in Chl-*a*. For open ocean air mass, The correlations of atmospheric DMS with the aerosol (CN) and CCN concentrations are presented are presented in the supplementary material, Figure 3.11, while those of surface seawater DMS concentration and the sea-to-air flux with CN and CCNs are also shown in supplementary material, Figure 3.12 and Figure 3.13, respectively. Comparatively, the correlations of fluorometer-measured and satellite-retrieved Chl-*a* concentration with CN and

CCNs are presented in Figure 3.14 and 3.16, respectively. Comparing the results of Figures 3.11-3.14, it is clear that the correlations between DMS and particles are visible while those between Chl-*a* and particles are not. In Figure 3.15, the correlations of both MODIS-retrieved (satellite) and fluorometer-retrieved (Ship) Chl-*a* with atmospheric and seawater DMS concentrations are presented. It is obvious that the correlations of fluorometer Chl-*a* with both DMS concentrations are better than those of satellite Chl-*a* (as also shown in Figure 3.16 that there is even negative correlation between Chl-*a* and CCN), indicated the issue of poor resolution inherent in satellite data retrieval. The visible correlation in Figure 3.11-3.13 and 3.15 are generally consistent with the CLAW hypothesis that nonlinear processes involved in both the reflection of DMS in response to primary production (Chl-*a*) changes and the reflection of CCN in response to DMS changes (Charlson et al., 1987; Andreae et al., 1995; Andreae and Crutzen, 1997;). Therefore, the absence of correlation as shown in Figure 3.14 reflected that the additive effects of multiple nonlinear processes may result in an invisible causal relationship between the start-up factor (enhanced phytoplankton growth) and the end result (CCN increase), if evaluated locally (Quinn and Bates, 2011).

Additional parameters are presented in Figure 3.6. From the plot, we can see that no measurements showed apparent diurnal cycles except the short wave irradiance. Not any two variables showed a similar time-series pattern either. Comparing the variations in Figure 3.5 and 3.6, we can notice that CN and CCN concentrations seem to be insensitive to the extremely heavy precipitation events during station I, corroborating with the previous finding that the horizontal mixing after precipitation is very fast after the wet deposition of submicron particles (Clarke et al., 1997; Katoshevski et al., 1999). Concentrations of large particles were also increased during precipitation events. The possibility of overcounting some large drops entering the sampling system during rain period cannot be rule out. Also during the “Continent” segment

CN and CCN concentrations are mostly correlated inversely with wind speed since pressure and wind speed are generally negatively correlated.

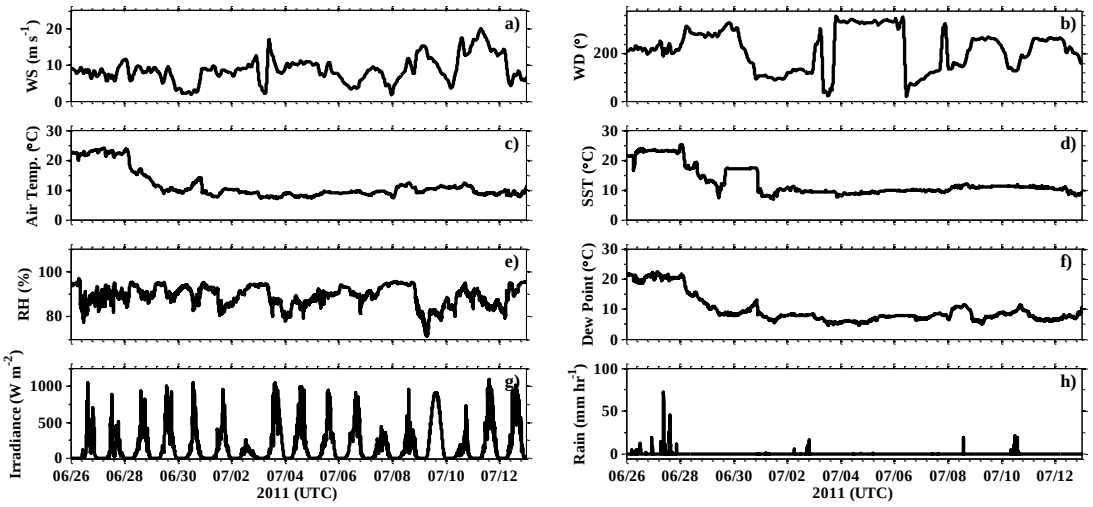

Figure 3.6 Overview of meteorological parameters during the cruise with the same time axes of the previous plot. "WS" stands for true wind speed calculated from measured relative wind speed and navigation speed; "WD" means true wind direction corrected from relative wind direction and navigation direction; "SST" represents sea surface temperature; "RH" is relative humidity in percent; Dew point is calculated based on relative humidity and air temperature.

3.3.2 Comparison of CCNs and CN influenced by different air masses

To further evaluate the cloud nucleation abilities of aerosols influenced by the open ocean, coastal and continental air mass, the average CCN/CN ratios at the five SS levels for the three air mass scenarios are plotted in Figure 3.7a. For comparison, ammonium sulfate calibration data is also plotted. Specific numbers of aerosol and CCN concentrations under different air mass scenarios are presented in Table 3.1. Averagely, the number concentrations of aerosols influenced by continental air mass which activate at SS levels ranging from 0.15% to

1.2% are 92.8% to 128.3% compared to the whole cruise. Similarly, those by coastal air mass and open ocean air mass range from 93.4% to 79.4% and from 114.3% to -81.7%, respectively. Based on the segment distinction in Figure 3.5a marked by colored bold lines, periods in which the influences of continental air mass on marine aerosol are widespread but highly variable and unpredictable. Aerosol influenced by continental air mass will have lower activation ratios (for all five SS levels) than those by coastal air mass, which are in turn have lower activations than that only influenced by pristine ocean air. By comparing the measured activation ratios with the activation curves of ammonium sulfate with different sizes, it is clear that the aerosol influenced by oceanic air masses has a larger effective average size than that influenced by coastal air mass, which is in turn larger than that influenced by continental air mass. This finding probably shows that more foreign aerosols will compete with the pristine marine aerosols (e.g. newly formed particles) for condensational vapors in growth. In addition, the invasion of more nonhygroscopic particles (such as black carbon) from the transported continental or coastal sources will decrease the cloud nucleation ability of marine aerosol.

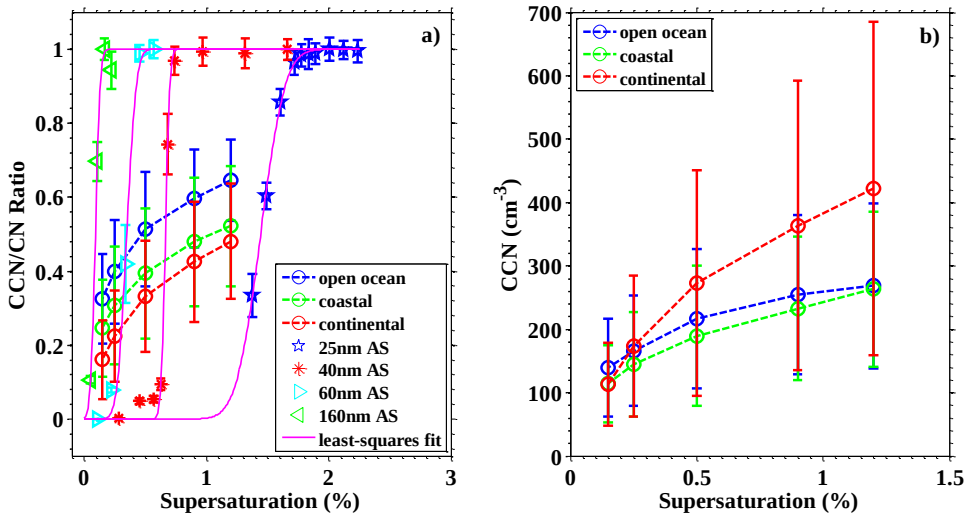

Figure 3.7 Spectrum of average activation ratios (a) and CCN concentrations (b) of aerosols at five supersaturation levels under the influence of three different air masses. Together shown in (a) are the activation curves of ammonium sulfate aerosols with different dry particle sizes and their fitted curves.

In addition to CCN/CN ratio, the CCN absolute concentration is also important in quantifying cloud formation potential of aerosol, which is compared for three different air masses in Figure 3.7b. Similar with the comparison for the single "Ocean" segment, all the segments influenced only by open ocean air mass has lower CCN than continental air mass when SS is equal or larger than 0.5%. The CCN concentration at SS 0.15% is higher for all open ocean air mass segments than all continental air mass segments, while their CCNs at SS 0.25% are similar. The CCNs for all coastal air mass segments are lower than or similar to the other two at all five SS levels. The orders of CCN concentrations in the three air mass scenarios are different from those of the CCN/CN activation ratios. However, it verified with the results that cloud formation potential at the lowest measured SS (0.15%) is the highest for open ocean air mass segments, which is the SS for common marine clouds. Therefore, continental air mass has a

potential to depress cloud activation of marine atmosphere even though they enhance total aerosol concentration.

Both the trends of CCN/CN ratios and CCN concentrations are similar to those of Northeast Atlantic aerosols in a field measurement carried out in Mace Head in 2008 (Dall'Osto et al., 2010). The Mace Head measurement also showed an increasing CCN concentration and a decreasing CCN activation ratio with the increasing of air mass pollution levels. However, the absolute CCN concentrations at the same or similar SS levels in the Mace Head measurement (as high as 1600 cm^{-3} for continental air mass) are much higher than this study, even though the activation ratios of both studies are close. The reason of the difference in CCN concentration is that the pollution in the Mace Head project is mainly from European continents while the pollution in this study is mainly from the Greenland and North Canadian continents, guaranteeing a much higher background aerosol and oxidants levels for the Mace Head project.

To compare the links among Chl-*a*, DMS, and CCN concentrations for different air mass influences, the correlations of atmospheric DMS, seawater DMS, and sea-to-air DMS flux with aerosol (CN) and CCN concentrations are presented in Table 3.3-3.5 respectively. It is obvious from the results that the correlations between DMS and CCN for the open ocean air mass are larger than those for coastal air mass, which is in turn larger than those for the continental air mass. This shows that the influence of continental and coastal air masses can weaken the response of CCN to DMS change in situ in a short period of time (half an hour). This also implies that the validating of CLAW hypothesis in an ever-increasingly polluted atmosphere becomes more difficult and requires more sophisticated measurement (Doraiswamy and Hogrefe, 2009).

In addition to differentiating aerosol and CCN concentrations between different air mass influences, differentiation between daytime and nighttime within each segment was also summarized in Table 3.1 to verify with the coming calculation of DMS oxidation rate. For instance, without differentiating between day and night, the CN concentration has an enhancement of 115% and 44% for continental and coastal air masses compared to open ocean air mass, respectively. If differentiating between night and day, the enhancements are 156% and 60% for continental and coastal air masses respectively during nighttime, and are 96% and 31% respectively during daytime. Comparatively, without differentiating day and night, continental and coastal air masses decrease CCN by 18% and 19% respectively compared to open ocean air mass at the SS level of 0.15%, which is a typical SS level of marine stratiform clouds. However, the relative CCN concentration at that level in nighttime to that in daytime is about 77% for open ocean air mass and the day and night CCNs are similar for the coastal and continental air masses. This may have to do with the increased amount of oxidant during nighttime under the influence of coastal and continental air masses, as will also discussed in the following section.

3.3.3 Oxidation of DMS in the atmosphere

There have been numerous laboratory and theoretical investigations of the mechanism for gas phase DMS oxidation, establishing OH and NO_3 as the main oxidants and leading to various products (Barnes et al., 2006; Stark et al., 2007 and references therein). In the marine atmosphere, DMS is mainly oxidized by OH and halogens (Cl atoms and BrO radicals) during daytime and NO_3 (nitrate) radicals during nighttime in the gaseous phase (Stark et al., 2007). The mechanisms responsible for atmospheric DMS oxidation during daytime and that during nighttime are almost mutually exclusive (Stark et al., 2007; Osthoff et al., 2009). During the day, OH is resultant from the photolysis of O_3, which will generate $O(^1D)$ to react with water vapors

as shown in the following reactions (Vaughan et al, 2012).

$O_3 + h\nu$ (< 340 nm) --> $O(^1D) + O_2$ R(3.1)

$O(^1D) + H_2O$ --> 2OH R(3.2)

Ozone could come from polluted air masses and local ship traffic (Dibb et al., 2004; Eyring et al., 2010) through photochemical reactions and can be entrained from the ozone-rich stratosphere (Ayers et al., 1992; Parrish et al., 2009). Another category of daytime oxidants, halogens, have a marine origin (Oum et al., 1998; Knipping et al., 2000; Saiz-Lopez et al., 2004; Breider et al., 2010). Comparatively, nitrate radicals, the nighttime oxidant, are evolved from NO_x in MBL which are mainly from anthropogenic origins over the North Atlantic (Jacob et al., 1996; Heard et al., 2006). Therefore, high nighttime oxidation rate is a clean sign of anthropogenic influence on DMS oxidation. Further, by comparing the oxidation rates during daytime and nighttime, it is possible to estimate the lower limit contribution of anthropogenic influence on total DMS oxidation (This is a lower limit since daytime oxidation occurs by both marine and anthropogenic oxidants). In addition, comparing the measured aerosol and CCN concentrations may provide insight in the relationship between DMS and cloud nucleation ability of aerosols.

Stark et al. (2007) measured NO_3 and DMS concentrations during a cruise research in the New England Coast. Assuming a constant DMS sea-to-air flux, it was found that 65%-90% DMS oxidation was due to NO_3. Later on in a study over the same region, Osthoff et al. (2009) showed that nitrate oxidation rates during nighttime were higher and more variable than OH oxidation rates. Both studies assumed a constantly low marine atmospheric boundary layer (MBL) height of 100 m. Even though multiple assumptions seriously undermined the accuracy

of their results, the analyses in their papers have effectively demonstrated the importance of NO_3 in DMS oxidation in marine atmosphere.

Adopting a mass balance approach, the variation of DMS concentration and its oxidation can be expressed as follows (Katoshevski et al., 1999):

$$\frac{d(DMS)}{dt} = \frac{F_{DMS}}{H} - k_{OH,Cl}[OH][DMS] - k_{NO_3}[NO_3][DMS] + \frac{v_e}{H}([DMS]_{FT} - [DMS]) \quad (3.1)$$

where *[DMS]* and $[DMS]_{FT}$ are atmospheric DMS concentration in MBL and FT respectively, *H* is the height of MBL. $k_{OH,\,Cl}$ is the effective reaction coefficient of OH (+ halogen) and DMS. To obtain this coefficient, Cl concentration is assumed to be linearly proportional to that of OH (Stark et al., 2007). k_{NO_3} is the effective reaction coefficient between NO_3 and DMS, and v_e is the entrainment velocity. The fourth term demonstrates the exchange of air masses between MBL and FT. Note that air mass entrainment in the MBL from the FT is usually accompanied by the same amount of air mass flowing in the opposite direction (Katoshevski et al., 1999).

Since oxidation of DMS during daytime and that during nighttime are mutually exclusive. In addition, DMS concentration in FT is usually much lower than that in MBL (Ferek et al., 1986). Therefore, the equation can be rewritten as follows:

$$\frac{d[DMS]}{dt} = \frac{F_{DMS}}{H} - \frac{v_e}{H}[DMS] - k_{oxi}[oxidants][DMS] \quad (3.2)$$

where *[oxidants]* stands for OH and halogen radical (mainly Cl) concentration during daytime, and represents NO_3 concentration alone during nighttime. The reaction coefficient k_{oxi} changes accordingly. *H* is the MBL height.

The sea-to-air flux of DMS can be calculated based on Liss and Merlivat (1986) mechanism:

$$F_{DMS} = k_w([DMS]_w - \frac{[DMS]}{\alpha}) \quad (3.3)$$

where k_w (cm hr^{-1}) is the overall transfer velocity, $[DMS]_w$ is the measured bulk water DMS concentration, and α is the dimensionless solubility based on Henry's law. The second term in the parenthesis is usually much smaller than the first term and can be dropped during the calculation.

Schmidt number (S_{ch}), a measure of the ratio of momentum diffusivity (viscosity) and mass diffusivity, can be approximated practically as follows (Saltzman et al., 1993):

$$S_{ch} = 2674.0 - 147.12t + 3.726t^2 - 0.038t^3 \quad (3.4)$$

where t is the atmospheric temperature in °C.

The transfer velocity at Schmidt number 660 can be calculated based on the following scheme (Goddijn-Murphy et al., 2012):

$$k_{W,660} = 2.3U_{10} - 4 \quad (3.5)$$

where U_{10} is the wind speed at 10 m above sea level, which is represented by the shipboard measurement of true wind speed (the height of wind sensors is very close to 10 m and the correction required is very small). Next, the actual overall transfer velocity can be related with the transfer velocity at Schmidt number of 660 by the following relationship:

$$\frac{k_w}{k_{w,660}} = (\frac{660}{S_{ch}})^{1/2} \quad (3.6)$$

where S_{ch} is Schmidt number, k_w and $k_{w,\,660}$ are actual transfer velocity and transfer velocity at Schmidt number of 660 respectively.

During Bloomcruise, DMS concentration in atmosphere and seawater were measured at 10 min and 5 min intervals, respectively. Wind speed and air temperature were recorded every minute. Therefore the time-series oxidation rates of DMS every 10 min can be calculated by combining equation (3.3 – 3.6) and omit negligible terms in equation (3.4):

$$\frac{d[DMS]_{oxi}}{dt} = k_{oxi}[oxidants][DMS] =$$

$$(2.3U_{10} - 4)\left(\frac{660}{2674.0 - 147.12t + 3.726t^2 - 0.038t^3}\right)^{\frac{1}{2}}\frac{[DMS]_w}{H} - \frac{v_e}{H}[DMS] - \frac{d[DMS]}{dt} \quad (3.7)$$

Kritz (1983) obtained an entrainment velocity of 0.3-0.4 cm s^{-1}. Boers and Betts (1988) reported a velocity of 1 cm s^{-1} in a stratus cloud capped situation. Raes et al. (1995) reported that a range of 0.3-0.6 cm s^{-1} is proper for both clear and cloudy situations in their own study. Stark et al. (2007) adopted a value of 0.25 cm s^{-1} for their model calculation. Osthoff et al. (2009) evaluated 0.4 cm s^{-1} as the best value for their study. Here, we set an entrainment velocity constant in each day proportional to the maximum short wave radiation in each day (a coarse indicator of cloudiness, reversely) measured aboard the cruise vessel. Daily values throughout the cruise were within the range of 0.3-0.6 cm s^{-1}, inversely.

MBL height (*H*) was not measured in this study. Following the work of Stark et al. (2007) and Osthoff et al. (2009), we chose a MBL of 100 m.

The average oxidation rates during different segments are presented in Table 3.2, together shown are the ratios of nighttime to daytime oxidation rates. Overall, the average

oxidation rate of DMS during nighttime is 85% of that during daytime. The ratios during Station II, III, and IV are smaller than that of the cruise average, from 0.26 to 0.57, whereas the ratio during Station V is almost equal to unity. The lowest oxidation rate during Station II, 39 pptv hr^{-1}, is much smaller than any other segments. This is apparently related to the low DMS flux resulting from low wind speed in this segment. Comparing the results in Table 3.2 and Figure 3.5b, magnitudes of oxidations rates during various segments are not proportional to the absolute atmospheric DMS concentrations, but to the differences between flux and concentration variation. Considering the three cases ("Ocean", "Coast" and "Continent"), the ratio of DMS nighttime to daytime oxidation is larger for the continental air mass than coastal air mass, which in turn is larger than the open ocean air mass. That result is consistent with previous reports in that air masses more influenced by continental sources contain more NO_x pollution (Stark et al., 2007; Osthoff et al., 2009). However, this result is also unique because here direct DMS measurements and back trajectories are used to arrive at this conclusion.

Table 3.2 Average oxidation rate of DMS during nighttime to that during daytime and the ratio between the two over different periods (four stations and three cases).

Oxidation	Overall	Station II	Station III	Station IV	Station V	"Ocean"	"Coast"	"Continent"
Unit: pptv hr^{-1}								
Day and night	146±117	39±40	105±68	150±61	220±84	200±108	103±51	207±100
Nighttime	130±116	26±15	32±19	89±23	219±105	160±118	111±53	219±123
Daytime	153±117	45±46	123±64	164±59	221±75	210±103	101±50	200±84
Night-to-day ratio	**0.85±0.76**	**0.57±0.33**	**0.26±0.16**	**0.54±0.14**	**0.99±0.48**	**0.76±0.56**	**1.09±0.53**	**1.09±0.62**

Note: The standard deviation of night-to-day ratio is calculated by the dividing the standard deviation of nighttime oxidation rate by the average of daytime oxidation rate.

Referring to the CN and CCN concentrations shown in Table 3.1, it can be seen that overall aerosol and CCN concentrations are similar during day and night. We note that daytime

aerosol and CCN concentrations are higher than those during nighttime for the open ocean air mass, possibly indicating less oxidation and less particulate products during nighttime than during daytime. For the coastal air mass, CCN concentrations are slightly higher during night than during day, with CN concentration in the opposite trend. Furthermore, CN and CCN concentrations during nighttime are either larger than or similar to those during daytime for the continental air mass. These results are also consistent with the fact that continental air mass bringing more oxidants (especially NO_x) to MBL than coastal air mass and further more than the open ocean air mass. For the case of "Ocean" segment which is the majority of all ocean open ocean air mass, the nighttime CN and CCN are less populous than those of daytime, consistent with the smaller oxidation rates during nighttime than during time for the same segment as shown in Table 3.2. Therefore, the calculation of oxidation rates has verified with the observed CCN concentrations concerning the influences of anthropogenic activities on marine aerosol.

3.3.4 Contribution of condensational growth to CCN activation

Condensational growth of DMS oxidation products may change the cloud activation potential of the aerosol population. To investigate their potential influence, the CCN activation ratio (CCN/CN) at five SS levels and critical supersaturation are plotted against atmospheric DMS concentration as shown in Figure 3.8. Data for air masses influenced by continental and coastal regions are included because condensational growth may modify all types of aerosols. The data points with DMS higher than 1000 pptv all occurred during the "Ocean" segment. These data will be further discussed in the nucleation event section following this section. The data fall into a triangular shaped pattern (when DMS is lower than 1000 pptv) of the scatter plots of CCN/CN ratios (Figure 3.8a-e) against DMS indicated the nonlinear response of CCN activation to increasing DMS. For a chosen DMS level, the activation ratio at an SS level can be

variable and at least higher than a level bounded by the hypotenuse of the triangle. The variation is believed to be due to variation in both nucleation and condensational growth.

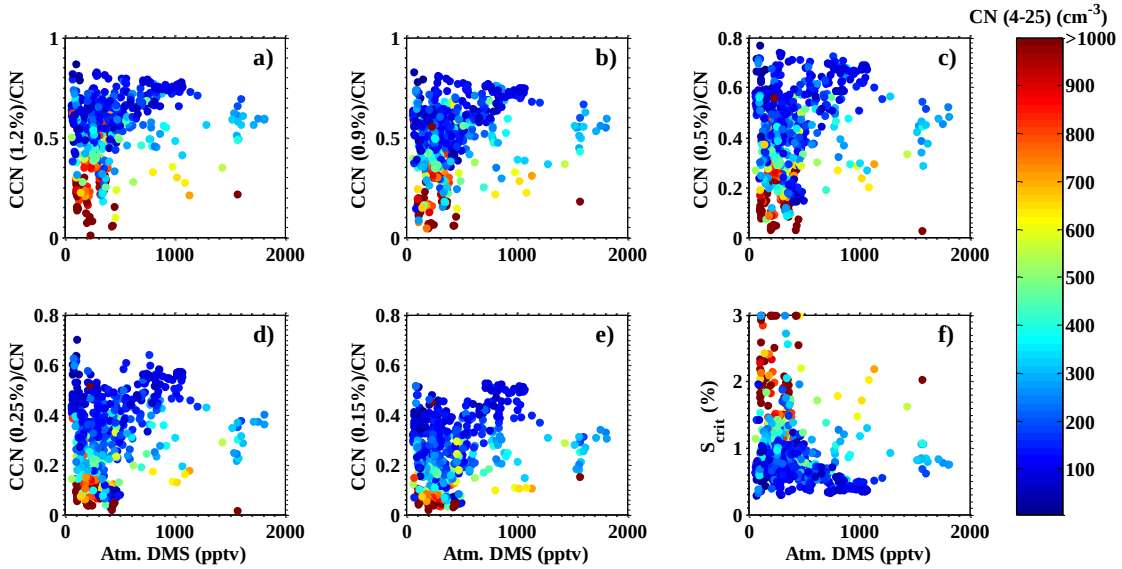

Figure 3.8 Scattered plots of cloud activation ability of aerosol against atmospheric DMS concentration. Panels (a-e) show the CCN/CN activation ratios at five supersaturation (SS) levels against DMS, while panel (f) shows the derived (operational) critical SS against DMS. Color bar shows the total CN concentration which is capped at 1000 cm^{-3}. The black lines are the least-squares linear regressions and the correlation coefficients of each plot are shown in the plots.

Figure 3.8f presents the S_{crit} against DMS level, which is a one-parameter indicator for cloud nucleation ability as introduced in the calibration section. Under high DMS conditions, aerosols have improved cloud nucleation abilities (signified by small S_{crit}). However, this trend is clearer when the DMS is lower than 1000 pptv. If DMS is higher than that, MBL nucleation might be easily achievable. When nucleation events in MBL are triggered, the CCN/CN activation ratio could become significantly lower because the bursts of nucleation mode (3-25

nm) particles are available, as shown by the CN and CCN at high SS levels in Figure 3.5a and Table 3.1. But with proper condensational growth, the effective CCN under these high DMS conditions are efficiently enhanced compared with other conditions.

Low volatility vapors responsible for condensation and those for nucleation could be different, but those for condensational growth are mainly derived from DMS (or SO_2) oxidation (Kulmala et al., 2004b). Also, the condensational growth rate of particles by vapors is similar in various environments since large vapor sources are usually accompanied by large condensational sinks (Kulmala et al., 2005). Therefore, it is not straightforward to view the influence of DMS amount on condensational growth of particles from Figure 3.8.

There are occasions that nucleation mode particle concentrations (majority of total aerosol concentration) are very high when DMS is both low and high. When DMS is high, the high CN concentration can be resultant from nucleation events. When DMS is very low, the high CN concentration can be transported from elsewhere, e.g. continental sources. In terms of the cloud nucleation ability, when DMS is very high, the activation ratios are usually low when nucleation mode particle concentration is too high, which suggests than condensational vapors are relatively insufficient or the condensational growth is relatively slower. The newly formed particles will need several hours to grow into sizes which can be counted as a CCN at the SS levels which we adopted in measurements (Kulmala et al., 2004a). So the activation of aerosol is still limited by time during the nucleation event even though there are enough condensational vapors. However, when DMS is low, the low activation at low DMS concentration could be simply due to lack of condensing vapors. Therefore, the low activation ratios in different conditions are due to different reasons.

Under high DMS conditions, one of the evidences of new nucleation events is the relative abundance of nucleation mode particles, which is embodied in the CN concentration since nucleation mode particles usually dominate CN numbers. In nucleation events, a higher fraction of the aerosol population is present as nucleation mode particles relative to non-nucleation time periods (Kulmala et al., 2004b; Ahlm et al., 2012). Hypothetically, the activation ratio of the aerosol will be increased by condensational growth and coagulation of small particles as aerosol transported along. The results shown in Figure 3.8 also verified that nucleation and condensation are not a coupled phenomenon (Kulmala et al., 2001).

The difference between new nucleation events and that after apparent growth under high DMS conditions is the relative abundance of nucleation mode particles, which is embodied in the CN concentration since nucleation mode particles usually dominate CN numbers. In the former case there should be a much higher concentration of nucleation mode particles than the latter since it has been grown to larger sizes or lost during coalescence with other particles during the process of evolution (Kulmala et al., 2004b; Ahlm et al., 2012). There is a good chance for the activation ratio of the aerosol to be enhanced along the route of transportation by condensational growth and coagulation between small particles. It is then true that higher DMS concentration will increase CCN unambiguously even though the CCN/CN could be low due to the happening of in situ nucleation.

3.3.5 Case study: extremely high DMS and CCN

As introduced in the introduction, nucleation in MBL could happen when DMS is higher than 400 pptv and the total aerosol surface area is lower than 60 μm^2 cm^{-3} (Pirjola et al., 2000). The total aerosol surface area measured by PAS (0.3 to 20 micron in aerodynamic diameter) is presented together with aerosol concentration in in the supplementary materials, Figure 3.17.

During the "Ocean" segment the total aerosol surface area is low (<10 μm^2 cm^{-3}), which is a favorable condition for nucleation to happen. However, not all segments with low aerosol surface area have initiated such nucleation events, perhaps due to the low DMS concentrations observed along these segments. Since the "Ocean" segment is accompanied by both high DMS (more than 80% measurements are higher than 400 pptv) and low aerosol surface, it is worthwhile to take a deeper look at periods of high CN and CCNs to evaluate what is the most possible mechanism to lead to these enhancements. Multiple nucleation mechanisms, including classical binary nucleation of H_2SO_4-H_2O (Doyle 1961), ternary nucleation of H_2SO_4-H_2O-ammonia /amine /organics (Kulmala et al., 2004a), ion-mediated nucleation of H_2SO_4-H_2O (Yu and Turco, 2000), iodine-enhanced nucleation (McFiggans et al., 2010), kinetic nucleation of H_2SO_4 and organic vapor(s) (Karl et al., 2012), as well as nanogel emission (Karl et al., 2013), have all been suggested to be responsible for new particle formation observed in ambient atmosphere at different locations. Suggested mechanisms vary with locations of these studies including the free troposphere (FT) (Clarke 1993; Weber et al., 1999, 2001), marine boundary layer (MBL) (Covert et al., 1992; Hoppel et al., 1994; Clarke et al., 1998a), arctic polar areas (Pirjola et al., 1998; Chang et al., 2011; Karl et al., 2012, 2013), coastal sites (O'Dowd et al., 1999; McFiggans et al., 2010), heavily polluted locations (Kerminen et al., 1996; Zheng et al., 2011), and boreal forest regions (Makela et al., 1997; Kulmala et al., 1998).

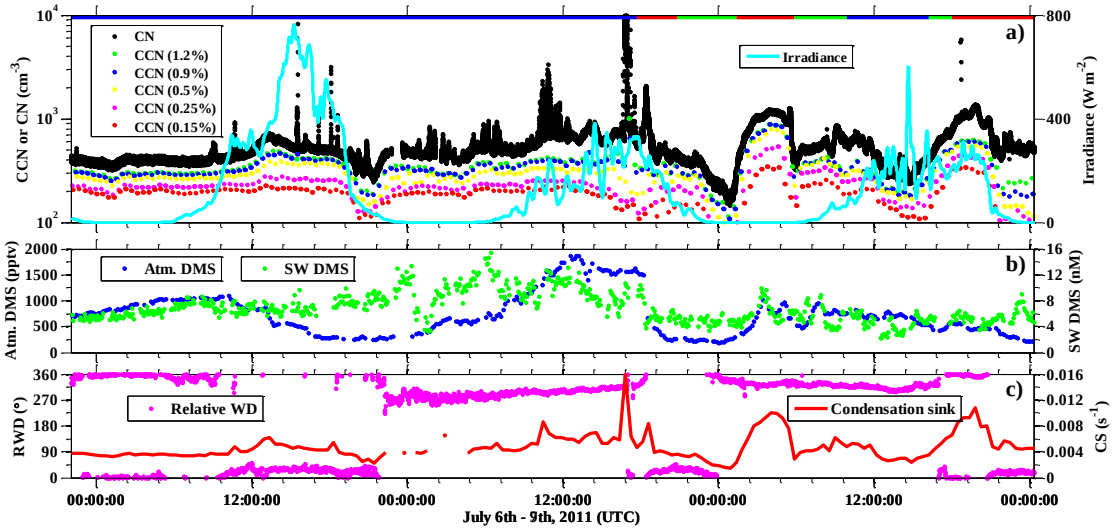

Figure 3.9 Various measurements for nucleation events during the segment with high DMS, including the special "Ocean" segment which has the least continental influence. Panel a) shows particle concentrations and short wave radiation levels; Panel b) shows DMS concentrations in both atmosphere and seawater; panel c) shows relative wind direction (an indication to preclude ship contamination) and the calculated condensation sink capped at 0.016 s^{-1}.

In Figure 3.9 aerosol and CCN concentrations, DMS levels, as well as radiation and aerosol condensation sinks for the segment with significantly enhanced DMS are shown. Constantly high CN and CCNs occur when the DMS is high. In Figure 3.9a, CN and CCN concentrations coinciding with the DMS bloom were shown, including both the "Ocean" case segment and a period following it. It is noticeable that during the "Ocean" segment the particle concentrations are generally more stable and higher than any other segments. The atmospheric DMS concentration peaks around 12 pm of July 7th (UTC), which is in the early morning. A peak in aerosol concentration and coincident shallower peaks in CCN concentrations occurred 3-4 hours later than the DMS peak. The trough of CN and CCNs that happened before 22:00 of July 6th was coincident with the DMS trough and the sunset, a time frame for lower oxidant concentration (Stark et al., 2007). This significant lowering of both CN and CCNs can possibly

be ascribed to the drop of DMS oxidation products, i.e. the vapors for condensation and nucleation, though the offset in timing makes this conclusion uncertain. In summary, significant enhancement of CN and CCNs occur when the DMS is high.

The original criterion for filtering the data for stack contamination was 90 to 270° relative wind speed, based on previous studies (Deng et al. 2013a). If we put a more stringent criterion on the stack contamination (e.g. exclude data when relative wind direction is between 60° and 300°), then many peaks of CN concentration during this segment disappeared. So, we chose not to treat the CN peaks from 1:00 to 8:00 of July 7th as newly formed particles. Then the peaks at the morning and afternoon of July 7th happened concurrently with high DMS concentration and moderate solar radiation, which is also part of the reason for the presence of the highest DMS (over 1800 pptv) detected during the cruise. Five hours after the highest DMS peak, there is a period of DMS trough accompanied by decreasing solar radiation, the aerosol and CCN concentrations also dropped several hours later than DMS.

The condensational sink was low during the whole segment in Figure 3.9 except the parts influenced by nucleation episodes and continental air mass. The peaks of condensation sink during nucleation episode proved the statement from Kulmala et al. (2005) that large vapor sources are usually accompanied by large condensational sinks.

The beginning segment marked by blue bold line (marked by "Ocean" in Figure 3.5a) could be influenced by both nucleation and condensational growth. Loss of particles possibly due to either reduced nucleation or increased coagulation happened at the sunset when OH production is switched off and NO_3 concentration is still low. None of the observed nucleation episodes happened during nighttime. Note that our earlier conclusion showed that DMS oxidation rate during nighttime (prodominantly by NO_3) was at most 85% of that during daytime

(predominantly by OH+Cl) in the whole cruise and 76% in the "Ocean" segment. Therefore, a seemingly small difference at oxidation rates could make a big difference in nucleation results.

DMS and aerosol and CCN data collected during Bloomcruise may result from both nucleation and condensational grwoth mechanism, although we have no way to determine the contribution from each, based on the available data. An alternative way to explain is to evaluate whether or not the H_2SO_4 mass evolved from DMS oxidation could explain the measured aerosol mass after treating all nucleation and condensation vapors as H_2SO_4 (as a surrogate). There are two steps to do this. The first step is to utilize the empirical relationship between gaseous phase concentration of H_2SO_4 and DMS to evaluate if gaseous H_2SO_4 concentration is adequate to sustain a critical nuceation rate. The second step is to evaulate if the calculated oxidant amount is sufficient to explain particle growth based on the oxidation rates derived in section 3.3.2.

Mikkonen et al. (2011) reported a statisical relationship between gaseous H_2SO_4 and SO_2 concentrations:

$$[H_2SO_4] = 8.21 \times 10^{-3} \cdot k \cdot Irradiance \cdot [SO_2]^{0.62} \cdot (CS \cdot RH)^{-0.13} \quad (3.8)$$

where k is a temperature dependent reaction constant and ranges from 0.8959 to 1.1740, *Irradiance* is the short wave irradiance (W m^{-2}), *CS* is condensational sink, and *RH* is relative humidity (%).

Condensation sink can be calculated based on Mikkonen et al. (2011):

$$CS = 2\pi D \int_0^\infty d_p \beta_M(d_p) n(d_p)\, dd_p = 2\pi D \sum_i \beta_M d_{p,i} N_i \quad (3.9)$$

where D is the diffusional coefficient (0.1 cm^2 s^{-1}), β_M is a transitional correction factor and can be expressed as:

$$\beta_M = \frac{K_n+1}{0.377K_n+1+\frac{4}{3}\alpha^{-1}K_n{}^2+\frac{4}{3}\alpha^{-1}K_n} \quad (3.10)$$

where α is the sticking coefficient (≈1), K_n is the Knudsen number which can be expressed as:

$$K_n = \frac{\lambda_v}{r} \quad (3.11)$$

where r is particle size (radius), λ_v is the mean free path of vapor molecules (sulfuric acid molecules) and is expressed as:

$$\lambda_v = 3D\sqrt{\frac{\pi m_v}{8kT}} \quad (3.12)$$

where D is the diffusional coefficient as used in Eq. (3.9), m_v is the molecular mass of sulfuric acid vapor, k is the Boltzmann constant, and T is the temperature in Kelvin.

To establish a scheme from DMS to H_2SO_4, a scheme from DMS to SO_2 should be first established. SO_2 yield from consumed DMS was reported to increase with increasing temperature within the range of 84.3%-99% under the temperature of 284 K to 306 K based on laboratory studies (Arsene et al., 1999). Barnes et al. (1996) reported a SO_2 yield of about 70% in chamber studies under low NO_x conditions, similar to the yields obtained in several field projects (Putaud et al., 1992; Bandy et al., 1996). Since the yield of SO_2 from DMS oxidation is stable, the variations of DMS and SO_2 will be anti-phased if DMS production is constant. Sciare et al. (2001) reported the ratio of DMS to SO_2 within a range of 0.08-0.59 (mean 0.23±0.17) at Amsterdam Island during January of 1998. De Bruyn et al. (1998) reported an observed average ratio between DMS and SO_2 at 13±9 and a modeled DMS to SO_2 conversion efficiency of 30%-50% over the oceans southeast of Austrialia in November and December of 1995. The same group later also reported a similar measured mixing ratios of DMS relative to SO_2 and modeled

DMS to SO_2 yield of 85% at Oahu, Hawayii during April and May of 2000 (De Bruyn et al., 2006). Bandy et al. (1996) reported that 62% of DMS was converted to SO_2 in Christmas islands during July and August of 1994. Other studies reported DMS-to-SO_2 conversion efficiency of 60-73% as well (Gray et al., 2011; Bandy et al., 2011). Ayers et al. (1997) reported the average summer time SO_2 to DMS ratio of 0.1 at Cape Grim, compared to a value of 0.2 reported by Putaud et al. (1992). Putaud et al. (1993) also reported a regressed relationship of $[SO_2]$ = 0.3*[DMS] + 0.2 when expressed in nmol m^{-3} (1 nmol m^{-3} corresponds to 22.4 pptv at standard temperature and pressure). Since the precise time series data of DMS oxidation rate is lacking, we choose to assume a reasonably higher limit ratio for SO_2/DMS in pptv:

$$[SO_2] \approx 0.3 \cdot [DMS] \ + 10 \tag{3.13}$$

Combining Eqs. (3.8) to (3.13) and assigning unity to *k*, we can get:

$$[H_2SO_4] = 8.21 \times 10^{-3} \cdot Irradiance \cdot (0.3 \cdot [DMS] + 10)^{0.62} \cdot (CS \cdot RH)^{-0.13} \tag{3.14}$$

Eq. (3.14) predicts daytime generation of sulfuric acid. However, multiple ambient phase measurement had shown that H_2SO_4 centration during nighttime is above the dection limit. The measurement showed the concentration at a magnitude of 10^6 molecules cm^{-3} is achievable during night when OH is not expected to result from by ozone photolysis (Eisele and Tanner, 1993; Zheng et al., 2011). The missing source of OH is beyond the scope of this research. Instead we set a lower limit of H_2SO_4 concentration at 10^6 molecules cm^{-3}.

The calculated gas phase H_2SO_4 concentration can be compared with a critical concentration, which is defined by the concentration required to achieve a critical nucleation rate of 1 cm^{-3} s^{-1} by sulfuric acid vapors. The critical nucleation rate is the minium rate to witness a

nucleation event. The critical concentration is given empirically by Seinfeld and Pandis (2006) as:

$$C_{crit} = 0.16 \cdot exp(0.1 \cdot T - 3.5 \cdot RH - 27.7) \qquad \text{in } \mu g\ m^{-3} \qquad (3.15\text{-a})$$

Here T is air temperature in Kelvin. RH is relative humidity in fraction (0-1). To convert the unit of gas phase sulfuric concentration to molecules cm^{-3}, Eq. (3.15-a) is transformed to:

$$C_{crit} = 9 \times 10^8 \cdot \exp(0.1 \cdot T - 3.5 \cdot RH - 27.7) \qquad \text{in molecules } cm^{-3} \qquad (3.15\text{-b})$$

Then we can compare the derived sulfuric acid concentration in gasous phase with the required concentration for a nucleation rate of 1 cm^{-3} s^{-1}, shown in the supplementary material, Figure 3.18. From the figure we can notice that the calculated sulfuric acid based on DMS concentration during daytime is adequate for a significant nucleation, and insufficient during nighttime. Even though the estimate of sulfuric acid during nighttime is short of accuracy, we still find the result is consistent with our observation. In Figure 3.9 there are nucleation episodes happening during daytime but not during nighttime.

Next, we estimate the growth rate of the existing particles based on the oxidation rate calculated in the previous section. The daytime and nighttime average oxidation rate of DMS during the "Ocean" segment is 0.05 pptv s^{-1} by referring to Table 3.2. The average particle diamater in this special segment is 88 nm assuming an inorganic chemical composition, which constitute good cloud nucleation ability. Assuming a sulfur molar yield of sulfuric acid from DMS oxidation at 1% (Chen and Jang, 2012), it will contribute to a growth rate of 2.2 nm hr^{-1} of the aerosol, within the typical range of growth rate of 1-20 nm hr^{-1} for nucleation events (Kulmala et al., 2004a). One caveat is that this calcuation does not include the surface of

supermicrometer particles lost in the sampling process, which could be a major sink of condensable vapors and is comparable or even larger than that of the submicron particles.

Therefore, during the "Ocean" segment the amount of sulfuric acid derived from DMS concentration is sufficient to sustain significant nucleation events even by the binary nucleation mechanism. Also, based on the calculated oxidation rate of DMS, the oxidation products can supply enough condensational vapors for aerosol to grow to effective CCN under achievable SS levels in the MBL. Thus, we regard this segment as a segment of nucleation which has due possibility of sulfuric acid-involved nucleation, and sure probability of consensational growth.

It should be noted that the contribution of marine primary organics, especially biologically derived nanogels which may contribute significantly to atmospheric aerosol number concentrations (Karl et al., 2012, 2013). As shown in Supplement Materials, Figure 3.12, seawater DMS is better correlated with CCN than atmospheric DMS with CCN (Figure 3.11.), possibly because seawater DMS could be a reasonable metric for those biologically derived organics (Bates et al., 2012; Gaston et al., 2011).

To reiterate, the constant CCN enhancement in this section has lasted for multiple days and it may have a bigger importance than have been treated previously (as unimportant), especially during summer time when phytoplankton blooms are frequent.

3.3.6 Influence of meteorological parameters on CN and CCN

To evaluate relationships between main meteorological parameters (pressure and wind speed) and the aerosol concentration (CN), we plot wind speed, sea surface pressure and CN concentration against each other in 27 min averages, as shown in Figure 3.10. From Figure 3.10a and 10b we can verify that wind speed and sea surface pressure are generally correlated

negatively, which is taken as a common meteorological rule to evaluate weather conditions based on pressure contour plots. It is noticeable from Figure 3.5 that CN and CCN concentrations dropped dramatically when both pressure and wind speed (refer to Figure 3.6a for wind speed) are low during "Station III". However, in this segment the minor peaks of particle concentrations are not concurrent with pressure peak but with small peaks of atmospheric DMS. By comparing Figure 3.5a with 3.5c, we can see the similar trend of sea surface pressure and CN concentration which are more pronounced during the segments marked with "pressure change". Therefore the scatter plot in Figure 3.10c indicates that there is a coarse proportionality between the logarithmic value of CN concentration and sea surface pressure.

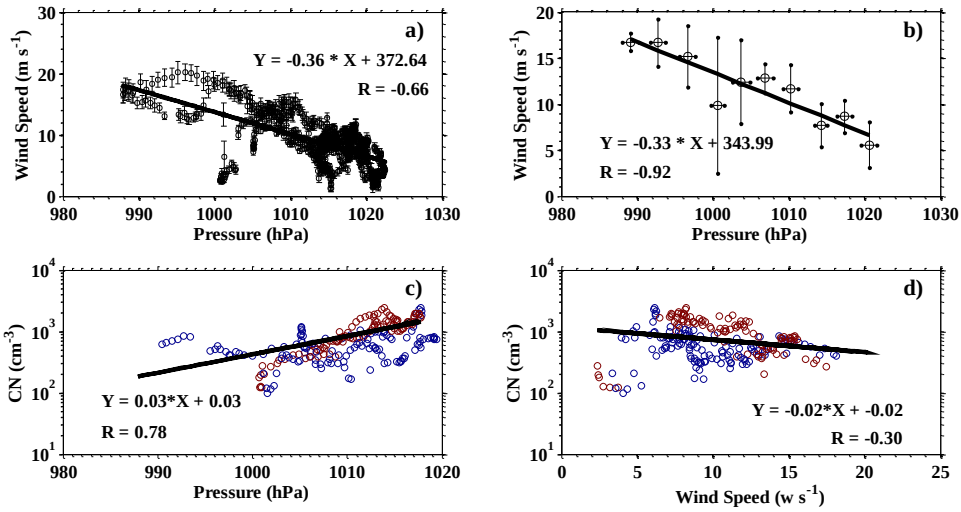

Figure 3.10 Relationship between sea surface pressure and wind speed and the correlation of them with CN in log scale during significant pressure change periods. a) shows the correlation between wind speed and pressure in 27-minute averages; b) shows the same correlations with data pairs binned into 10 ranges based on gradually increasing pressure values; c) shows CN in log scale in correlation with pressure during obvious pressure change period; d) shows CN in log scale in correlation with wind speed during obvious pressure change period. In c) and d), red color shows pressure increasing and blue shows decreasing.

The reason of the correlation could be interpreted by the vertical movement of air masses signified by sea surface pressure, as Katoshevski et al. (1999) reported that entrainment of air from free troposphere was found to be indicative for aerosol number concentration. When sea surface pressure is high there must be more air sinking from upper atmosphere to surface layer than air ventilated from surface layer to upper atmosphere, and vice versa. There are plenty of evidences that ultrafine particle concentration in upper troposphere is much higher (orders of magnitude) than surface layer over global oceans (Clarke 1993; Spracklen et al., 2005; Mann et al., 2012). Friedlander (1977) proposed the self-preserving theory of ultrafine particles in upper troposphere resulting from new particle formation by binary homogeneous nucleation and a balance between coagulation and nucleation. There are measurements showing that the ultrafine CN concentration in free troposphere is not constant though (Peter et al., 2010). Nevertheless, even though the CN concentration in free troposphere cannot be treated as constant, there is still a good chance for CN to be signified by the pressure level since it is significantly higher in UT than in MBL. However, the influence of vertical movement to marine CN and CCNs relative to that of continental transport is not evaluated quantitatively here due to lack of data. Qualitatively, vertical downward entrainment tends to increase CCN as shown in Figure 3.5, whereas transport from continental sources tends to decrease CCN as analyzed in section 3.3.2.

3.4 Conclusions

Aerosol and CCN concentrations under a wide range of conditions, including extremely high DMS levels (1800 pptv), were measured during the Bloomcruise research.Our data show that, atmospheric aerosol in the North Atlantic were signicantly influenced by continental air mass, even over remote regions. The average aerosol number concentration influenced by continental air mass was 115% higher than pristine marine aerosols, while that by coastal air

mass has an enhancement of 44% compared with pristine air. On the contrary, in continental and coastal air masses, CCN concentrations are decreased by 18% and 19% compared with open ocean air mass, at the SS level of 0.15%, a SS level typical of marine stratiform clouds. While total aerosol concentrations for continental air mass are elevated due to continental polluation, the number of aersosol capabile of forming cloud drops is not nesseaily increased and in some instances, is lower than open ocean air mass. Esimated oxidation rates based on measured DMS concentrations illustrated influence of anthropogenic acitivities on marine atmosphere. Overall, the oxidation rate of DMS during nighttime is 85% of that during daytime. Therefore, continental or anthropogenic sources generally provide aerosols of decreased cloud activation potential in MBL over the North Atlantic Ocean during summer.

In the Bloomcuirse research which is the first to report the aerosol and CCN concentration during such a high DMS level as 1800 pptv. The highest DMS was observed when the atmospehre is not influenced by continental air mass. In the two-day sustained nucleation event, we estimated that the sulfuric acid concentration derived from DMS concentration was adequate to explain the observed particle concentration due to nucleation. Therefore, the importance of contributions from marine biota to atmospheric aerosols are significant, at least over the North Atlantic and during summer season when phytoplankton blooms are frequent.

In addition, our measurements indicate that meteorological parameters play an important role in the modificaiton of cloud nucleation ability of marine aerosols. Increases in sea surface pressure may correspond to downward vertical air movement which bring increases in total aerosol concentrations due to the much higher nucleation mode particle concentration in UT than in MBL.

3.5 Supplementary materials

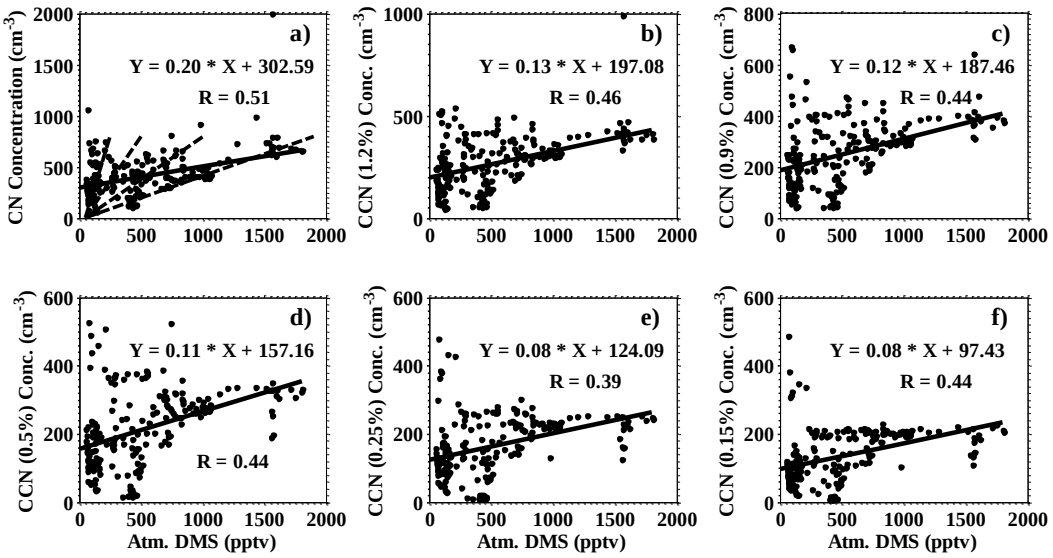

Figure 3.11 Condensation nuclei (CN, or total aerosol) and cloud condensation nuclei (CCN) at five supersaturation levels plotted against atmospheric DMS concentration for data pairs when air masses stayed over the open ocean during the past 48-hr. Black straight lines are least-squares fit between data pairs and R value is correlation coefficient. Extremely high CN and CCN (1.2%) concentrations are due to nucleation episodes and are capped at 2000 and 1000 cm^{-3} respectively. Dashed lines in panel a) are imagined linear fit for different DMS ranges. Data pairs when CN is larger than 1000 cm^{-3} are excluded from linear regression.

Table 3.3 Correlation coefficients between particle concentrations and atmospheric DMS concentration under three air mass scenarios.

particle concentrations	open ocean air mass	coastal air mass	continental air mass	all air masses
Aerosol (CN)	0.51	0.18	-0.27	0.14

Table 3.3 Continued

CCN (1.2%)	0.46	0.30	-0.27	0.23
CCN (0.9%)	0.44	0.32	-0.21	0.25
CCN (0.5%)	0.44	0.30	-0.04	0.30
CCN (0.25%)	0.39	0.31	-0.07	0.29
CCN (0.15%)	0.44	0.28	-0.05	0.36

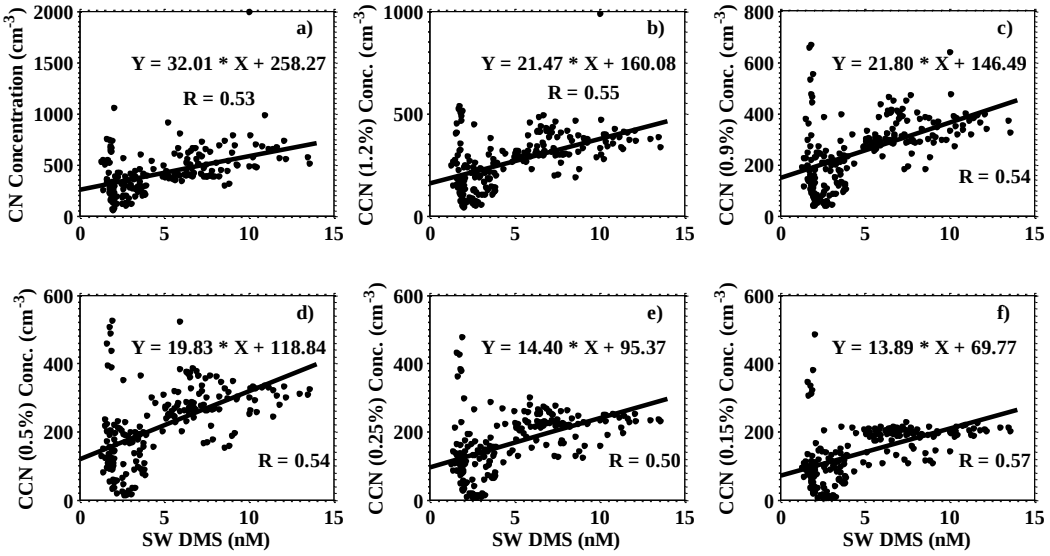

Figure 3.12 Condensation nuclei (CN, or total aerosol) and cloud condensation nuclei (CCN) at five supersaturation levels plotted against seawater DMS concentration when air masses stayed over the open ocean during the past 48-hr. Black straight lines are least-squares fit between data pairs and R value is correlation coefficients. Extremely high CN and CCN (1.2%) concentrations are due to nucleation episodes and are capped at 2000 and 1000 cm^{-3} respectively. Data pairs when CN is larger than 1000 cm^{-3} are excluded from linear regression.

Table 3.4 Correlation coefficients between particle concentrations and seawater DMS concentration under three air mass scenarios.

particle concentrations	open ocean air mass	coastal air mass	continental air mass	all air masses
Aerosol (CN)	0.53	0.23	-0.19	0.18
CCN (1.2%)	0.55	0.41	-0.01	0.34
CCN (0.9%)	0.54	0.45	-0.02	0.36
CCN (0.5%)	0.54	0.46	-0.01	0.39
CCN (0.25%)	0.50	0.44	-0.06	0.37
CCN (0.15%)	0.57	0.40	-0.10	0.44

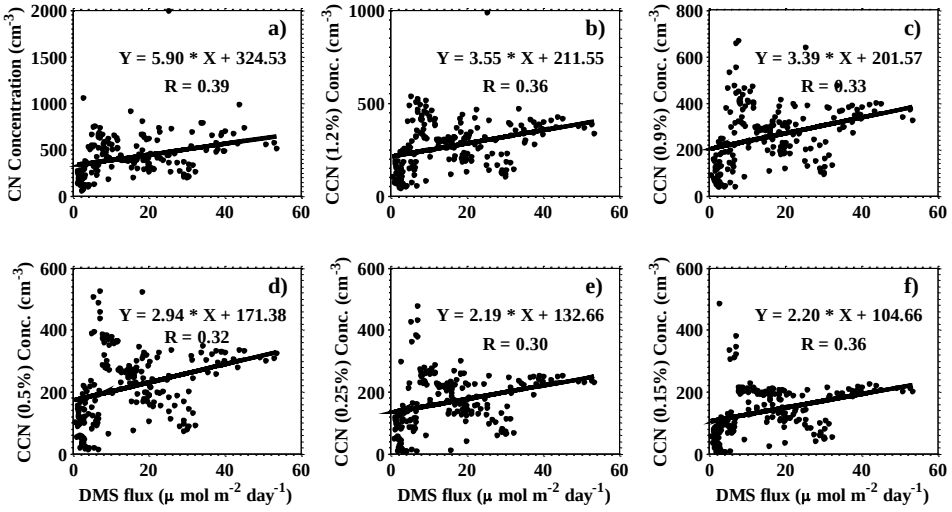

Figure 3.13 Scatter plot of CN (or CCNs) against DMS flux for the pristine marine air masses (DMS flux is calculated based on the scheme proposed by Goddijn-Murphy et al. (2012)).

Table 3.5 Correlation coefficients between particle concentrations and DMS sea-to-air flux under three air mass scenarios.

particle concentrations	open ocean air mass	coastal air mass	continental air mass	all air masses
Aerosol (CN)	0.39	0.23	-0.23	0.15
CCN (1.2%)	0.36	0.45	-0.16	0.21
CCN (0.9%)	0.33	0.45	-0.22	0.18
CCN (0.5%)	0.32	0.40	-0.23	0.17
CCN (0.25%)	0.30	0.37	-0.23	0.16
CCN (0.15%)	0.36	0.35	-0.25	0.20

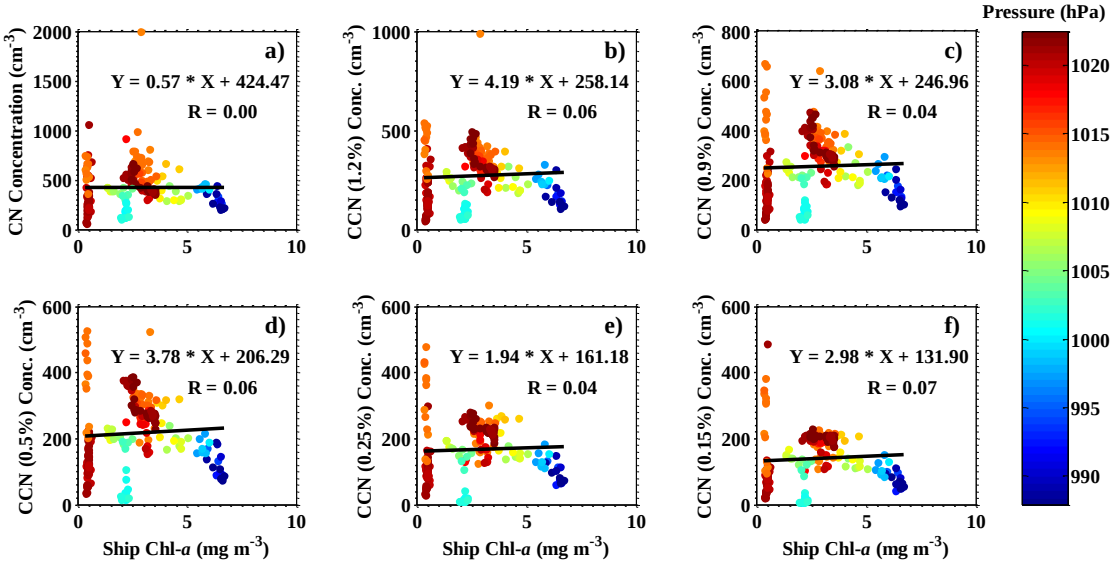

Figure 3.14 Scatter plot of CN (and CCNs) against ship-aboard fluorometer measured chlorophyll *a* for the open ocean air mass.

Table 3.6 Correlation coefficients between particle concentrations and fluorometer measured chlorophyll *a* concentration under three air mass scenarios.

particle concentrations	open ocean air mass	coastal air mass	continental air mass	all air masses
Aerosol (CN)	0.02	0.23	0.31	0.24
CCN (1.2%)	0.05	0.54	0.34	0.30
CCN (0.9%)	0.04	0.55	0.23	0.25
CCN (0.5%)	0.06	0.51	0.07	0.19
CCN (0.25%)	0.05	0.47	-0.12	0.11
CCN (0.15%)	0.14	0.45	-0.26	0.07

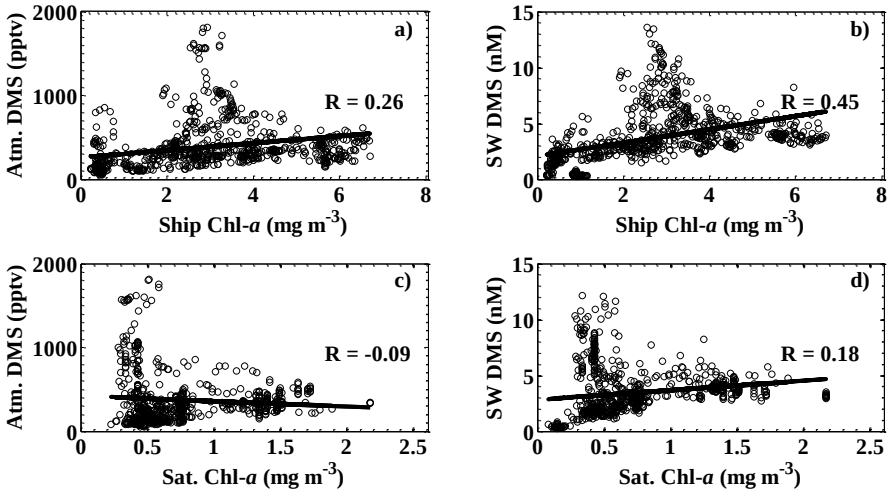

Figure 3.15 Correlation of Chlorophyll *a* and DMS concentrations. Ship Chl-*a* is calculated from ship-board fluorometer reading. Satellite Chl-*a* (Sat. Chl-*a*) is retrieved from MODIS satellite. Scattered open circles are measurements and lines are fitted linear relationship. Correlations coefficients are shown in the plot. Values are averages of 27 min required for a CCN cycle measurement.

Table 3.7 Correlation coefficients between chlorophyll *a* (Chl-*a*) and DMS.

	Ship Chl-*a*	Sat. Chl-*a*	Ship Chl-*a* × Irradiance	Sat. Chl-*a* × Irradiance
Atm. DMS	0.26	-0.09	0.12	-0.06
SW DMS	0.45	0.18	0.19	0.05

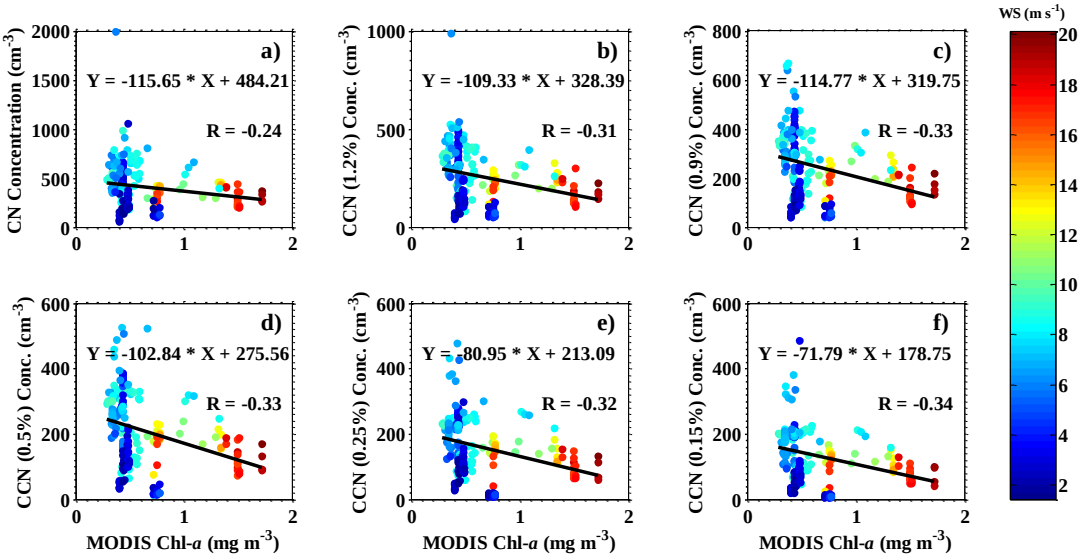

Figure 3.16 Scatter plot of CN (or CCNs) against MODIS retrieved Chl-*a* for the open ocean air mass.

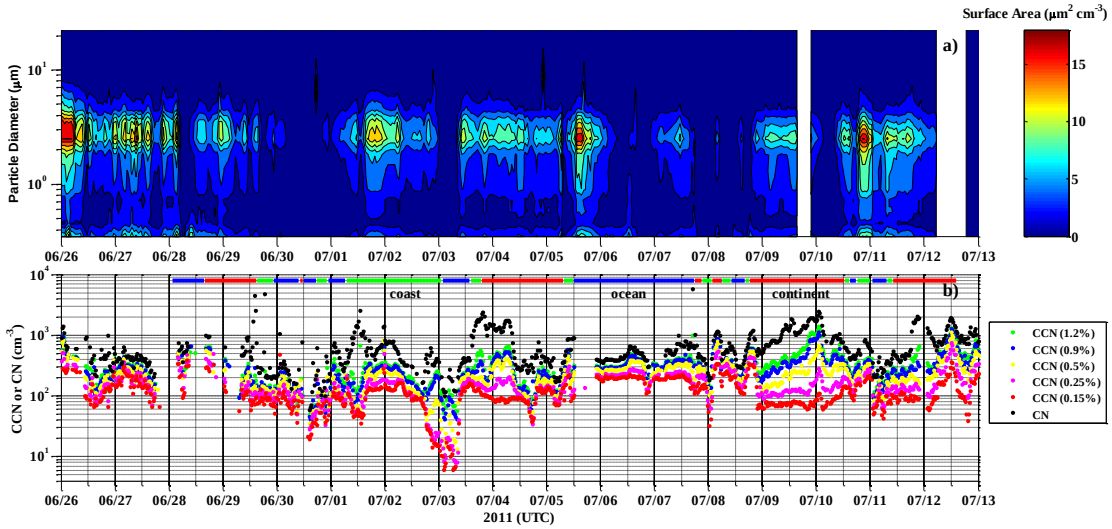

Figure 3.17 Observed PAS derived aerosol surface area (0.3 – 20 micron) in comparison with measured CN and CCNs concentration.

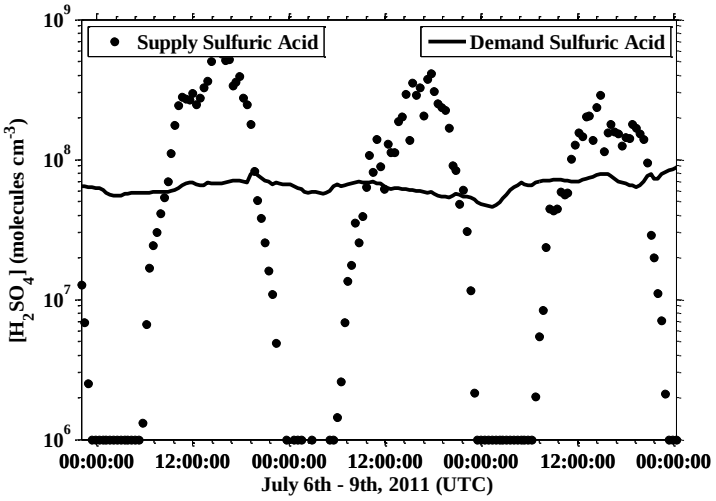

Figure 3.18 Comparison of supply sulfuric acid concentration and the concentration required for a significant nucleation to occur.

4. AN ANALYSIS OF SMALL SEA SPRAY PARTICLE PRODUCTION OVER THE NORTH ATLANTIC OCEAN

4.1 Introduction

Constraining marine aerosol concentration is vital for understanding the direct and indirect effects of aerosol on the global climate since ocean covers over 70% of the earth surface (Bigg 2007). Marine aerosols in the marine boundary layer (MBL) over pristine oceanic areas comprise mainly of sea salts, primary organic aerosols with biological origins, as well as the non-sea-salt (nss-) sulfate derived from phytoplankton-excreted DMS (Charlson et al., 1987; Lewis and Schwartz, 2004).

The production flux of SSA is usually parameterized by wind speed at 10 m above sea level and is termed as its source function or production flux (Lewis and Schwartz, 2004; Martensson et al., 2003). The production flux of SSA can be parameterized in terms of its number, surface area, volume, as well as its mass (de Leeuw et al., 2011). One of the earliest and most commonly used source (or flux) functions of sea salt aerosol is proposed by Monahan and colleagues (Monahan and Muircheartaigh, 1980; Monahan et al., 1986). Monahan and fitted the relationship of whitecap (white areas of the sea surface resulting from breaking waves) coverage and wind speed at the power law relationship of $W_{cap}=3.84\times10^{-6}\ U_{10}^{3.41}$ (Monahan and Muircheartaigh, 1980). The source function of sea salt aerosol per whitecap area is usually determined in laboratory and assumed to be independent of wind speed (Lewis and Schwartz, 2004; de Leeuw et al., 2011). Monahan et al. (1986) incorporated the laboratory results of aerosol flux versus whitecap area and field data fitting of whitecap coverage versus wind speed and obtained the source function as Eq. (4.1):

$$\frac{dF_{int}}{dlogr_{80}} = 3.2U_{10}^{3.41}r_{80}^{-2}(1 + 0.057r_{80}^{1.05}) \times exp\{2.74 \times \exp[-2.4(0.38 - logr_{80})^2]\} \quad (4.1)$$

This source function is applicable for particles of radius at 80% RH from 0.8 μm to 8 μm. In addition to the whitecap method, other methods can also be used to derive the SSA source function, including steady state dry deposition method, concentration buildup method, statistical wet deposition method, micrometeorological method, bubble method, along-wind flux method, direct observation method, etc. (Lewis and Schwartz, 2004; de Leeuw et al., 2011). Exponential dependence on wind speed was also obtained by these methods during source function derivation (Petelski 2005; de Leeuw et al., 2011).

It is widely accepted that SSA comprised the majority of the marine aerosol mass due to the dominance of coarse particles in mass and its undeniable source function in coarse size mode (Bates et al., 2006; Prather et al., 2013). Source functions of SSA mass or volume has been parameterized with wind speed at 10 m height as power law or exponential relationships within an uncertainty of two orders of magnitude due to the different dependence on wind and the different upper size cut (Monahan et al., 1986; Lewis and Schwartz, 2004; de Leeuw et al., 2011). Furthermore, the number source function of SSA is subjected to even larger uncertainties because SSA number concentration is dominated by small particles which may be composed of many constituents other than sea salt (Geever et al., 2005). In fact, presence of sea salt particles smaller than 200 nm in marine atmosphere is still debatable (Clarke et al., 2006; Bigg 2007). Bigg (2007) contended that essentially no sea salt particles smaller than 200 nm are existent in MBL, while others reported that significant fluxes of sea salt particles down to 10 nm were detected (O'Dowd and Smith, 1993; Nilsson et al., 2001; Geever et al., 2005; Clarke et al., 2006; O'Dowd et al., 2008). One distinction is that those submicrometer SSA fluxes were detected at a fixed station rather than during a cruise, making it not universally convincing. Recent researches

have detected NaCl from SSA generated from real seawater in an experimental system simulating the ambient wave processes but excluding possible terrestrial contamination (Prather et al., 2013; Ault et al., 2013). The same groups also verified that the presence of NaCl in SSA smaller than 200 nm and that organic species in SSA has an increasing contribution with decreasing sizes, which is consistent with the findings of previous studies (O'Dowd et al., 2004; Keene et al., 2007). Tiny particles are very important for cloud formation and climate (Russell and Singh, 2006). Given all the complexities in aerosol properties and source functions, there is urgent need of further theoretical and experimental investigations to unveil the chemical composition and mixing state of SSA smaller than 200 nm.

The uncertain source function of sea salt particles smaller than 200 nm causes uncertainties in assessing both the direct aerosol radiative forcing (Kahn 2012) and the indirect aerosol radiative forcing (Ma et al., 2008). However, both the magnitude (negative) and the uncertainty of indirect forcing due to sea salt aerosols are much larger than their direct forcing (Satheesh and Moorthy, 2005). In addition, the total aerosol forcing due to sea salt particles is much larger in both magnitude (negative) and uncertainty than anthropogenic aerosols (Satheesh and Moorthy, 2005; IPCC 2007). Therefore, the chance to narrow the gap in understanding the total aerosol forcing lies well in quantitatively understanding the indirect effect of sea salt aerosols. Size-resolved hygroscopicity of pure NaCl is known unambiguously. Hence, its ability of serving as cloud condensation nuclei (CCN) can be well quantified. However, the composition of SSA is unknown. Therefore, the uncertainty of sea salt aerosol's indirect effect originates from its size-resolved and composition-dependent source function, as well as the poorly understood physical processes that regulate cloud droplet numbers (Ma et al., 2008).

An additional difficulty arises from complex nature of organic species which contribute to differences in aerosol properties including CCN activation potential. In addition, the likelihood of particles to act as sites for heterogeneous oxidation of trace gases depends, in part, on their compositions and uptake coefficients (Quinn et al., 2002; Bigg 2007). An array of organic species have been found in sea spray aerosols with various solubilities and hygroscopicities (O'Dowd et al., 2004; Bigg and Leck, 2008; Deng et al., 2013a). Some organics (especially gel-like organics) can serve as CCN by themselves (Leck and Bigg, 2005a, b, 2007), while others are water insoluble and reduce the cloud nucleation ability of SSA by reducing its hygroscopicity (Wex et al., 2010b; Fuentes et al., 2011). Variation in mixing states of sea salts and organics is also a large barrier in evaluating the indirect effect of sea spray aerosols (Gaston et al., 2011; Ault et al., 2013).

Previous SSA source functions all have an important restriction of only applicable to particles larger than 0.5 μm in dry diameter, with most of them only applicable to 1.0 μm (Martensson et al., 2003; de Leeuw et al., 2011). Martensson et al. (2003) measured fluxes for particles with sizes down to 20 nm by bubbling simulated seawater using a sintered glass filter in laboratory. More recently, Fuentes et al. (2010) extended the primary particle (number) source function down to 3 nm with the differentiation of phytoplankton levels in the water which is used to generate particles. However, the extended lab-generated source functions were proved to have overestimated the real world source flux significantly (Ovadnevaite et al., 2012). Therefore, models (Spracklen et al., 2007; Pierce and Adams, 2006) using the Martensson et al. (2003) and Gong (2003) source functions have overestimated the contribution of SSA to marine aerosol number concentration. Regardless of the various source functions, if SSA smaller than 200 nm dominates the number concentration of marine aerosol in the same size range, a positive correlation should exist between wind speed and total aerosol number concentration.

The extent to which sea spray aerosol contributes to marine CCN has been studies for over 130 years and no conclusive implication has been derived (Aitken 1880; Kohler 1936). Here we do an analysis based on our measured data to shed a little light on the above mentioned enigmatic question.

4.2 Experimental section

4.2.1 CCN and CN measurement

The purpose of this chapter was to understand the relationship of aerosol concentrations and meteorological parameters. The details of the Bloomcruise were elaborated in the previous chapter and only necessary details are repeated here. CCN number concentrations were measured at five SS levels in rotation by a CCN counter (DMT technologies) continuously. The five SS levels of 1.2%, 0.9%, 0.5%, 0.25% and 0.15% were allowed 7 min, 5 min, 5 min, 5 min and 5 min respectively in a single cycle, constituting the whole cruise as a series of 27 min cycles in terms of CCN measurements. By bifurcating the main inlet after removing the excess humid by dryers and large particles by a cyclone impactor (remove particles larger than 1.5 micron), CN (total particle from 4.5 nm to 3000 nm) measurement was made by a GRIMM CPC instrument, in parallel with CCN.

Calibration of CCN and CPC instruments using lab-generated ammonium sulfate aerosol particles were carried out both before and after the cruise. Details of the calibration were presented in the previous chapter.

4.2.2 Approximation of particle size derived from CCN measurement

Cloud nucleation ability of soluble inorganic aerosol particles is well understood based on Köhler theory (Seinfeld and Pandis, 2006). For a species with known chemical composition, the critical SS at which 50% of the particle populations activate as CCN can be calculated for different dry particle sizes. For pure inorganic aerosol particles with mono-disperse size distribution, their activation at varying SS levels can be fitted with an accumulated Gaussian curve to compute the SS required for 50% activation. The details of those fittings were shown in the CCN and CN calibration in the previous chapter. Similarly, we can derive the critical dry diameter of inorganic aerosol particles with different mono-disperse sizes at which 50% of the particle population achieves activation at an SS level. Therefore, for single component aerosol, we can use the CCN concentration measured at an SS level to determine its critical dry particle diameter. For a single component aerosol with polydisperse size distribution, the CCN concentration measured at one SS level corresponds to the number concentration of particles larger than the critical dry diameter at that SS level.

Sodium chloride (NaCl) is the main component of sea salt aerosols (Lewis and Schwartz, 2004). Ammonium sulfate ($(NH_4)_2SO_4$) is a common secondary aerosol species (Seinfeld and Pandis, 2006). Sulfuric acid (H_2SO_4) is the most important species for new particle formation resulting from oxidation products of DMS (Clarke et al., 1998b). Here we employ the highly idealized cases to examine differences in CCN activation of three hypothetical types of single component aerosol. In the first case, we assume that all the marine aerosols encountered during Bloomcruise were composed of pure sodium chloride particles. In the second and third cases, we assume all particles were pure ammonium sulfate particles, and pure sulfuric acid particles,

respectively. In reality marine aerosol has much more complex composition and should not substitute those simplified sizes as its real size.

In Table 4.1, we reported the results of the critical dry diameters of three inorganic aerosols (Row 2 to 4) at the five SS levels that we have adopted to measure CCN concentration. Therefore, each CCN concentration is labeled as number concentration of particles larger than its critical dry diameter. Also important to note is that the CPC instrument used in the measurement has a lower limit of 4.5 nm. In the last row of the table, the values assumed for a mixture of the three inorganic aerosols were reported.

Table 4.1 Particle size (dry diameter) ranges of assumed inorganic aerosols detectable at measurements.

Meas. / **Species**	**CN (by CPC)**	**CCN (1.2%)**	**CCN (0.9%)**	**CCN (0.5%)**	**CCN (0.25%)**	**CCN (0.15%)**
NaCl	>4.5 nm	> 20 nm	> 25 nm	> 36 nm	> 58 nm	> 82 nm
$(NH_4)_2SO_4$	>4.5 nm	> 26 nm	> 32 nm	> 48 nm	> 75 nm	> 105 nm
H_2SO_4	>4.5 nm	> 24 nm	> 29 nm	> 43 nm	> 69 nm	> 97 nm
Assumed mixture	>4.5 nm	> 25 nm	> 30 nm	> 45 nm	> 70 nm	> 100 nm

If marine ambient aerosol measured is a mixture of the above three species and the mixing ratios of each component were known, then the critical sizes of aerosol population measured by CCN counter would correspond to particles of the size shown in the last row. In reality, the addition of marine primary organic aerosol has complicated the problem (Prather et al., 2013). Multiple studies have showed only minor reduction in cloud nucleation ability of

primary inorganic aerosol per the addition of organic species unless the organic species are exudates from nanoplankton (Wex et al., 2010b; Fuentes et al., 2011). Therefore, the real critical diameter of ambient marine aerosol may differ a lot from that of the assumed mixture of three inorganic species as shown in the last row of Table 4.1.

4.2.3 PAS measurement

Meanwhile, particle size distribution for particles with aerodynamic diameter between 0.3 and 20 micron were recorded every six seconds with 15 bins by a portable aerosol spectrometer (PAS) from GRIMM technologies.

4.2.4 Shipboard measurements

Shipboard measurement from meteorological sensors on different positions of the ships (main mast, forward mast port side and starboard side) were carried out continuously and data were recorded every minute. These parameters include air temperature (three sensors), barometric pressure (three sensors), shortwave irradiance (one sensor), rain intensity (two sensors) and rain accumulation (two sensors), wind speed and direction (three sensors). The values from different sensors were averaged for each meteorological parameter in this study for use. The navigation direction and speed of the ship were also logged to derive the true wind direction and speed based on the measured relative wind direction and speed. Sea surface temperature (two sensors) and salinity (two sensors) of seawater were measured by sensors located in the bow chamber outboard of the surface water pump. A fluorometer sensor was aboard the research vessel. The reading was used to derive chlorophyll *a* (Chl-*a*) concentration along the cruise track.

4.3 Results and discussion

4.3.1 An overview of measurement results

The overview of the variation of multiple measurements and parameters are presented in Figure 4.1. Figure 4.1a shows the particle concentrations in averages of 27 min. Figure 4.1b presents the variations of wind speed and rain intensity. Figure 4.1c reveals the change of sea surface pressure and chlorophyll *a* concentration derived from fluorometer reading. We note that unfortunately the most recent calibration of the fluorometer occurred two years before Bloomcruise. While absolute values are uncertain, the fluorometer does provide a measure of relative changes in the fluorometer measurements throughout the cruise, and an indication of the relative highs and lows in Chl-*a* conditions measured throughout the cruise. In general, particle concentrations did not vary in the same direction with wind speed. An exception occurs during the abrupt change in particle concentrations can be attributed in part to the wind speed during "Station III" and "Station V". It is also interesting to notice that precipitation does not lower particle concentrations as expected. No simple correlation between particle concentrations and phytoplankton amount signified by Chl-*a* level is traceable in the figure.

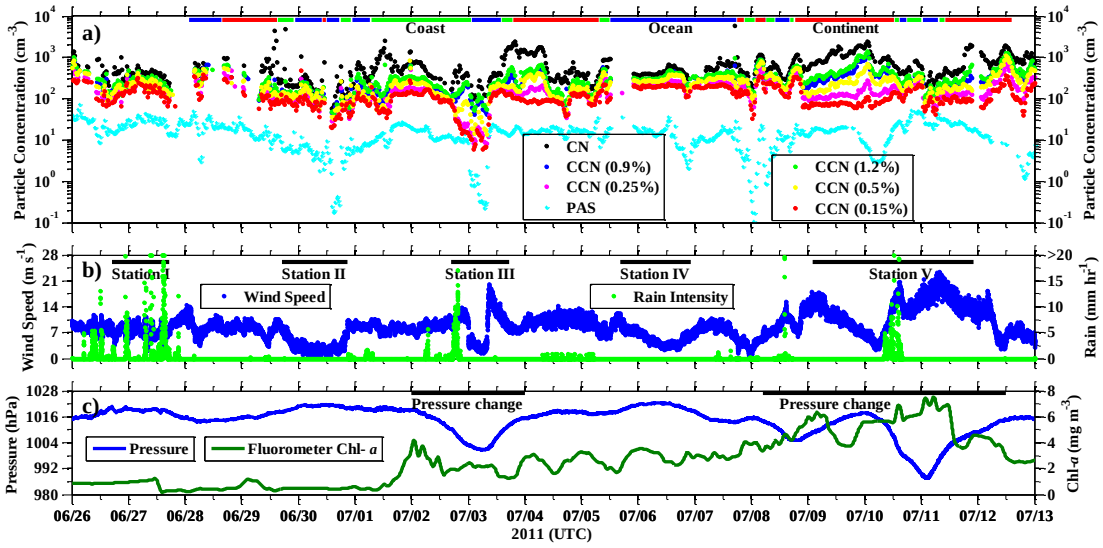

Figure 4.1 Time series measurements during the cruise. Panel a) shows the variation of 27 min averages of CN concentration and CCN concentrations at five different SS levels, as well as the total concentration from PAS. Bold line with blue, green and red colors in the panel show segments when their air masses passed through the open ocean, coasts, and continents in the past 48 hours respectively; Panel b) shows variation of true wind speed and rain intensity. Segments marked by bold black lines and marked with segment numbers are the periods with no spatial variation; Panel c) shows the fluorometer-measured chlorophyll *a* concentration and shipboard barometric reading. The two segments marked with bold black line and marked underneath with "Pressure change" are the phases with apparent sea surface pressure change.

4.3.2 Relationship between wind speed and particle concentration

The correlational analyses between wind speed and particle concentrations with different sizes derived from various measurements are carried out in this section. Prior to making any correlation analysis, it is necessary to clarify relationships between the parameters used in previous literature and those measured by us during the cruise. It is the wind speed at a height of 10 m above sea surface (referred to as U_{10}) that has been widely used to parameterize SSA source functions, especially for field data (O'Dowd and Smith, 1993; Clarke et al., 2006; de

Leeuw et al., 2011). The wind speed in the marine boundary layer is only weakly dependent on measured height under neutrally stable conditions and the measurement uncertainty usually overwhelms the height dependence (Lewis and Schwartz, 2004). The deployed heights of wind sensors in the cruise are very close to the height of 10 m (within a range of ±2 m). Therefore, it is unambiguous that our measured wind speed is a valid surrogate for U_{10}, adding to the confidence is the fact that the wind speed values we adopted are the averages of three sensors. So wind speed and U_{10} are used equivalently in this manuscript.

In source function parameterization, the size of SSA is usually expressed as the radius of particles measured when the relative humidity (RH) is at 80%, expressed as r_{80} (Lewis and Schwartz, 2004). The RH at which SSA is formed at sea surface is very close to saturation (close to 98% for most of the oceans) and the radius at formation is usually termed as r_{form}, practically approximated by r_{98}. The particle concentration or size distribution is usually measured at a dry condition (corresponding radius termed as r_{dry}), as we did for our measurement. In our case, ambient samples were passed through a heater and dryers prior to measurement. The hygroscopicity of NaCl is well-known (Seinfeld and Pandis, 2006). If we assume the marine particles are single-component NaCl particles, a relationship between particle size and the RH can be explicitly expressed as $r_{98} = 2r_{80} = 4r_{dry}$ (Lewis and Schwartz, 2004). The measurement of particle concentrations for each size range, either by CPC or PAS, is distinguished by the aerodynamic diameter (d_P). Therefore the diameter at dry condition is equal to the radius at 80% RH and they are used interchangeably in this manuscript, $d_P = r_{80}$.

Since the relation between size-resolved SSA (number) source function and the wind speed at 10 m above sea surface (U_{10}) is well confined to a power law relationship (Martensson et al., 2003; Fuentes et al., 2010), there should be a discernible positive correlation coefficient

between the size-segregated number concentration of aerosols at lower atmosphere and U_{10} if SSA possess an appreciable portion of the marine aerosol number concentration. The correlation plots between small particle number concentrations measured by CPC or CCN counter and the wind speed is shown in Figure 4.2. From the figure we can see that they are barely correlated (correlation coefficients vary from -0.16 to 0.07). Precluding data with air masses influenced by continental and coastal air masses results in no better correlation either. Conversely, the correlations between large particle concentrations derived from CPC measurement and U_{10}, as shown in Figure 4.3, are significant (correlation coefficients vary from 0.38 to 0.57) for either submicron particles (0.3 to 1 micron), or supermicron particles (1 - 20 micron), or the sum of the two. In addition, the correlations between large particles and wind speed were evaluated for the number concentration, the surface area concentration, as well as the volume concentration. Therefore, it is reasonable to speculate that SSA comprises a significant fraction of large particles (>0.3 micron) in marine boundary layer, whereas it constitutes a lesser fraction of smaller particles (<0.3 micron). Previous investigations have tried to separate source function parameterizations for particles down to 10 nm into several functions based on the ranges of wind speed (Martensson et al., 2003) as well as the trend of wind change, i.e., wind increasing or decreasing (Ovadnevaite et al., 2012). However, these parameterizations only differ slightly in the constants, not in the types of the function. Particle concentrations and wind speed are plotted in Figure 4.2. The data appear to follow two different separate trends for wind speeds smaller and larger than 8 m s^{-1}. Then, if we were to fit the data at different ranges of wind speed, one positive and one negative value will be obtained for the wind speed smaller than and larger than 8 m s^{-1} separately. Since no previous studies have suggested opposite trends based on different wind speed range, the separate retrieval of correlation coefficients is not well-founded even though reasonable correlation coefficients can be resulted in.

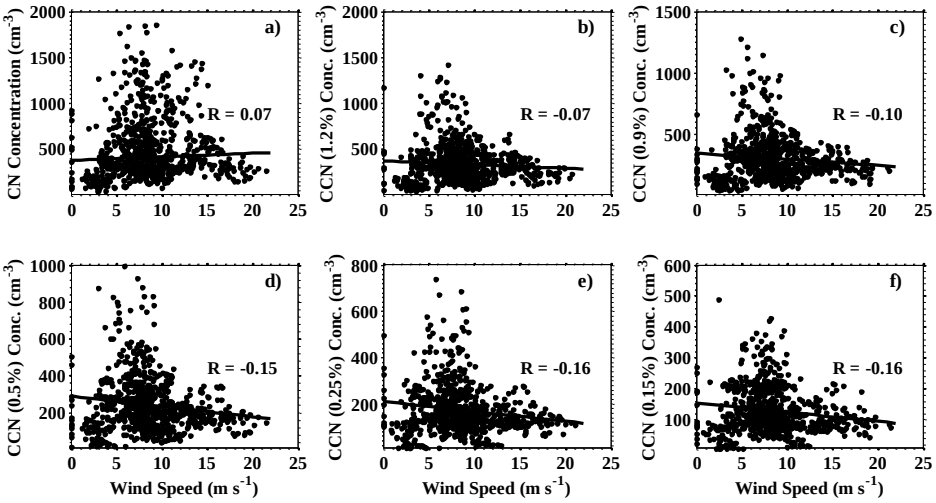

Figure 4.2 Scatterplots of particle concentrations measured by CPC (CN concentration) and CCN counter against wind speed. Solid lines are fitted by least-squares method. Correlation coefficients (R values) are shown for each plot. Each data point is derived from a 27 minute cycle.

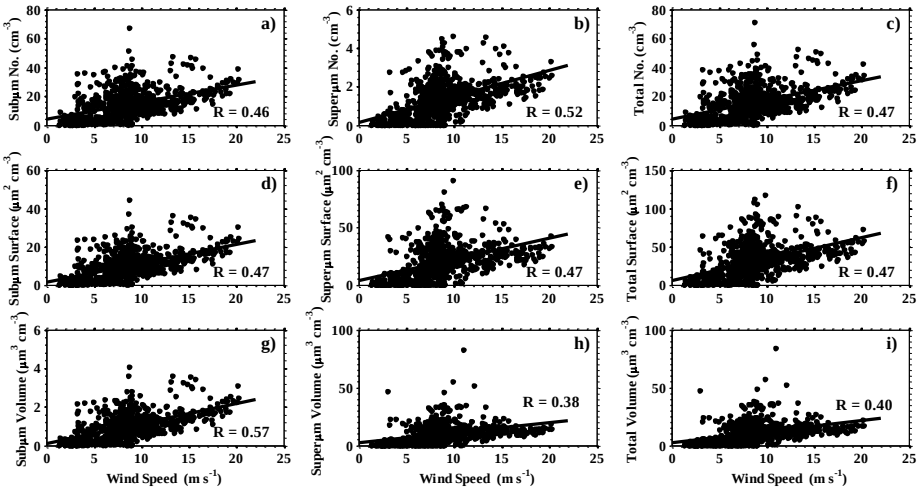

Figure 4.3 Scatterplots of particle concentrations measured by PAS against wind speed. Panels (a-c) show the correlations of aerosol number concentration with wind speed; Panels (d-f) show those between aerosol surface concentration and wind speed; Panels (g-i) show those between aerosol volume concentration and wind speed. Panels (a, d and g) present correlations for submicron particles (diameter between 0.3 and 1 micron); Panels (b, e and h) present correlations for supermicron particles (diameter between 1 and 20 micron); and panels (c, f and i) present correlations for all PAS particles (diameter between 0.3 and 20 micron). Solid lines are fitted by least-squares method. Correlation coefficients (R values) are shown for each plot. Data points are the averages of 27 min's measurement.

As mentioned in the introduction section, the smallest size of SSA is still under discussion (Prather et al., 2013). Multiple groups reported real world SSA with sizes smaller than 200 nm and parameterized the size-differentiated concentration with U_{10} (O'Dowd and Smith, 1993; Clarke et al., 2006). However, Bigg and Leck (2008) reported the absence of NaCl, the most important species in SSA, in particles < 200 nm during their long-term field observations, and explained the possible reason why other researches could have erroneously detected NaCl in that size range (Bigg 2007). Therefore, an indirect way to prove the presence or

absence of NaCl for particles in a size range is to compare the size-dependent correlation coefficients between particle number concentrations and wind speed, as shown in Figure 4.4. It is noticeable that for particles smaller than 0.5 micron, the aerosol number concentration and wind speed is barely correlated (R value ranges from -0.2 to 0.2). The correlation between number concentration and wind speed improves with the increasing particle size when $r_{80} > 0.5$, leveled off at 1 micron and then dropped sharply after 3 micron. The increasing and plateauing of R values are attributable to the increasing dominance of SSA aerosol in marine aerosol particles with increasing size. However, the decease after 3 micron is likely to be a result of particle losses during the sampling system resulting in undercounting large particles by the PAS. We have no intention of corroborating the importance of SSA to marine aerosol >3 micron so the size-dependent particle loss rate is not discussed further. However, the increasing trend of SSA contribution to marine aerosol <3 micron is clearly shown in the figure. We hypothesize two possibilities to explain why the measured number concentration of aerosols < 0.5 micron are not correlated with wind speed. First, the SSA particles are not a significant component of marine aerosols smaller than 0.5 micron but meanwhile the source function of SSA <0.5 micron can be similarly parameterized by wind speed as that of larger SSA particles (0.5 to 10 micron). Second, the SSA particles contribute significantly to marine aerosols <0.5 micron but meanwhile those small SSA particles have a different production process from larger SSA particles (0.5 to 10 micron). Either of the two hypotheses will result in similar correlational results as shown by our results.

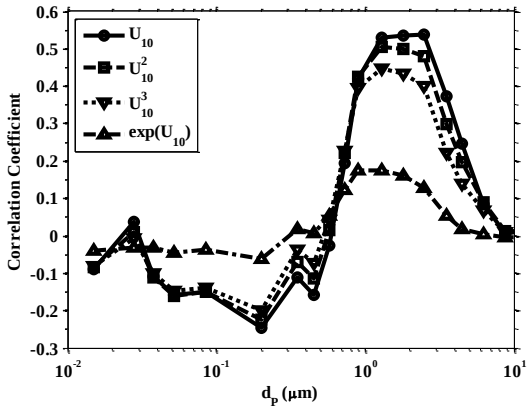

Figure 4.4 Correlation coefficients between particle concentrations with different sizes (as shown in abscissa) and derivatives of wind speed (as shown in the legend).

Also shown in Figure 4.4 are the comparison of various different parameterizations of wind speed, including power-law and exponential relationships. The size-differentiated correlation coefficients between particle number concentration and four different parameterizations of wind speed are compared. It is visible that for particles between 0.5 and 3 micron the best correlations exist between particle concentration and wind speed itself, which is better than its squared and cubic values, and further better than its exponential value. As shown in Eq. (4.1), the most cited source function initiated from the mechanism proposed by Monahan and Muircheartaigh (1980) between wind speed and the oceanic whitecap fraction which itself suffered from an uncertainty of an order of magnitude due to different ways of measurement (de Leeuw et al., 2011).

$$W(U_{10}) = 3.84 \times 10^{-6} U_{10}^{3.41} \tag{4.2}$$

The SSA flux function and its contained size distribution per whitecap area, which are dependent on a number of factors including bubble generation methods, salinity, water temperature, surfactant amount (de Leeuw et al., 2011), are independent of wind speed and can be as detailed as presented in Martensson et al. (2003). Therefore, the source function should also correlate with the same raised power of wind speed as shown in Eq. (4.2). For those size ranges that SSA makes a significant contribution to aerosol populations, the aerosol number concentration should be well correlated to the 3rd power of wind speed based on Eq. (4.2). Other than that, there is also an energy flux consideration from wind to the waves, as pointed out by Wu (1982) in defending a slightly different form of whitecap function from Eq. (4.2). Energy carried by the wind is proportional to the cube of the wind speed. However, that is the total energy available carried by the wind. The extent to which the wind energy is utilized in generating whitecaps and whether or not a fixed fraction of wind energy can be used in generating whitecaps are both unknown. Nevertheless, a correlation between particle number concentration and cube of wind speed is expected to corroborate any source function evolved from Eq. (4.2). Based on our data, the correlation of the cube of wind speed and particles are not better than the wind itself. The random variations of a number of environmental parameters such as temperature and salinity may have caused this behavior (Martensson et al., 2003).

To reiterate, using our data we were unable to verify the actual dependence of source function of small particles on wind speed. This lack of details is also reflected in the similar correlation coefficients achieved between wind speed and the number, surface area and volume concentrations, as shown in Figure 4.3. Another reason of this inconsistence is that the particle loss rate of the sampling system dependent on its size may have a bearing on the relationship of wind speed and particle concentration.

4.3.3 Relationship between precipitation and particle concentration

The concentration of small particles and large particles are plotted against precipitation intensity are presented in Figure 4.5 and Figure 4.6, respectively. From Figure 4.5 we can conclude that smaller particles (<100 nm) are not correlated in any way with rain intensity, implying either a nonexistence of linear relationship or a lack of causal relationship. It is also possible that small particles are replenished from surrounding regions (horizontal and vertical) without precipitation (Clarke et al., 1997; Katoshevshi et al., 1999). However, from Figure 4.6 we can see that the number concentrations of large particles are significantly correlated with rain intensity positively, implying that precipitation is overall a source of SSA rather than a sink. Rain can generate SSA when they impinge the sea surface and remove SSA from MBL by direct scavenging (de Leeuw et al., 2011). Indirectly, raindrops can also influence SSA production by entraining bubbles, lowering the seawater salinity, changing the seawater temperature, as well as by interrupting the sea surface organic microlayer (Lewis and Schwartz, 2004). The positive correlation coefficients between particle concentrations measured by PAS and the rain intensity indicated that precipitation promote more SSA generation than removing it from MBL.

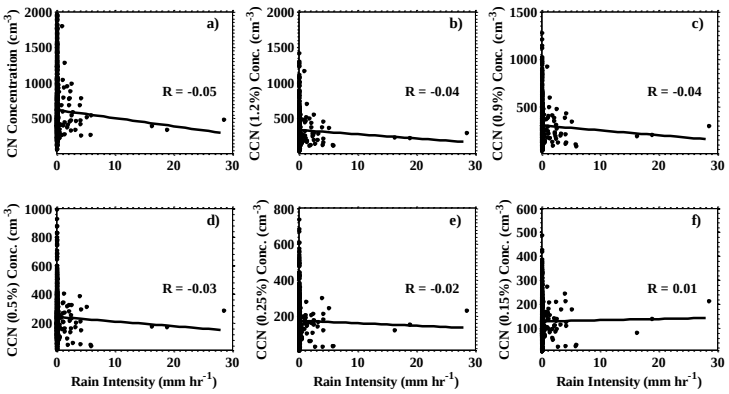

Figure 4.5 Scatterplots of particle concentrations measured by CPC (CN concentration) and CCN counter against rain intensity. Solid lines are fitted by least-squares method. Correlation coefficients are shown for each plot. Data points are averages of 27 min.

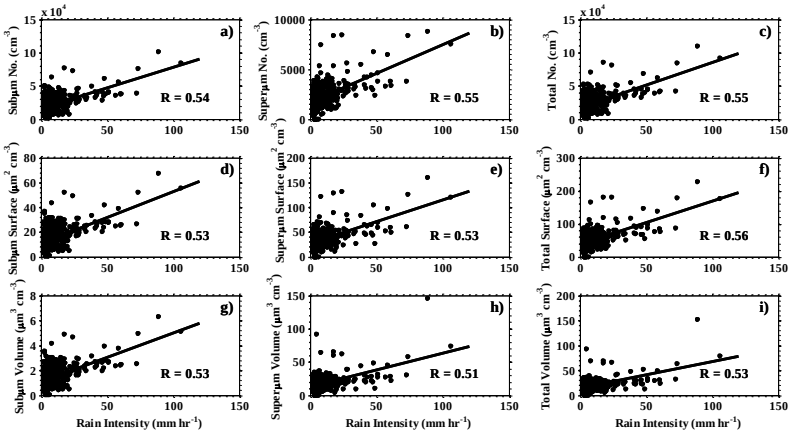

Figure 4.6 Scatterplots of particle concentrations measured by PAS against rain intensity. Panels (a-c) show the correlations of number concentration with rain intensity; Panels (d-f) show those between surface concentration and rain intensity; Panels (g-i) show those between volume concentration and rain intensity. Panels (a, d and g) present correlations for submicron particles (diameter between 0.3 and 1 micron); Panels (b, e and h) present correlations for supermicron particles (diameter between 1 and 20 micron); and panels (c, f and i) present correlations for all PAS particles (diameter between 0.3 and 20 micron). Solid lines are fitted by least-squares method. Correlation coefficients are shown for each plot. Data points are averages of 27 min data.

The correlation levels of size-segregated particle number concentration and rain intensity are presented in Figure 4.7. Particle concentration and precipitation rate become significantly correlated with each other when particle sizes increase to larger than 0.2 micron. The correlations are relatively constant between 0.2 and 3 micron. There are a few ways we can hypothesize the SSA production mechanisms due to precipitation. First, SSA production resulting from precipitation does not contain a significant fraction of particles smaller than 0.2 micron. Second, it is possible that SSA particles smaller than 0.2 micron produced by precipitation are significant but SSA production and removal by precipitation in the size range are comparable in magnitude and opposite in sign. Third, it is possible that precipitation produces SSA particles <0.2 micron but they only comprise a negligible fraction of marine aerosol in that range.

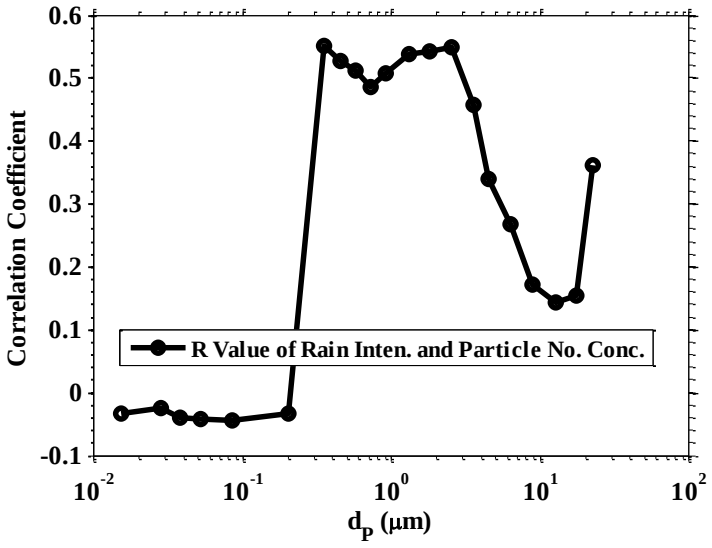

Figure 4.7 Correlation coefficients between particle concentrations with different sizes (as shown in abscissa) and rain intensity.

4.3.4 Relationship between sea surface pressure and particle concentration

Plots of the number concentrations of small particles (measured by CPC and CCN counter) and larger particles (measured by PAS) versus pressure are presented in Figure 4.8 and Figure 4.9, respectively. As shown in the previous chapter, the correlation between small particles and pressure is significant (R value of logarithm of CN vs. pressure is 0.78) when there is an apparent pressure change (about 2% change within one day). We attribute such change to the much higher concentration of small particles in upper troposphere than in MBL (entrainment from UT to MBL indicated by pressure level). However, the correlation evades when apply to all the dataset. That is understandable because other factors overwhelm the influence of entrainment on concentration of small particles. This also implies the inadequacy of representing particle concentration of small particles by sea surface pressure alone. On the contrary, the correlations between particle concentration of large particles and pressure are weak but sometimes visible (R value -0.06 to -0.3). The negative correlation between them is due to the combined effect of positive correlation between particle and wind speed, and the inherent negative correlation between wind speed and pressure (Deng et al., 2013b).

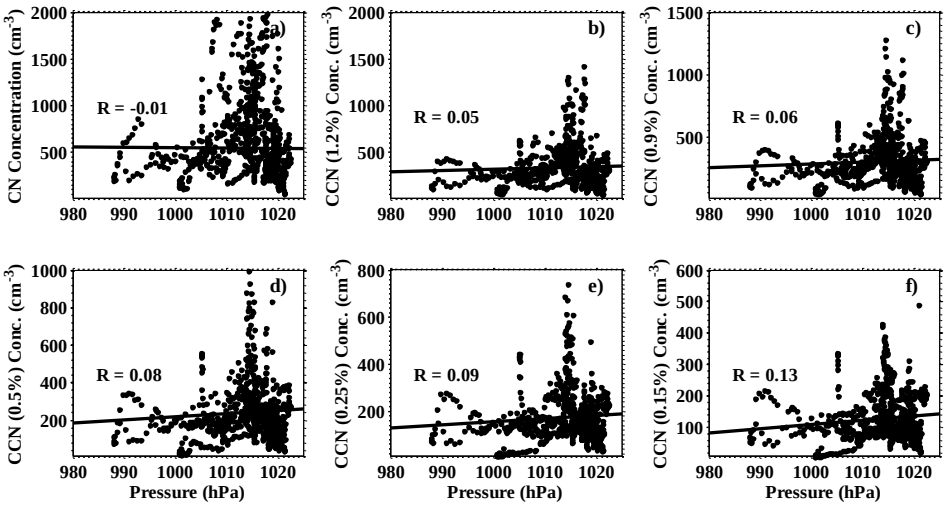

Figure 4.8 Scatterplots of particle concentrations measured by CPC (CN concentration) and CCN counter against sea surface pressure. Solid lines are fitted by least squares method. Correlation coefficients are shown for each plot.

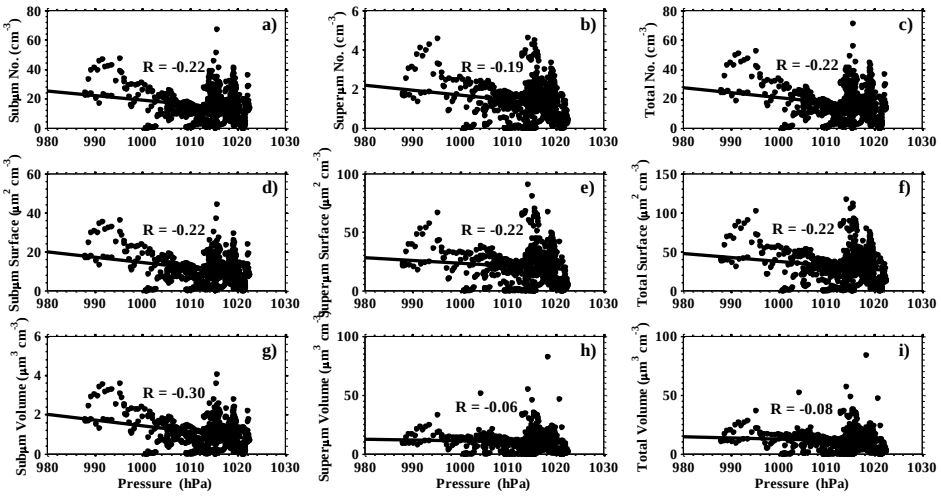

Figure 4.9 Scatterplots of particle concentrations measured by PAS against sea surface pressure. Panels (a-c) show the correlations of number concentration with pressure; Panels (d-f) show those between aerosol surface area concentration and pressure; Panels (g-i) show those between volume concentration and pressure. Panels (a, d and g) present correlations for submicron particles (diameter between 0.3 and 1 micron); Panels (b, e and h) present correlations for supermicron particles (diameter between 1 and 20 micron); and panels (c, f and i) present correlations for all PAS particles (diameter between 0.3 and 20 micron). Solid lines are fitted by least squares method. Correlation coefficients are shown for each plot.

4.3.5 Case studies

In Figure 4.10 we plotted number concentrations of small particle against wind speed during a special period during which the pressure change is significant. It is visible from Figure 4.1 that the concentrations from CPC and CCN followed the trend of pressure rather than wind speed. That reinforced our hypothesis about the claims of small SSA particles. From Figure 10 we see that small particle numbers are negatively significantly correlated with wind speed. That is explainable because pressure and number concentration of small particles are positively

correlated (as shown in the previous chapter), while pressure and wind speed is positively correlated. However, there is no physical basis to explain the negative correlation between pressure and number concentration of small aerosols directly. We can also notice that the magnitude of the negative correlation is decreasing with increasing particle size (decreasing SS level from CCN data, as shown in Table 4.1). This reinforces the above evidence that pressure has a larger influence on smaller particles, and that wind speed has larger impact on larger particles.

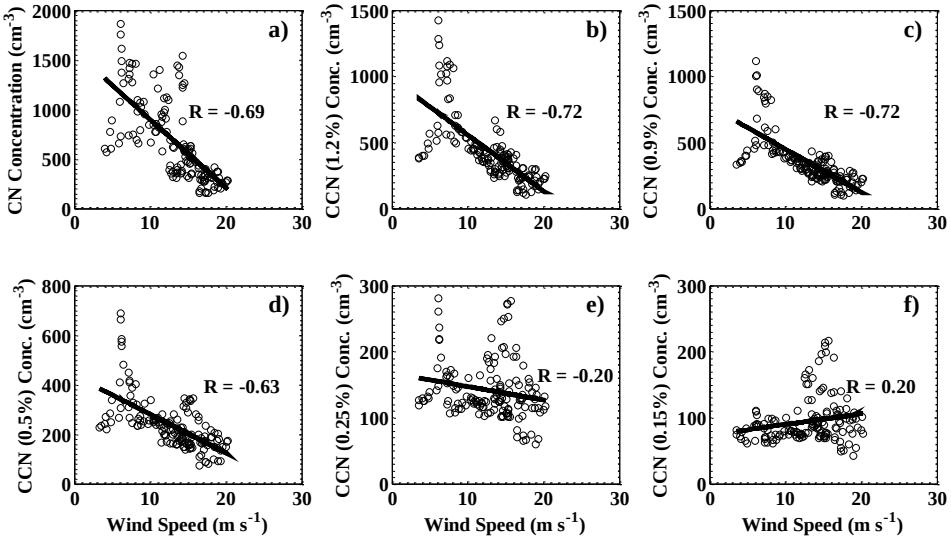

Figure 4.10 Scatterplots of number concentration of small particles against wind speed during station V, a period with significant pressure change.

4.3.6 Further analysis and future research demands

From the correlations between particle number concentrations and wind speed above, as well as those between number concentrations and precipitation, we hypothesized either the

possibility of a limited fraction small SSA particles in marine aerosol or a different source function of small SSA aerosols from large aerosols, over the North Atlantic open ocean. However, multiple investigations support the presence of primary marine aerosols smaller than 0.2 micron using sophisticated single particle detection techniques in both field and laboratory (O'Dowd and Smith, 1993; Martensson et al., 2003*;* O'Dowd et al., 2004; Clarke et al., 2006; Bigg 2007; Bigg and Leck, 2008; Prather et al., 2013; Ault et al., 2013). Among them, O'Dowd and Smith (1993) found a significant correlation between primary marine particles down to 0.05 micron and wind speed for air masses over the Northeast Atlantic. Clarke et al. (2006) were able to derive a sea salt flux parameterized on wind speed for particles down to 0.01 micron from open ocean air masses measured in a Hawaii station. They also reported a contribution of 5-90% to marine CCN by those small sea salt particles, with the remaining part mainly from UT entrainment of particles resulting from new particle formation. On the contrary, Bigg (2007) found no sea salt particles smaller than 200 nm during their 6 years of sampling in Cape Grim. Instead, they found the particles smaller than 200 nm are microgels resulting from marine microorganisms and their fraction without any association with sea salts (Bigg and Leck, 2008), while Prather and colleagues found mixtures of sea salt and organic carbon in particles smaller than 200 nm (Prather et al., 2013; Ault et al., 2013). Therefore, the clear understanding of production and characteristics of SSA smaller than 200 nm requires more sophisticated studies. The contribution of sea salt particles to the local marine aerosol for sizes < 200 nm is determined by a number of factors, including the production mechanism of these small SSA aerosols (Martensson et al., 2003), local primary production level (Bigg 2007), surfactant levels (Sellegri et al., 2006), sea surface salinity and temperature (Martensson et al., 2003), entrainment levels (Raes 1995; Deng et al., 2013b), influences from continental and anthropogenic sources, and wind conditions.

Among the above mentioned factors, the production mechanisms of primary marine particles need to be understood with first priority. The question should be answered from three aspects. First, since these small sea salt particles are much less frequently observed than larger ones over the open ocean, are the small sea salt particles generated the same way as large sea salt particles from bubble bursting processes? For the first question, Martensson et al. (2003) indicated the possibility that the droplet formation process of sea salt particles smaller than 200 nm are different from those large than that size, based on different influence of salinity on them. Second, are those organic aerosols, which have an increasing and overwhelming fraction with decreasing sizes, produced the same way as the large sea salt particles from bubble bursting processes? For the second question, Bigg (2007) indicated that the gel-like organic particles smaller than 200 nm could also be injected from the oceanic surface microlayer in the bubbling process. Third, are the small SSA, i.e., mixtures of sea salts and organics, produced the same way as large sea salt particles? For the third question, recent laboratory studies indicated the high possibility of different production processes of mixed sea salt and organic particles, with shapes of those particles changed from more cubic to more rounded with decreasing sizes (Ault et al., 2013), accompanying with an increasing fraction of organic species (O'Dowd et al., 2004; Ault et al., 2013).

Therefore, investigations should be carried out in the following directions: (1) Using microscopic techniques to monitor SSA particle evolution processes in laboratory environments, for both small and large particles, as well as for both pure sea salt particles and those containing organic components. (2) Investigate if there are chemical processes other than physical processes (e.g. crystallization) responsible for small SSA evolution after bubbles burst. (3) Using an atomic structure detection technique such as x-ray diffraction (XRD) to determine the atomic arrangement of small sea salt particles mixed with organic species. Sea salt particles (mainly

composed by NaCl) are cubic since the NaCl crystals possess a face centered cubic (fcc) structure. Since the small SSA particles containing organic species present themselves as a rounded shape, the crystallization of NaCl must have be altered significantly and it would be worthwhile to investigate how it is changed.

4.4 Summary and atmospheric implication

Through the analysis of marine aerosol concentrations within different size ranges and several meteorological parameters, a set of hypotheses are presented and several suggestions for future relevant researches were proposed. Based on our data, it is either that small SSA particles (<200 nm) do not contribute significantly to marine aerosol number concentration or that small SSA particles are produced in a different way from large SSA particles so that their number concentrations is not correlated with wind speed, at least over the North Atlantic open ocean during summer. Identification of the formation processes of these small SSA particles is important for assessments of the direct and indirect effect of aerosols on climate. It is also important to understand how organic species are transferred from oceanic surface to the marine atmosphere in addition to understanding their hygroscopic properties. Not until we understand their production processes could we represent their flux from sea to air correctly. Small particles tend to dominate marine aerosol number concentration. Since CCN property could be influenced more by particle number than mass, understanding the factors which control small SSA particle concentration is key to determining indirect radiative forcing on global climate.

5. CONCLUSIONS AND FUTURE DIRECTIONS

Two cruise researches were carried out to study the chemical composition and cloud nucleation ability of marine aerosol, one carried out over Pacific Ocean during March to April of 2010 and another over North Atlantic Ocean during June to July of 2011. The purpose of the HaloCAST cruise over the Pacific Ocean was to study the chemical composition and mixing state of marine aerosol. The Atlantic cruise was mainly used to study the cloud nucleation ability of marine aerosol under a wide range of DMS concentrations. An additional goal of the Atlantic cruise was to analyze the sea spray aerosol production under various meteorological conditions.

5.1 Chemical composition and mixing states of Pacific marine aerosol

Raman microspectroscopy was utilized to determine that long chain organic compounds were consistently a major component in Pacific marine aerosol. Analysis of aerosol composition on the ~11,000 km HaloCAST cruise indicated that long chain organic species were the most common aerosol composition observed. This result corroborates previous reports of high concentrations of organics in marine aerosol, and extends previous knowledge in several significant ways. Our data include the aerosol composition, concentration and cloud nucleation ability in the marine boundary layer over understudied areas in the Pacific Ocean. While most previous reports have focused on organics found in submicron aerosols, our collection technique included coarse mode aerosol (>1.0 μm diameter). The percentage of particles containing pure and predominately long chain organics were 8% or more and 28% or more for all conditions in both the Northern and Southern Hemispheres. The prevalence of organics observed in samples far removed from continental anthropogenic effects strongly suggests a marine source. Also, these organic components were detected in autumn (in the Southern Hemisphere) and in spring

(in the Northern hemisphere), suggesting that organics may be present throughout much of the annual cycle.

Water soluble inorganic species such as sulfate and nitrate were observed in higher frequency in the northern segments of the open ocean cruise track, possibly suggesting a stronger influence from anthropogenic activity in the northern hemisphere.

Despite the insensitivity of Raman to some compounds, the majority of particles collect in this Pacific cruise were classified as internally mixed. Long chain organics were found in mixtures with other compounds 57 to 72% of the time. Based on our observations, long chain organic species tended to be mixed most often with HULIS, and frequently with other organic and inorganic species.

Both the consistent prevalence of long chain organic species throughout the wide range of conditions and locations sampled during this cruise indicate that organics must be considered in modeling studies of marine aerosol. Furthermore, the variable composition and mixing states observed here suggest a need to treat marine organic aerosol in a more detailed manner for accurate modeling of the role of marine aerosols in cloud formation and climate. The complex marine aerosol composition and prevalence of organic aerosols must be considered in assessments of marine aerosol direct and indirect effects on climate.

5.2 Aerosol and CCN concentration under high DMS concentrations

Aerosol and CCN concentrations under a wide range of conditions, including extremely high DMS levels (1800 pptv), were measured during the Bloomcruise research. Our data shows that, atmospheric aerosol in the North Atlantic were signicantly influenced by continental air mass, even over remote regions. The average aerosol number concentration influenced by

continental air mass was 115% higher than pristine marine aerosols, while that by coastal air mass has an enhancement of 44% compared with pristine air. On the contrary, in continental and coastal air masses, CCN concentrations are decreased by 18% and 19%, at the SS level of 0.15%, a SS level typical of marine stratiform clouds. While total aerosol concentrations are elevated due to continental polluation, the number of aersosol capabile of forming cloud drops is not nesseaily increased and in some instances, is lower than in marine air. Esimated oxidation rates based on measured DMS concentrations illustrated influence of anthropogenic acitivities on marine atmosphere. Overall, the oxidation rate of DMS during nighttime is 85% of that during daytime. Therefore, continental or anthropogenical sources generally provide aerosols of decreased cloud activation potential in marine boundary layer over the North Atlantic Ocean during summer.

In the Bloomcruise research which is the first to report the aerosol and CCN concentration during such a high DMS level as 1800 pptv. The highest DMS was observed when the atmospehre is not influenced by continental air mass. In the two-day sustained nucleation event, we estimate that the sulfuric acid concentration derived from DMS concentration is adequate to explain the observed particle concentration by nucleation. Therefore, the importance of contributions from marine biota to atmospheric aerosols are significant, at least over the North Atlantic and during summer season when phytoplankton blooms are frequent.

In addition, our measurements indicate that meteorological parameters play an important role in the modificaiton of cloud nucleation ability of marine aerosols. Increases in sea surface pressure may correspond to downward vertical air movement which bring increases in total aerosol concentrations due to the much higher nucleation mode particle concentration in upper troposphere than in marine boundary layer.

5.3 Sea spray aerosol production by wind and precipitation

Through the analysis of marine aerosol concentrations within different size ranges and several meteorological parameters, a set of hypotheses are presented and several suggestions for future relevant researches were proposed. Based on our data, either small sea spray aerosol (SSA) particles (<200 nm) do not contribute significantly to marine aerosol number concentration or small SSA particles are produced in a different way from large SSA particles so that their number concentrations is not correlated with wind speed, at least over the North Atlantic open ocean during summer. Identification of the formation processes of these small SSA particles is important for assessments of the direct and indirect effect of aerosols on climate. In addition, until we understand the production processes of sea spray aerosol, we cannot parameterize their flux from sea to air correctly. Small particles tend to dominate marine aerosol number concentration. Since CCN property is influenced more by particle number than mass, understanding the factors which control small SSA particle concentration is key to determining indirect radiative forcing on global climate.

5.4 Future research directions

Field studies covering more meteorological and environmental conditions will be complementary to Bloomcruise and HaloCAST cruise researches. More CCN measurements are also wanted to understand cloud nucleation ability of marine aerosol in deeper extent, especially under an ever-increasingly polluted world.

The uncertainty of the generation and mixing state of sea spray aerosol with dry diameter smaller than 200 nm is vital to better evaluate the direct radiative forcing on global climate, in both its accuracy and precision. In spite of significant progress made in recent years,

more laboratory and filed studies are required to understand those small SSA particles and their generation mechanism.

REFERENCES

ABBATT, J. P. D., BROEKHUIZEN, K. & KUMAL, P. P. 2005. Cloud condensation nucleus activity of internally mixed ammonium sulfate/organic acid aerosol particles. *Atmospheric Environment,* 39**,** 4767-4778.

AHLM, L., LIU, S., DAY, D. A., RUSSELL, L. M., WEBER, R., GENTNER, D. R., GOLDSTEIN, A. H., DIGANGI, J. P., HENRY, S. B., KEUTSCH, F. N., VANDENBOER, T. C., MARKOVIC, M. Z., MURPHY, J. G., REN, X. R. & SCHELLER, S. 2012. Formation and growth of ultrafine particles from secondary sources in Bakersfield, California. *Journal of Geophysical Research-Atmospheres,* 117, 1-13.

AITKEN, J. 1880. On dust, fogs, and clouds. *Trans. R. Soc. Edinburgh 30,* 337-368.

ALLER, J. Y., KUZNETSOVA, M. R., JAHNS, C. J. & KEMP, P. F. 2005. The sea surface microlayer as a source of viral and bacterial enrichment in marine aerosols. *Journal of Aerosol Science,* 36**,** 801-812.

ANDREAE, M. O., ELBERT, W. & DEMORA, S. J. 1995. Biogenic sulfur emissions and aerosols over the tropical South Atlantic 3. Atmospheric dimethylsulfide, aerosols and cloud condensation nuclei. *Journal of Geophysical Research-Atmospheres,* 100**,** 11335-11356.

ANDREAE, M. O. & CRUTZEN, P. J. 1997. Atmospheric aerosols: Biogeochemical sources and role in atmospheric chemistry. *Science,* 276**,** 1052-1058.

ANDREAE, M. O., ELBERT, W., CAI, Y., ANDREAE, T. W. & GRAS, J. 1999. Non-sea-salt sulfate, methanesulfonate, and nitrate aerosol concentrations and size distributions at

Cape Grim, Tasmania. *Journal of Geophysical Research-Atmospheres,* 104**,** 21695-21706.

ANDREAE, M. O. & ROSENFELD, D. 2008. Aerosol-cloud-precipitation interactions. Part 1. The nature and sources of cloud-active aerosols. *Earth-Science Reviews,* 89**,** 13-41.

ARSENE, C., BARNES, I. & BECKER, K. H. 1999. FT-IR product study of the photo-oxidation of dimethyl sulfide: Temperature and O-2 partial pressure dependence. *Physical Chemistry Chemical Physics,* 1**,** 5463-5470.

ARSENE, C., BARNES, I., OLARIU, R. I. & BECKER, K. H. 2005a. Dimethyl sulphide photo-oxidation at various NO2 concentrations. 1 Product study and mechanistic investigation. *Revue Roumaine De Chimie,* 50**,** 359-369.

ARSENE, C., OLARIU, R. I. & BARNES, I. 2005b. Dimethyl sulphide photo-oxidation at various NO2 concentrations. 2 Investigation on particle formation. *Revue Roumaine De Chimie,* 50**,** 485-490.

ASA-AWUKU, A., NENES, A., GAO, S., FLAGAN, R. C. & SEINFELD, J. H. 2010. Water-soluble SOA from Alkene ozonolysis: composition and droplet activation kinetics inferences from analysis of CCN activity. *Atmospheric Chemistry and Physics,* 10**,** 1585-1597.

AULT, A. P., MOFFET, R. C., BALTRUSAITIS, J., COLLINS, D. B., RUPPEL, M. J., CUADRA-RODRIGUEZ, L. A., ZHAO, D. F., GUASCO, T. L., EBBEN, C. J., GEIGER, F. M., BERTRAM, T. H., PRATHER, K. A. & GRASSIAN, V. H. 2013. Size-dependent changes in sea spray aerosol composition and properties with different seawater conditions. *Environmental Science & Technology,* 47**,** 5603-5612.

AVZIANOVA, E. & BROOKS, S. D. 2013. Raman spectroscopy of glyoxal oligomers in aqueous solutions. *Spectrochimica Acta Part a-Molecular and Biomolecular Spectroscopy,* 101**,** 40-48.

AYERS, G. P., PENKETT, S. A., GILLETT, R. W., BANDY, B., GALBALLY, I. E., MEYER, C. P., ELSWORTH, C. M., BENTLEY, S. T. & FORGAN, B. W. 1992. Evidence for photochemical control of ozone concentrations in unpolluted marine air. *Nature,* 360**,** 446-449.

AYERS, G. P., CAINEY, J. M., GILLETT, R. W. & IVEY, J. P. 1997. Atmospheric sulphur and cloud condensation nuclei in marine air in the Southern Hemisphere. *Philosophical Transactions of the Royal Society of London Series B-Biological Sciences,* 352**,** 203-211.

AYERS, G. P. & CAINEY, J. M. 2007. The CLAW hypothesis: a review of the major developments. *Environmental Chemistry,* 4**,** 366-374.

AZATYAN, V. V., KALKANOV, V. A. & SHAVARD, A. A. 1980. Mechanism of silane oxidation. *Reaction Kinetics and Catalysis Letters,* 15**,** 367-372.

BANDY, A., THORNTON, D. C., BLOMQUIST, B. W., CHEN, S., WADE, T. P., IANNI, J. C., MITCHELL, G. M. & NADLER, W. 1996. Chemistry of dimethyl sulfide in the equatorial Pacific atmosphere. *Geophysical Research Letters,* 23**,** 741-744.

BANDY, A., FALOONA, I. C., BLOMQUIST, B. W., HUEBERT, B. J., CLARKE, A. D., HOWELL, S. G., MAULDIN, R. L., CANTRELL, C. A., HUDSON, J. G., HEIKES, B. G., MERRILL, J. T., WANG, Y. H., O'SULLIVAN, D. W., NADLER, W. & DAVIS, D. D. 2011. Pacific Atmospheric Sulfur Experiment (PASE): dynamics and chemistry of the south Pacific tropical trade wind regime. *Journal of Atmospheric Chemistry,* 68**,** 5-25.

BARLETTA, R. E. 2012. Raman analysis of blue ice tephra: an approach to tephrachronological dating of ice cores. *Antarctic Science,* 24**,** 202-208.

BARNES, I., BECKER, K. H. & PATROESCU, I. 1996. FTIR product study of the OH initiated oxidation of dimethyl sulphide: Observation of carbonyl sulphide and dimethyl sulphoxide. *Atmospheric Environment,* 30**,** 1805-1814.

BARNES, I., HJORTH, J. & MIHALOPOULOS, N. 2006. Dimethyl sulfide and dimethyl sulfoxide and their oxidation in the atmosphere. *Chemical Reviews,* 106**,** 940-975.

BATES, T. S., ANDERSON, T. L., BAYNARD, T., BOND, T., BOUCHER, O., et al. 2006. Aerosol direct radiative effects over the northwest Atlantic, northwest Pacific, and North Indian Oceans: estimates based on in-situ chemical and optical measurements and chemical transport modeling. *Atmospheric Chemistry and Physics,* 6**,** 1657-1732.

BATES, T. S., QUINN, P. K., FROSSARD, A. A., RUSSELL, L. M., HAKALA, J., et al. 2012. Measurements of ocean derived aerosol off the coast of California. *Journal of Geophysical Research-Atmospheres,* 117, 1-13.

BAUMGARDNER, D., JONSSON, H., DAWSON, W., O'CONNOR, D. & NEWTON, R. 2001. The cloud, aerosol and precipitation spectrometer: A new instrument for cloud investigations. *Atmospheric Research,* 59**,** 251-264.

BAUSTIAN, K. J., CZICZO, D. J., WISE, M. E., PRATT, K. A., KULKARNI, G., HALLAR, A. G. & TOLBERT, M. A. 2012. Importance of aerosol composition, mixing state, and morphology for heterogeneous ice nucleation: A combined field and laboratory approach. *Journal of Geophysical Research-Atmospheres,* 117, 1-13.

BIGG, E. K. 2007. Sources, nature and influence on climate of marine airborne particles. *Environmental Chemistry,* 4**,** 155-161.

BIGG, E. K. & LECK, C. 2008. The composition of fragments of bubbles bursting at the ocean surface. *Journal of Geophysical Research-Atmospheres,* 113, 1-7.

BLANCHARD, D. C. & WOODCOCK, A. H. 1957. Bubble formation and modification in the sea and its meteorological significance. *Tellus,* 9**,** 145-158.

BLANCHARD, D. C. 1963. The electrification of the atmosphere by particles from bubbles in the sea. *Progress in Oceanography,* 1**,** 71-202.

BLANCHARD, D. C. 1964. Sea-to-air transport of surface active material. *Science,* 146**,** 396-397.

BLANCHARD, D. C. & SYZDEK, L. 1970. Mechanism for water-to-air transfer and concentration of bacteria. *Science,* 170**,** 626-627.

BLANCHARD, D. C. & SYZDEK, L. D. 1982. Water-to-air transfer and enrichment of bacteria in drops from bursting bubbles. *Applied and Environmental Microbiology,* 43**,** 1001-1005.

BLANCHARD, D. C. 1983. The production, distribution and bacterial enrichment of the sea-salt aerosol. *In:* LISS, P. S. & SLINN, W. G. N. (eds.) *The Air-Sea Exchanges of Gases and Particles.* Norwell, Mass.: D. Reidel.

BOERS, R. & BETTS, A. K. 1988. Saturation point structure of marine stratocumulus clouds. *Journal of the Atmospheric Sciences,* 45**,** 1156-1175.

BREIDER, T. J., CHIPPERFIELD, M. P., RICHARDS, N. A. D., CARSLAW, K. S., MANN, G. W. & SPRACKLEN, D. V. 2010. Impact of BrO on dimethylsulfide in the remote marine boundary layer. *Geophysical Research Letters,* 37, 1-6.

BROOKS, S. D., GONZALES, M. & FARIAS, R. 2009. Using surface tension measurements to understand how pollution can influence cloud formation, fog, and precipitation. *Journal of Chemical Education,* 86**,** 838-841.

CAVALLI, F., FACCHINI, M. C., DECESARI, S., MIRCEA, M., EMBLICO, L., FUZZI, S., CEBURNIS, D., YOON, Y. J., O'DOWD, C. D., PUTAUD, J. P. & DELL'ACQUA, A.

2004. Advances in characterization of size-resolved organic matter in marine aerosol over the North Atlantic. *Journal of Geophysical Research-Atmospheres,* 109, 1-14.

CEBURNIS, D., O'DOWD, C. D., JENNINGS, G. S., FACCHINI, M. C., EMBLICO, L., DECESARI, S., FUZZI, S. & SAKALYS, J. 2008. Marine aerosol chemistry gradients: Elucidating primary and secondary processes and fluxes. *Geophysical Research Letters,* 35, 1-5.

CEBURNIS, D., GARBARAS, A., SZIDAT, S., RINALDI, M., FAHRNI, S., PERRON, N., WACKER, L., LEINERT, S., REMEIKIS, V., FACCHINI, M. C., PREVOT, A. S. H., JENNINGS, S. G., RAMONET, M. & O'DOWD, C. D. 2011. Quantification of the carbonaceous matter origin in submicron marine aerosol by C-13 and C-14 isotope analysis. *Atmospheric Chemistry and Physics,* 11**,** 8593-8606.

CHANG, R. Y. W., SJOSTEDT, S. J., PIERCE, J. R., PAPAKYRIAKOU, T. N., SCARRATT, M. G., MICHAUD, S., LEVASSEUR, M., LEAITCH, W. R. & ABBATT, J. P. D. 2011. Relating atmospheric and oceanic DMS levels to particle nucleation events in the Canadian Arctic. *Journal of Geophysical Research-Atmospheres,* 116, 1-10.

CHARLSON, R. J., LOVELOCK, J. E., ANDREAE, M. O. & WARREN, S. G. 1987. Oceanic phytoplankton, atmospheric sulfur, cloud albedo and climate. *Nature,* 326**,** 655-661.

CHEN, T. & JANG, M. 2012. Chamber simulation of photooxidation of dimethyl sulfide and isoprene in the presence of NOx. *Atmospheric Chemistry and Physics,* 12**,** 10257-10269.

CHIN, M., JACOB, D. J., GARDNER, G. M., FOREMANFOWLER, M. S., SPIRO, P. A. & SAVOIE, D. L. 1996. A global three-dimensional model of tropospheric sulfate. *Journal of Geophysical Research-Atmospheres,* 101**,** 18667-18690.

CIURARU, R., GOSSELIN, S., VISEZ, N. & PETITPREZ, D. 2011. Heterogeneous reactivity of chlorine atoms with sodium chloride and synthetic sea salt particles. *Physical Chemistry Chemical Physics,* 13**,** 19460-19470.

CLARKE, A. D. 1993. Atmospheric nuclei in the Pacific midtroposphere: Their nature, concentration, and evolution. *Journal of Geophysical Research-Atmospheres,* 98**,** 20633-20647.

CLARKE, A. D., UEHARA, T. & PORTER, J. N. 1997. Atmospheric nuclei and related aerosol fields over the Atlantic: Clean subsiding air and continental pollution during ASTEX. *Journal of Geophysical Research-Atmospheres,* 102**,** 25281-25292.

CLARKE, A. D., VARNER, J. L., EISELE, F., MAULDIN, R. L., TANNER, D. & LITCHY, M. 1998a. Particle production in the remote marine atmosphere: Cloud outflow and subsidence during ACE 1. *Journal of Geophysical Research-Atmospheres,* 103**,** 16397-16409.

CLARKE, A. D., DAVIS, D., KAPUSTIN, V. N., EISELE, F., CHEN, G., et al. 1998b. Particle nucleation in the tropical boundary layer and its coupling to marine sulfur sources. *Science,* 282**,** 89-92.

CLARKE, A. D., OWENS, S. R. & ZHOU, J. C. 2006. An ultrafine sea-salt flux from breaking waves: Implications for cloud condensation nuclei in the remote marine atmosphere. *Journal of Geophysical Research-Atmospheres,* 111, 1-14.

COVERT, D. S., KAPUSTIN, V. N., QUINN, P. K. & BATES, T. S. 1992. New particle formation in the marine boundary layer. *Journal of Geophysical Research-Atmospheres,* 97**,** 20581-20589.

CROPP, R. A., GABRIC, A. J., MCTAINSH, G. H., BRADDOCK, R. D. & TINDALE, N. 2005. Coupling between ocean biota and atmospheric aerosols: Dust, dimethylsulphide, or artifact? *Global Biogeochemical Cycles,* 19, 1-13.

CROPP, R., NORBURY, J. & BRADDOCK, R. 2007. Dimethylsulphide, clouds, and phytoplankton: Insights from a simple plankton ecosystem feedback model. *Global Biogeochemical Cycles,* 21, 1-17.

CUNLIFFE, M., SALTER, M., MANN, P. J., WHITELEY, A. S., UPSTILL-GODDARD, R. C. & MURRELL, J. C. 2009. Dissolved organic carbon and bacterial populations in the gelatinous surface microlayer of a Norwegian fjord mesocosm. *Fems Microbiology Letters,* 299**,** 248-254.

CUNLIFFE, M. & MURRELL, J. C. 2010. Eukarya 18S rRNA gene diversity in the sea surface microlayer: implications for the structure of the neustonic microbial loop. *Isme Journal,* 4**,** 455-458.

CUNLIFFE, M., ENGEL, A., FRKA, S., GASPAROVIC, B., GUITART, C., MURRELL, J. C., SALTER, M., STOLLE, C., UPSTILL-GODDARD, R. & WURL, O. 2013. Sea surface microlayers: A unified physicochemical and biological perspective of the air-ocean interface. *Progress in Oceanography,* 109**,** 104-116.

DALL'OSTO, M., CEBURNIS, D., MARTUCCI, G., BIALEK, J., DUPUY, R., JENNINGS, S. G., BERRESHEIM, H., WENGER, J., HEALY, R., FACCHINI, M. C., RINALDI, M., GIULIANELLI, L., FINESSI, E., WORSNOP, D., EHN, M., MIKKILA, J., KULMALA, M. & O'DOWD, C. D. 2010. Aerosol properties associated with air masses arriving into the North East Atlantic during the 2008 Mace Head EUCAARI intensive observing period: An overview. *Atmospheric Chemistry and Physics,* 10**,** 8413-8435.

DARQUENNE, C. 2012. Aerosol deposition in health and disease. *Journal of Aerosol Medicine and Pulmonary Drug Delivery*, 25**,** 140-147.

DE BRUYN, W. J., BATES, T. S., CAINEY, J. M. & SALTZMAN, E. S. 1998. Shipboard measurements of dimethyl sulfide and SO2 southwest of Tasmania during the First Aerosol Characterization Experiment (ACE 1). *Journal of Geophysical Research-Atmospheres,* 103**,** 16703-16711.

DE BRUYN, W. J., DAHL, E. & SALTZMAN, E. S. 2006. DMS and SO2 measurernents in the tropical marine boundary layer. *Journal of Atmospheric Chemistry,* 53**,** 145-154.

DE LEEUW, G., ANDREAS, E. L., ANGUELOVA, M. D., FAIRALL, C. W., LEWIS, E. R., O'DOWD, C., SCHULZ, M. & SCHWARTZ, S. E. 2011. Production flux of sea spray aerosol. *Reviews of Geophysics,* 49, 1-39.

DEBOUDT, K., FLAMENT, P., CHOEL, M., GLOTER, A., SOBANSKA, S. & COLLIEX, C. 2010. Mixing state of aerosols and direct observation of carbonaceous and marine coatings on African dust by individual particle analysis. *Journal of Geophysical Research-Atmospheres,* 115, 1-14.

DECESARI, S., MIRCEA, M., CAVALLI, F., FUZZI, S., MORETTI, F., TAGLIAVINI, E. & FACCHINI, M. C. 2007. Source attribution of water-soluble organic aerosol by nuclear magnetic resonance spectroscopy. *Environmental Science & Technology,* 41**,** 2479-2484.

DENG, C., BROOKS, S. D., VIDAURRE, G., and THORNTON, D. C.O. 2013a. Using Raman microspectroscopy to determine chemical composition and mixing state of airborne marine aerosols over the Pacific Ocean, Aerosol Science and Technology, in press.

DENG, C., BROOKS, S. D., THORNTON, D. C.O., BELL, T. G., SALZMAN, E. S., and DE BRYUN W. J. 2013b. Cloud condensation nuclei and aerosol concentrations under extremely high DMS levels over the North Atlantic Ocean, in preparation.

DIBB, J. E., SCHEUER, E., WHITLOW, S. I., VOZELLA, M., WILLIAMS, E. & LERNER, B. M. 2004. Ship-based nitric acid measurements in the gulf of Maine during New England Air Quality Study 2002. *Journal of Geophysical Research-Atmospheres,* 109, 1-13.

DIERSSEN, H. M. 2010. Perspectives on empirical approaches for ocean color remote sensing of chlorophyll in a changing climate. *Proceedings of the National Academy of Sciences of the United States of America,* 107**,** 17073-17078.

DORAISWAMY, P., HOGREFE, C., HAO, W., HENRY, R. F., CIVEROLO, K., KU, J.-Y., SISTLA, G., SCHWAB, J. J. & DEMERJIAN, K. L. 2009. A diagnostic comparison of measured and model-predicted speciated VOC concentrations. *Atmospheric Environment,* 43**,** 5759-5770.

DOYLE, G. J. 1961. Self-nucleation in sulfuric acid-water system. *Journal of Chemical Physics,* 35**,** 795-799.

Draxler, R.R. and Rolph, G.D.: HYSPLIT (HYbrid Single-Particle Lagrangian Integrated Trajectory) Model access via NOAA ARL READY Website (http://www.arl.noaa.gov/HYSPLIT.php). NOAA Air Resources Laboratory, College Park, MD., 2013.

DU, L., XU, Y., GE, M., JIA, L., YAO, L. & WANG, W. 2007. Rate constant of the gas phase reaction of dimethyl sulfide (CH3SCH3)with ozone. *Chemical Physics Letters,* 436**,** 36-40.

DUSEK, U., FRANK, G. P., HILDEBRANDT, L., CURTIUS, J., SCHNEIDER, J., WALTER, S., CHAND, D., DREWNICK, F., HINGS, S., JUNG, D., BORRMANN, S. & ANDREAE, M. O. 2006. Size matters more than chemistry for cloud-nucleating ability of aerosol particles. *Science,* 312**,** 1375-1378.

EISELE, F. L. & TANNER, D. J. 1993. Measurement of the gas-phase concentration of H2SO4 and methane sulfonic-acid and estimates of H2SO4 production and loss in the atmosphere. *Journal of Geophysical Research-Atmospheres,* 98**,** 9001-9010.

EYRING, V., ISAKSEN, I. S. A., BERNTSEN, T., COLLINS, W. J., CORBETT, J. J., ENDRESEN, O., GRAINGER, R. G., MOLDANOVA, J., SCHLAGER, H. & STEVENSON, D. S. 2010. Transport impacts on atmosphere and climate: Shipping. *Atmospheric Environment,* 44**,** 4735-4771.

FACCHINI, M. C., DECESARI, S., MIRCEA, M., FUZZI, S. & LOGLIO, G. 2000. Surface tension of atmospheric wet aerosol and cloud/fog droplets in relation to their organic carbon content and chemical composition. *Atmospheric Environment,* 34**,** 4853-4857.

FACCHINI, M. C., DECESARI, S., RINALDI, M., CARBONE, C., FINESSI, E., MIRCEA, M., FUZZI, S., MORETTI, F., TAGLIAVINI, E., CEBURNIS, D. & O'DOWD, C. D. 2008a. Important Source of Marine Secondary Organic Aerosol from Biogenic Amines. *Environmental Science & Technology,* 42**,** 9116-9121.

FACCHINI, M. C., RINALDI, M., DECESARI, S., CARBONE, C., FINESSI, E., MIRCEA, M., FUZZI, S., CEBURNIS, D., FLANAGAN, R., NILSSON, E. D., DE LEEUW, G., MARTINO, M., WOELTJEN, J. & O'DOWD, C. D. 2008b. Primary submicron marine aerosol dominated by insoluble organic colloids and aggregates. *Geophysical Research Letters,* 35, 1-5.

FAN, T. & TOON, O. B. 2011. Modeling sea-salt aerosol in a coupled climate and sectional microphysical model: mass, optical depth and number concentration. *Atmospheric Chemistry and Physics,* 11**,** 4587-4610.

FAUCHEREAU, N., TAGLIABUE, A., BOPP, L. & MONTEIRO, P. M. S. 2011. The response of phytoplankton biomass to transient mixing events in the Southern Ocean. *Geophysical Research Letters,* 38**,** 1-6.

FEREK, R. J., CHATFIELD, R. B. & ANDREAE, M. O. 1986. Vertical-distribution of dimethylsulfide in the marine atmosphere. *Nature,* 320**,** 514-516.

FRIEDLANDER, S. K. 1977. *Smoke, Dust, and Haze: Fundamentals of Aerosol Behaviors,* New York, Wiley-Interscience.

FUENTES, E., COE, H., GREEN, D., DE LEEUW, G. & MCFIGGANS, G. 2010. On the impacts of phytoplankton-derived organic matter on the properties of the primary marine aerosol - Part 1: Source fluxes. *Atmospheric Chemistry and Physics,* 10**,** 9295-9317.

FUENTES, E., COE, H., GREEN, D. & MCFIGGANS, G. 2011. On the impacts of phytoplankton-derived organic matter on the properties of the primary marine aerosol - Part 2: Composition, hygroscopicity and cloud condensation activity. *Atmospheric Chemistry and Physics,* 11**,** 2585-2602.

GALLAVARDIN, S., LOHMANN, U. & CZICZO, D. 2008. Analysis and differentiation of mineral dust by single particle laser mass spectrometry. *International Journal of Mass Spectrometry,* 274**,** 56-63.

GANTT, B., MESKHIDZE, N., FACCHINI, M. C., RINALDI, M., CEBURNIS, D. & O'DOWD, C. D. 2011. Wind speed dependent size-resolved parameterization for the organic mass fraction of sea spray aerosol. *Atmospheric Chemistry and Physics,* 11**,** 8777-8790.

GANTT, B., XU, J., MESKHIDZE, N., ZHANG, Y., NENES, A., GHAN, S. J., LIU, X., EASTER, R. & ZAVERI, R. 2012. Global distribution and climate forcing of marine

organic aerosol – Part 2: Effects on cloud properties and radiative forcing. *Atmos. Chem. Phys.,* 12**,** 6555-6563.

GANTT, B. & MESKHIDZE, N. 2013. The physical and chemical characteristics of marine primary organic aerosol: a review. *Atmospheric Chemistry and Physics,* 13**,** 3979-3996.

GASTON, C. J., FURUTANI, H., GUAZZOTTI, S. A., COFFEE, K. R., BATES, T. S., QUINN, P. K., ALUWIHARE, L. I., MITCHELL, B. G. & PRATHER, K. A. 2011. Unique ocean-derived particles serve as a proxy for changes in ocean chemistry. *Journal of Geophysical Research-Atmospheres,* 116, 1-13.

GEEVER, M., O'DOWD, C. D., VAN EKEREN, S., FLANAGAN, R., NILSSON, E. D., DE LEEUW, G. & RANNIK, U. 2005. Submicron sea spray fluxes. *Geophysical Research Letters,* 32, 1-4.

GERSHENZON, M., DAVIDOVITS, P., JAYNE, J. T., KOLB, C. E. & WORSNOP, D. R. 2001. Simultaneous uptake of DMS and ozone on water. *Journal of Physical Chemistry A,* 105**,** 7031-7036.

GHAN, S. J., LIU, X., EASTER, R. C., ZAVERI, R., RASCH, P. J., YOON, J. H. & EATON, B. 2012. Toward a minimal representation of aerosols in climate models: Comparative decomposition of aerosol direct, semidirect, and indirect radiative forcing. *Journal of Climate,* 25**,** 6461-6476.

GLAGOLENKO, S. & PHARES, D. J. 2004. Single-particle analysis of ultrafine aerosol in College Station, Texas. *Journal of Geophysical Research-Atmospheres,* 109, 1-12.

GODDIJN-MURPHY, L., WOOLF, D. K. & MARANDINO, C. 2012. Space-based retrievals of air-sea gas transfer velocities using altimeters: Calibration for dimethyl sulfide. *Journal of Geophysical Research-Oceans,* 117, 1-14.

GONG, S. L. 2003. A parameterization of sea-salt aerosol source function for sub- and super-micron particles. *Global Biogeochemical Cycles,* 17(4), 1-7.

GRAY, B. A., WANG, Y. H., GU, D. S., BANDY, A., MAULDIN, L., CLARKE, A., ALEXANDER, B. & DAVIS, D. D. 2011. Sources, transport, and sinks of SO2 over the equatorial Pacific during the Pacific Atmospheric Sulfur Experiment. *Journal of Atmospheric Chemistry,* 68**,** 27-53.

HANSELL, D. A., CARLSON, C. A., REPETA, D. J. & SCHLITZER, R. 2009. Dissolved organic matter in the ocean: A controversy stimulates new insights. *Oceanography,* 22**,** 202-211.

HASEGAWA, T. 2004. Structural analysis of biological aliphatic compounds using surface-enhanced Fourier transform Raman spectroscopy. *Biopolymers,* 73**,** 457-462.

HAWKINS, L. N. & RUSSELL, L. 2010. Polysaccharides, proteins, and phytoplankton fragments: Four chemically distinct types of marine primary organic aerosol classified by single particle spectromicroscopy. *Advances in Meteorology,* 2010, 1-14.

HEARD, D. E., READ, K. A., METHVEN, J., AL-HAIDER, S., BLOSS, W. J., et al. 2006. The North Atlantic Marine Boundary Layer Experiment (NAMBLEX). Overview of the campaign held at Mace Head, Ireland, in summer 2002. *Atmospheric Chemistry and Physics,* 6**,** 2241-2272.

HEGG, D. A., FEREK, R. J., HOBBS, P. V. & RADKE, L. F. 1991. Dimethyl sulfide and cloud condensation nucleus correlations in the northeast Pacific Ocean. *Journal of Geophysical Research-Atmospheres,* 96**,** 13189-13191.

HIRANUMA, N., BROOKS, S. D., GRAMANN, J. & AUVERMANN, B. W. 2011. High concentrations of coarse particles emitted from a cattle feeding operation. *Atmospheric Chemistry and Physics,* 11**,** 8809-8823.

HOPPEL, W. A., FRICK, G. M., FITZGERALD, J. & LARSON, R. E. 1994. Marine boundary layer measurements of new particle formation and the effects nonprecipitating clouds have on aerosol size distribution. *Journal of Geophysical Research-Atmospheres,* 99**,** 14443-14459.

HYVARINEN, A. R., LIHAVAINEN, H., GAMAN, A., VAIRILA, L., OJALA, H., KULMALA, M. & VIISANEN, Y. 2006. Surface tensions and densities of oxalic, malonic, succinic, maleic, malic, and cis-pinonic acids. *Journal of Chemical and Engineering Data,* 51**,** 255-260.

IPCC 2007. *Climate Change 2007: The Physical Science Basis. Contribution of Working Group I to the Fourth Assessment Report of the Intergovernmental Panel on Climate Change*. [SOLOMON, S., QIN, D., MANNING, M., CHEN, Z., MARQUIS, M., AVERYT, K. B., TIGNOR, M. & MILLER, H. L. (eds.)]. Cambridge, U. K.: Cambridge University Press.

IRWIN, M., GOOD, N., CROSIER, J., CHOULARTON, T. W. & MCFIGGANS, G. 2010. Reconciliation of measurements of hygroscopic growth and critical supersaturation of aerosol particles in central Germany. *Atmospheric Chemistry and Physics,* 10**,** 11737-11752.

IVLEVA, N. P., MCKEON, U., NIESSNER, R. & POSCHL, U. 2007. Raman microspectroscopic analysis of size-resolved atmospheric aerosol particle samples collected with an ELPI: Soot, humic-like substances, and inorganic compounds. *Aerosol Science and Technology,* 41**,** 655-671.

JACOB, D. J., HEIKES, B. G., FAN, S. M., LOGAN, J. A., MAUZERALL, D. L., BRADSHAW, J. D., SINGH, H. B., GREGORY, G. L., TALBOT, R. W., BLAKE, D. R. & SACHSE, G. W. 1996. Origin of ozone and NOx in the tropical troposphere: A

photochemical analysis of aircraft observations over the South Atlantic basin. *Journal of Geophysical Research-Atmospheres,* 101**,** 24235-24250.

JUNGE, C. E. 1956. Recent investigations in air chemistry. *Tellus,* 8**,** 127-139.

KAHN, R. A. 2012. Reducing the uncertainties in direct aerosol radiative forcing. *Surveys in Geophysics,* 33**,** 701-721.

KARL, M., LECK, C., GROSS, A. & PIRJOLA, L. 2012. A study of new particle formation in the marine boundary layer over the central Arctic Ocean using a flexible multicomponent aerosol dynamic model. *Tellus Series B-Chemical and Physical Meteorology,* 64, 1-24.

KARL, M., LECK, C., COZ, E. & HEINTZENBERG, J. 2013. Marine nanogels as a source of atmospheric nanoparticles in the high Arctic. *Geophysical Research Letters,* 40**,** 3738-3743.

KATOSHEVSKI, D., NENES, A. & SEINFELD, J. H. 1999. A study of processes that govern the maintenance of aerosols in the marine boundary layer. *Journal of Aerosol Science,* 30**,** 503-532.

KAVOURAS, I. G. & KOUTRAKIS, P. 2001. Use of polyurethane foam as the impaction substrate/collection medium in conventional inertial impactors. *Aerosol Science and Technology,* 34**,** 46-56.

KAWAMURA, K. & SAKAGUCHI, F. 1999. Molecular distributions of water soluble dicarboxylic acids in marine aerosols over the Pacific Ocean including tropics. *Journal of Geophysical Research-Atmospheres,* 104**,** 3501-3509.

KEENE, W. C., MARING, H., MABEN, J. R., KIEBER, D. J., PSZENNY, A. A. P., DAHL, E. E., IZAGUIRRE, M. A., DAVIS, A. J., LONG, M. S., ZHOU, X. L., SMOYDZIN, L. & SANDER, R. 2007. Chemical and physical characteristics of nascent aerosols produced

by bursting bubbles at a model air-sea interface. *Journal of Geophysical Research-Atmospheres,* 112, 1-16.

KERMINEN, V. M. & WEXLER, A. S. 1996. The occurrence of sulfuric acid-water nucleation in plumes: Urban environment. *Tellus Series B-Chemical and Physical Meteorology,* 48**,** 65-82.

KHAN, M. A. H., ASHFOLD, M. J., NICKLESS, G., MARTIN, D., WATSON, L. A., HAMER, P. D., WAYNE, R. P., CANOSA-MAS, C. E. & SHALLCROSS, D. E. 2008. Night-time NO3 and OH radical concentrations in the United Kingdom inferred from hydrocarbon measurements. *Atmospheric Science Letters,* 9**,** 140-146.

KING, S. M., ROSENOERN, T., SHILLING, J. E., CHEN, Q. & MARTIN, S. T. 2009. Increased cloud activation potential of secondary organic aerosol for atmospheric mass loadings. *Atmospheric Chemistry and Physics,* 9**,** 2959-2971.

KIRKEVAG, A., IVERSEN, T., SELAND, O., DEBERNARD, J. B., STORELVMO, T. & KRISTJANSSON, J. E. 2008. Aerosol-cloud-climate interactions in the climate model CAM-Oslo. *Tellus Series a-Dynamic Meteorology and Oceanography,* 60**,** 492-512.

KNIPPING, E. M., LAKIN, M. J., FOSTER, K. L., JUNGWIRTH, P., TOBIAS, D. J., GERBER, R. B., DABDUB, D. & FINLAYSON-PITTS, B. J. 2000. Experiments and simulations of ion-enhanced interfacial chemistry on aqueous NaCl aerosols. *Science,* 288**,** 301-306.

KOHLER, H. 1936. The nucleus in and the growth of hygroscopic droplets. *Transactions of the Faraday Society,* 32**,** 1152-1161.

KORHONEN, H., CARSLAW, K. S., SPRACKLEN, D. V., MANN, G. W. & WOODHOUSE, M. T. 2008. Influence of oceanic dimethyl sulfide emissions on cloud condensation nuclei concentrations and seasonality over the remote Southern Hemisphere oceans: A global model study. *Journal of Geophysical Research-Atmospheres,* 113, 1-16.

KRITZ, M. A. 1983. Use of long-lived radon daughters as indicators of exchange between the free troposphere and the marine boundary layer. *Journal of Geophysical Research-Oceans and Atmospheres,* 88**,** 8569-8573.

KRIVACSY, Z., KISS, G., CEBURNIS, D., JENNINGS, G., MAENHAUT, W., SALMA, I. & SHOOTER, D. 2008. Study of water-soluble atmospheric humic matter in urban and marine environments. *Atmospheric Research,* 87**,** 1-12.

KRUEGER, B. J., GRASSIAN, V. H., IEDEMA, M. J., COWIN, J. P. & LASKIN, A. 2003. Probing heterogeneous chemistry of individual atmospheric particles using scanning electron microscopy and energy-dispersive X-ray analysis. *Analytical Chemistry,* 75**,** 5170-5179.

KULMALA, M., TOIVONEN, A., MAKELA, J. M. & LAAKSONEN, A. 1998. Analysis of the growth of nucleation mode particles observed in Boreal forest. *Tellus Series B-Chemical and Physical Meteorology,* 50**,** 449-462.

KULMALA, M., DAL MASO, M., MAKELA, J. M., PIRJOLA, L., VAKEVA, M., AALTO, P., MIIKKULAINEN, P., HAMERI, K. & O'DOWD, C. D. 2001. On the formation, growth and composition of nucleation mode particles. *Tellus Series B-Chemical and Physical Meteorology,* 53**,** 479-490.

KULMALA, M., KERMINEN, V. M., ANTTILA, T., LAAKSONEN, A. & O'DOWD, C. D. 2004a. Organic aerosol formation via sulphate cluster activation. *Journal of Geophysical Research-Atmospheres,* 109, 1-7.

KULMALA, M., VEHKAMAKI, H., PETAJA, T., DAL MASO, M., LAURI, A., KERMINEN, V. M., BIRMILI, W. & MCMURRY, P. H. 2004b. Formation and growth rates of ultrafine atmospheric particles: A review of observations. *Journal of Aerosol Science,* 35**,** 143-176.

KULMALA, M., PETAJA, T., MONKKONEN, P., KOPONEN, I. K., DAL MASO, M., AALTO, P. P., LEHTINEN, K. E. J. & KERMINEN, V. M. 2005. On the growth of nucleation mode particles: Source rates of condensable vapor in polluted and clean environments. *Atmospheric Chemistry and Physics,* 5**,** 409-416.

KULMALA, M. & KERMINEN, V. M. 2008. On the formation and growth of atmospheric nanoparticles. *Atmospheric Research,* 90**,** 132-150.

LANA, A., SIMO, R., VALLINA, S. M. & DACHS, J. 2012. Potential for a biogenic influence on cloud microphysics over the ocean: A correlation study with satellite-derived data. *Atmospheric Chemistry and Physics,* 12**,** 7977-7993.

LARA, R. J. & THOMAS, D. N. 1995. Formation of recalcitrant organic matter: Humification dynamics of algal derived dissolved organic carbon and its hydrophobic fractions. *Marine Chemistry,* 51**,** 193-199.

LECK, C. & BIGG, E. K. 2005a. Biogenic particles in the surface microlayer and overlaying atmosphere in the central Arctic Ocean during summer. *Tellus Series B-Chemical and Physical Meteorology,* 57**,** 305-316.

LECK, C. & BIGG, E. K. 2005b. Source and evolution of the marine aerosol - A new perspective. *Geophysical Research Letters,* 32, 1-4.

LECK, C. & BIGG, E. K. 2007. A modified aerosol-cloud-climate feedback hypothesis. *Environmental Chemistry,* 4**,** 400-403.

LECK, C. & BIGG, E. K. 2008. Comparison of sources and nature of the tropical aerosol with the summer high Arctic aerosol. *Tellus Series B-Chemical and Physical Meteorology,* 60**,** 118-126.

LECK, C. & BIGG, E. K. 2010. New particle formation of marine biological origin. *Aerosol Science and Technology,* 44**,** 570-577.

LEWIS, E. R. & SCHWARTZ, S. E. 2004. *Sea salt aerosol production: Mechanisms, methods, measurements, and models*, Washington, DC, American Geophysical Union.

LI, Z. D., WILLIAMS, A. L. & ROOD, M. J. 1998. Influence of soluble surfactant properties on the activation of aerosol particles containing inorganic solute. *Journal of the Atmospheric Sciences,* 55**,** 1859-1866.

LIMBECK, A., KULMALA, M. & PUXBAUM, H. 2003. Secondary organic aerosol formation in the atmosphere via heterogeneous reaction of gaseous isoprene on acidic particles. *Geophysical Research Letters,* 30(19), 1-4.

LISS, P. S. & MERLIVAT, L. 1986. Air-sea gas exchange rates: Introduction and synthesis. *In:* BUAT-MENARD, P. (ed.) *The Role of Air-Sea Gas Exchange in Geochemical Cycling.* Norwell, Mass., USA: D. Reidel Publishing Company.

LISS, P. S., HATTON, A. D., MALIN, G., NIGHTINGALE, P. D. & TURNER, S. M. 1997. Marine sulphur emissions. *Philosophical Transactions of the Royal Society B-Biological Sciences,* 352**,** 159-168.

LISS, P. S. & LOVELOCK, J. E. 2007. Climate change: The effect of DMS emissions. *Environmental Chemistry*, 4**,** 377-378.

LOHMANN, U., STIER, P., HOOSE, C., FERRACHAT, S., KLOSTER, S., ROECKNER, E. & ZHANG, J. 2007. Cloud microphysics and aerosol indirect effects in the global climate model ECHAM5-HAM. *Atmospheric Chemistry and Physics,* 7**,** 3425-3446.

MA, X., VON SALZEN, K. & LI, J. 2008. Modelling sea salt aerosol and its direct and indirect effects on climate. *Atmospheric Chemistry and Physics,* 8**,** 1311-1327.

MAHOWALD, N., WARD, D. S., KLOSTER, S., FLANNER, M. G., HEALD, C. L., HEAVENS, N. G., HESS, P. G., LAMARQUE, J.-F. & CHUANG, P. Y. 2011. Aerosol

impacts on climate and biogeochemistry. *Annual Review of Environment and Resources,* 36, 45-74.

MAKELA, J. M., AALTO, P., JOKINEN, V., POHJA, T., NISSINEN, A., PALMROTH, S., MARKKANEN, T., SEITSONEN, K., LIHAVAINEN, H. & KULMALA, M. 1997. Observations of ultrafine aerosol particle formation and growth in boreal forest. *Geophysical Research Letters,* 24**,** 1219-1222.

MAMANE, Y. & GOTTLIEB, J. 1992. Nitrate formation on sea-salt and mineral particles: A single-particle approach. *Atmospheric Environment Part a-General Topics,* 26**,** 1763-1769.

MANN, G. W., CARSLAW, K. S., RIDLEY, D. A., SPRACKLEN, D. V., PRINGLE, K. J., MERIKANTO, J., KORHONEN, H., SCHWARZ, J. P., LEE, L. A., MANKTELOW, P. T., WOODHOUSE, M. T., SCHMIDT, A., BREIDER, T. J., EMMERSON, K. M., REDDINGTON, C. L., CHIPPERFIELD, M. P. & PICKERING, S. J. 2012. Intercomparison of modal and sectional aerosol microphysics representations within the same 3-D global chemical transport model. *Atmospheric Chemistry and Physics,* 12**,** 4449-4476.

MARANDINO, C. A., DE BRUYN, W. J., MILLER, S. D. & SALTZMAN, E. S. 2007. Eddy correlation measurements of the air/sea flux of dimethylsulfide over the North Pacific Ocean. *Journal of Geophysical Research-Atmospheres,* 112, 1-12.

MARTENSSON, E. M., NILSSON, E. D., DE LEEUW, G., COHEN, L. H. & HANSSON, H. C. 2003. Laboratory simulations and parameterization of the primary marine aerosol production. *Journal of Geophysical Research-Atmospheres,* 108, 1-12.

MARTINEZ, R. I. & HERRON, J. T. 1978. Stopped-flow study of gas-phase reaction of ozone with organic sulfides: Dimethyl sulfide. *International Journal of Chemical Kinetics,* 10**,** 433-452.

MAYO, D. W., MILLER, F. A. & HANNAH, R. W. 2003. *Course Notes on the Interpretation of Infrared and Raman Spectra,* New Jersey, John Wiley & Sons, Inc.

MCFIGGANS, G., BALE, C. S. E., BALL, S. M., BEAMES, J. M., BLOSS, W. J., et al. 2010. Iodine-mediated coastal particle formation: an overview of the Reactive Halogens in the Marine Boundary Layer (RHaMBLe) Roscoff coastal study. *Atmospheric Chemistry and Physics,* 10**,** 2975-2999.

MENON, S., DEL GENIO, A. D., KOCH, D. & TSELIOUDIS, G. 2002. GCM simulations of the aerosol indirect effect: Sensitivity to cloud parameterization and aerosol burden. *Journal of the Atmospheric Sciences,* 59**,** 692-713.

MESKHIDZE, N. & NENES, A. 2006. Phytoplankton and cloudiness in the Southern Ocean. *Science,* 314**,** 1419-1423.

MESKHIDZE, N., XU, J., GANTT, B., ZHANG, Y., NENES, A., GHAN, S. J., LIU, X., EASTER, R. & ZAVERI, R. 2011. Global distribution and climate forcing of marine organic aerosol: 1. Model improvements and evaluation. *Atmospheric Chemistry and Physics,* 11**,** 11689-11705.

MIKKONEN, S., ROMAKKANIEMI, S., SMITH, J. N., KORHONEN, H., PETAJA, T., PLASS-DUELMER, C., BOY, M., MCMURRY, P. H., LEHTINEN, K. E. J., JOUTSENSAARI, J., HAMED, A., MAULDIN, R. L., BIRMILI, W., SPINDLER, G., ARNOLD, F., KULMALA, M. & LAAKSONEN, A. 2011. A statistical proxy for sulphuric acid concentration. *Atmospheric Chemistry and Physics,* 11**,** 11319-11334.

MIYAZAKI, Y., KAWAMURA, K. & SAWANO, M. 2010. Size distributions and chemical characterization of water-soluble organic aerosols over the western North Pacific in summer. *Journal of Geophysical Research-Atmospheres,* 115, 1-13.

MOCHIDA, M., KAWABATA, A., KAWAMURA, K., HATSUSHIKA, H. & YAMAZAKI, K. 2003. Seasonal variation and origins of dicarboxylic acids in the marine atmosphere over the western North Pacific. *Journal of Geophysical Research-Atmospheres,* 108**,** 1-11.

MOCHIDA, M., UMEMOTO, N., KAWAMURA, K., LIM, H. J. & TURPIN, B. J. 2007. Bimodal size distributions of various organic acids and fatty acids in the marine atmosphere: Influence of anthropogenic aerosols, Asian dusts, and sea spray off the coast of East Asia. *Journal of Geophysical Research-Atmospheres,* 112, 1-13.

MONAHAN, E. C. & MUIRCHEARTAIGH, I. O. 1980. Optimal power-law description of oceanic whitecap coverage dependence on wind speed. *Journal of Physical Oceanography,* 10**,** 2094-2099.

MONAHAN, E. C., FAIRALL, C. W., DAVIDSON, K. L. & BOYLE, P. J. 1983. Observed interrelations between 10m winds, ocean whitecaps and marine aerosols. *Quarterly Journal of the Royal Meteorological Society,* 109**,** 379-392.

MONAHAN, E. C., SPIEL, D. E. & DAVIDSON, K. L. 1986. A model of marine aerosol generation via whitecaps and wave disruption. *In:* MONAHAN, E. C. & MACNIOCHAILL, G. (eds.) *Oceanic Whitecaps.* Norwell, Mass.: D. Reidel.

MOON, S.-G. 2011. Chemical and physical properties of atmospheric aerosols (a) a case study in the unique properties of agricultural aerosols (b) the role of chemical composition in ice nucleation during the Arctic spring. College Station, Tex.: Texas A&M University.

NAKAMOTO, K. 2009. *Infrared and Raman Spectra of Inorganic and Coordination Compound Part A: Theory and Applications in Inorganic Chemistry* New Jersey, John Wiley & Sons, Inc.

NILSSON, E. D., RANNIK, U., SWIETLICKI, E., LECK, C., AALTO, P. P., ZHOU, J. & NORMAN, M. 2001. Turbulent aerosol fluxes over the Arctic Ocean 2. Wind-driven sources from the sea. *Journal of Geophysical Research-Atmospheres,* 106**,** 32139-32154.

OCKO, I. B., RAMASWAMY, V., GINOUX, P., MING, Y. & HOROWITZ, L. W. 2012. Sensitivity of scattering and absorbing aerosol direct radiative forcing to physical climate factors. *Journal of Geophysical Research-Atmospheres,* 117, 1-13.

O'DOWD, C. D. & SMITH, M. H. 1993. Physicochemical properties of aerosols over the northeastern Atlantic: Evidence for wind-speed-related submicron sea-salt production. *Journal of Geophysical Research-Atmospheres,* 98**,** 1137-1149.

O'DOWD, C., MCFIGGANS, G., CREASEY, D. J., PIRJOLA, L., HOELL, C., SMITH, M. H., ALLAN, B. J., PLANE, J. M. C., HEARD, D. E., LEE, J. D., PILLING, M. J. & KULMALA, M. 1999. On the photochemical production of new particles in the coastal boundary layer. *Geophysical Research Letters,* 26**,** 1707-1710.

O'DOWD, C. D., FACCHINI, M. C., CAVALLI, F., CEBURNIS, D., MIRCEA, M., DECESARI, S., FUZZI, S., YOON, Y. J. & PUTAUD, J. P. 2004. Biogenically driven organic contribution to marine aerosol. *Nature,* 431**,** 676-680.

O'DOWD, C. D. & DE LEEUW, G. 2007. Marine aerosol production: a review of the current knowledge. *Philosophical Transactions of the Royal Society a-Mathematical Physical and Engineering Sciences,* 365**,** 1753-1774.

O'DOWD, C. D., LANGMANN, B., VARGHESE, S., SCANNELL, C., CEBURNIS, D. & FACCHINI, M. C. 2008. A combined organic-inorganic sea-spray source function. *Geophysical Research Letters,* 35, 1-5.

OHDE, T. & SIEGEL, H. 2010. Biological response to coastal upwelling and dust deposition in the area off Northwest Africa. *Continental Shelf Research,* 30**,** 1108-1119.

OLIVEIRA, J. E., MENDES, J. & MOREIRA, J. E. 1981. Raman spectra of NaCl:Pb crystals. *Journal of Physics C-Solid State Physics,* 14**,** 2527-2533.

ORELLANA, M. V., MATRAI, P. A., LECK, C., RAUSCHENBERG, C. D., LEE, A. M. & COZ, E. 2011. Marine microgels as a source of cloud condensation nuclei in the high Arctic. *Proceedings of the National Academy of Sciences of the United States of America,* 108**,** 13612-13617.

OSTHOFF, H. D., BATES, T. S., JOHNSON, J. E., KUSTER, W. C., GOLDAN, P., SOMMARIVA, R., WILLIAMS, E. J., LERNER, B. M., WARNEKE, C., DE GOUW, J. A., PETTERSSON, A., BAYNARD, T., MEAGHER, J. F., FEHSENFELD, F. C., RAVISHANKARA, A. R. & BROWN, S. S. 2009. Regional variation of the dimethyl sulfide oxidation mechanism in the summertime marine boundary layer in the Gulf of Maine. *Journal of Geophysical Research-Atmospheres,* 114, 1-13.

OUM, K. W., LAKIN, M. J., DEHAAN, D. O., BRAUERS, T. & FINLAYSON-PITTS, B. J. 1998. Formation of molecular chlorine from the photolysis of ozone and aqueous sea-salt particles. *Science,* 279**,** 74-77.

OVADNEVAITE, J., CEBURNIS, D., MARTUCCI, G., BIALEK, J., MONAHAN, C., RINALDI, M., FACCHINI, M. C., BERRESHEIM, H., WORSNOP, D. R. & O'DOWD, C. 2011a. Primary marine organic aerosol: A dichotomy of low hygroscopicity and high CCN activity. *Geophysical Research Letters,* 38**,** 1-5.

OVADNEVAITE, J., O'DOWD, C., DALL'OSTO, M., CEBURNIS, D., WORSNOP, D. R. & BERRESHEIM, H. 2011b. Detecting high contributions of primary organic matter to marine aerosol: A case study. *Geophysical Research Letters,* 38, 1-5.

OVADNEVAITE, J., CEBURNIS, D., CANAGARATNA, M., BERRESHEIM, H., BIALEK, J., MARTUCCI, G., WORSNOP, D. R. & O'DOWD, C. 2012. On the effect of wind speed on submicron sea salt mass concentrations and source fluxes. *Journal of Geophysical Research-Atmospheres,* 117, 1-11.

PARRISH, D. D., MILLET, D. B. & GOLDSTEIN, A. H. 2009. Increasing ozone in marine boundary layer inflow at the west coasts of North America and Europe. *Atmospheric Chemistry and Physics,* 9**,** 1303-1323.

PETELSKI, T. 2005. Coarse aerosol concentration over the north polar waters of the Atlantic. *Aerosol Science and Technology,* 39**,** 695-700.

PETER, J. R., SIEMS, S. T., JENSEN, J. B., GRAS, J. L., ISHIZAKA, Y. & HACKER, J. M. 2010. Airborne observations of the effect of a cold front on the aerosol particle size distribution and new particle formation. *Quarterly Journal of the Royal Meteorological Society,* 136**,** 944-961.

PIERCE, J. R. & ADAMS, P. J. 2006. Global evaluation of CCN formation by direct emission of sea salt and growth of ultrafine sea salt. *Journal of Geophysical Research-Atmospheres,* 111, 1-16.

PHARES, D. J., RHOADS, K. P., JOHNSTON, M. V. & WEXLER, A. S. 2003. Size-resolved ultrafine particle composition analysis - 2. Houston. *Journal of Geophysical Research-Atmospheres,* 108, 1-14.

PIRJOLA, L., LAAKSONEN, A., AALTO, P. & KULMALA, M. 1998. Sulfate aerosol formation in the Arctic boundary layer. *Journal of Geophysical Research-Atmospheres,* 103**,** 8309-8321.

PIRJOLA, L., O'DOWD, C. D., BROOKS, I. M. & KULMALA, M. 2000. Can new particle formation occur in the clean marine boundary layer? *Journal of Geophysical Research-Atmospheres,* 105**,** 26531-26546.

POPOVIC, D. M., MILOSAVLJEVIC, V., ZEKIC, A., ROMCEVIC, N. & DANIELS, S. 2011. Raman scattering analysis of silicon dioxide single crystal treated by direct current plasma discharge. *Applied Physics Letters,* 98, 1-3.

POSCHL, U. 2005. Atmospheric aerosols: Composition, transformation, climate and health effects. *Angewandte Chemie-International Edition,* 44**,** 7520-7540.

PRATHER, K. A., BERTRAM, T. H., GRASSIAN, V. H., DEANE, G. B., STOKES, M. D., et al. 2013. Bringing the ocean into the laboratory to probe the chemical complexity of sea spray aerosol. *Proceedings of the National Academy of Sciences of the United States of America,* 110**,** 7550-7555.

PRISLE, N. L., RAATIKAINEN, T., LAAKSONEN, A. & BILDE, M. 2010. Surfactants in cloud droplet activation: mixed organic-inorganic particles. *Atmospheric Chemistry and Physics,* 10**,** 5663-5683.

PUTAUD, J. P., MIHALOPOULOS, N., NGUYEN, B. C., CAMPIN, J. M. & BELVISO, S. 1992. Seasonal variations of atmospheric sulfur dioxide and dimethylsulfide and dimethylsulfide concentrations at Amsterdam island in the southern Indian Ocean. *Journal of Atmospheric Chemistry,* 15**,** 117-131.

PUTAUD, J. P., BELVISO, S., NGUYEN, B. C. & MIHALOPOULOS, N. 1993. Dimethylsulfide, aerosols, and condensation nuclei over the tropical northeastern Atlantic Ocean. *Journal of Geophysical Research-Atmospheres,* 98**,** 14863-14871.

QUINN, P. K., MILLER, T. L., BATES, T. S., OGREN, J. A., ANDREWS, E. & SHAW, G. E. 2002. A 3-year record of simultaneously measured aerosol chemical and optical properties at Barrow, Alaska. *Journal of Geophysical Research-Atmospheres,* 107.

QUINN, P. K. & BATES, T. S. 2011. The case against climate regulation via oceanic phytoplankton sulphur emissions. *Nature,* 480**,** 51-56.

RAES, F. 1995. Entrainment of free tropospheric aerosols as a regulating mechanism for cloud condensation nuclei in the remote marine boundary layer. *Journal of Geophysical Research-Atmospheres,* 100**,** 2893-2903.

RAMAN, C. V. 1929. Part II. -The Raman effect: Investigation of molecular structure by light scattering. *Transactions of the Faraday Society*, 25**,** 0781-0791.

RIEMER, N. & WEST, M. 2013. Quantifying aerosol mixing state with entropy and diversity measures. *Atmos. Chem. Phys. Discuss.* , 13**,** 15615 - 15662.

RINALDI, M., DECESARI, S., FINESSI, E., GIULIANELLI, L., CARBONE, C., FUZZI, S., O'DOWD, C. D., CEBURNIS, D. & FACCHINI, M. C. 2010. Primary and secondary organic marine aerosol and oceanic biological activity: Recent results and new perspectives for future studies. *Advances in Meteorology*, 2010, 1-10.

ROSE, D., GUNTHE, S. S., MIKHAILOV, E., FRANK, G. P., DUSEK, U., ANDREAE, M. O. & POSCHL, U. 2008. Calibration and measurement uncertainties of a continuous-flow cloud condensation nuclei counter (DMT-CCNC): CCN activation of ammonium sulfate and sodium chloride aerosol particles in theory and experiment. *Atmospheric Chemistry and Physics,* 8**,** 1153-1179.

RUEHL, C. R., CHUANG, P. Y., NENES, A., CAPPA, C. D., KOLESAR, K. R. & GOLDSTEIN, A. H. 2012. Strong evidence of surface tension reduction in microscopic aqueous droplets. *Geophysical Research Letters,* 39, 1-5.

RUSSELL, L. M., SEINFELD, J. H., FLAGAN, R. C., FEREK, R. J., HEGG, D. A., HOBBS, P. V., WOBROCK, W., FLOSSMANN, A. I., O'DOWD, C. D., NIELSEN, K. E. & DURKEE, P. A. 1999. Aerosol dynamics in ship tracks. *Journal of Geophysical Research-Atmospheres,* 104**,** 31077-31095.

RUSSELL, L. M. & SINGH, E. G. 2006. Submicron salt particle production in bubble bursting. *Aerosol Science and Technology,* 40**,** 664-671.

RUSSELL, L. M., HAWKINS, L. N., FROSSARD, A. A., QUINN, P. K. & BATES, T. S. 2010. Carbohydrate-like composition of submicron atmospheric particles and their production from ocean bubble bursting. *Proceedings of the National Academy of Sciences of the United States of America,* 107**,** 6652-6657.

RUSSELL, L. M., BAHADUR, R. & ZIEMANN, P. J. 2011. Identifying organic aerosol sources by comparing functional group composition in chamber and atmospheric particles. *Proceedings of the National Academy of Sciences of the United States of America,* 108**,** 3516-3521.

SADEZKY, A., MUCKENHUBER, H., GROTHE, H., NIESSNER, R. & POSCHL, U. 2005. Raman micro spectroscopy of soot and related carbonaceous materials: Spectral analysis and structural information. *Carbon,* 43**,** 1731-1742.

SAIZ-LOPEZ, A., PLANE, J. M. C. & SHILLITO, J. A. 2004. Bromine oxide in the mid-latitude marine boundary layer. *Geophysical Research Letters,* 31, 1-4.

SALTZMAN, E. S., KING, D. B., HOLMEN, K. & LECK, C. 1993. Experimental determination of the diffusion coefficient of dimethylsulfide in water. *Journal of Geophysical Research-Oceans,* 98**,** 16481-16486.

SANDER, R., KEENE, W. C., PSZENNY, A. A. P., ARIMOTO, R., AYERS, G. P., BABOUKAS, E., CAINEY, J. M., CRUTZEN, P. J., DUCE, R. A., HONNINGER, G., HUEBERT, B. J., MAENHAUT, W., MIHALOPOULOS, N., TUREKIAN, V. C. & VAN DINGENEN, R. 2003. Inorganic bromine in the marine boundary layer: A critical review. *Atmospheric Chemistry and Physics,* 3**,** 1301-1336.

SATHEESH, S. K. & MOORTHY, K. K. 2005. Radiative effects of natural aerosols: A review. *Atmospheric Environment,* 39**,** 2089-2110.

SCHAUFEL, R. F. & SHIMANOU, T. 1967. Longitudinal acoustical vibrations of finite polymethylene chains. *Journal of Chemical Physics,* 47**,** 3605-3610.

SCHUMACHER, W., KUHNERT, M., ROSCH, P. & POPP, J. 2011. Identification and classification of organic and inorganic components of particulate matter via Raman spectroscopy and chemometric approaches. *Journal of Raman Spectroscopy,* 42**,** 383-392.

SCIARE, J., BABOUKAS, E. & MIHALOPOULOS, N. 2001. Short-term variability of atmospheric DMS and its oxidation products at Amsterdam Island during summer time. *Journal of Atmospheric Chemistry,* 39**,** 281-302.

SEBEK, J., PELE, L., POTMA, E. O. & GERBER, R. B. 2011. Raman spectra of long chain hydrocarbons: anharmonic calculations, experiment and implications for imaging of biomembranes. *Physical Chemistry Chemical Physics,* 13**,** 12724-12733.

SEINFELD, J. H. & PANDIS, S. N. 2006. *Atmospheric chemistry and physics: from air pollution to climate change,* Hoboken, NJ, John Wiley & Sons, Inc.

SELLEGRI, K., O'DOWD, C. D., YOON, Y. J., JENNINGS, S. G. & DE LEEUW, G. 2006. Surfactants and submicron sea spray generation. *Journal of Geophysical Research-Atmospheres,* 111, 1-12.

SHANK, L. M., HOWELL, S., CLARKE, A. D., FREITAG, S., BREKHOVSKIKH, V., KAPUSTIN, V., MCNAUGHTON, C., CAMPOS, T. & WOOD, R. 2012. Organic matter and non-refractory aerosol over the remote Southeast Pacific: oceanic and combustion sources. *Atmospheric Chemistry and Physics,* 12**,** 557-576.

SIMO, R. & PEDROS-ALIO, C. 1999. Role of vertical mixing in controlling the oceanic production of dimethyl sulphide. *Nature,* 402**,** 396-399.

SNYDER, R. G. & SCHACHTSCHNEIDER, J. H. 1963. Vibrational analysis of the n-paraffins. 1. Assignments of infrared bands in the spectra of C3H8 through n-C19H40. *Spectrochimica Acta,* 19**,** 85-116.

SNYDER, R. G., CAMERON, D. G., CASAL, H. L., COMPTON, D. A. C. & MANTSCH, H. H. 1982. Studies on determining conformational order in *n*-alkanes and phospholipids from the 1130 cm^{-1} raman band. *Biochimica et Biophysica Acta (BBA) - Biomembranes* 684**,** 1-6.

SOBANSKA, S., HWANG, H., CHOEL, M., JUNG, H. J., EOM, H. J., KIM, H., BARBILLAT, J. & RO, C. U. 2012. Investigation of the chemical mixing state of individual Asian dust particles by the combined use of electron Probe X-ray microanalysis and Raman microspectrometry. *Analytical Chemistry,* 84**,** 3145-3154.

SORJAMAA, R., SVENNINGSSON, B., RAATIKAINEN, T., HENNING, S., BILDE, M. & LAAKSONEN, A. 2004. The role of surfactants in Kohler theory reconsidered. *Atmospheric Chemistry and Physics,* 4**,** 2107-2117.

SPIEL, D. E. 1998. On the births of film drops from bubbles bursting on seawater surfaces. *Journal of Geophysical Research-Oceans,* 103**,** 24907-24918.

SPRACKLEN, D. V., PRINGLE, K. J., CARSLAW, K. S., CHIPPERFIELD, M. P. & MANN, G. W. 2005. A global off-line model of size-resolved aerosol microphysics: I. Model development and prediction of aerosol properties. *Atmospheric Chemistry and Physics,* 5**,** 2227-2252.

SPRACKLEN, D. V., PRINGLE, K. J., CARSLAW, K. S., MANN, G. W., MANKTELOW, P. & HEINTZENBERG, J. 2007. Evaluation of a global aerosol microphysics model against size-resolved particle statistics in the marine atmosphere. *Atmospheric Chemistry and Physics,* 7**,** 2073-2090.

STARK, H., BROWN, S. S., GOLDAN, P. D., ALDENER, M., KUSTER, W. C., JAKOUBEK, R., FEHSENFELD, F. C., MEAGHER, J., BATES, T. S. & RAVISHANKARA, A. R. 2007. Influence of nitrate radical on the oxidation of dimethyl sulfide in a polluted marine environment. *Journal of Geophysical Research-Atmospheres,* 112, 1-11.

SVENNINGSSON, B., RISSLER, J., SWIETLICKI, E., MIRCEA, M., BILDE, M., FACCHINI, M. C., DECESARI, S., FUZZI, S., ZHOU, J., MONSTER, J. & ROSENORN, T. 2006. Hygroscopic growth and critical supersaturations for mixed aerosol particles of inorganic and organic compounds of atmospheric relevance. *Atmospheric Chemistry and Physics,* 6**,** 1937-1952.

SWIETLICKI, E., HANSSON, H. C., HAMERI, K., SVENNINGSSON, B., MASSLING, A., MCFIGGANS, G., MCMURRY, P. H., PETAJA, T., TUNVED, P., GYSEL, M., TOPPING, D., WEINGARTNER, E., BALTENSPERGER, U., RISSLER, J., WIEDENSOHLER, A. & KULMALA, M. 2008. Hygroscopic properties of submicrometer atmospheric aerosol particles measured with H-TDMA instruments in

various environments - a review. *Tellus Series B-Chemical and Physical Meteorology,* 60**,** 432-469.

TERVAHATTU, H., HARTONEN, K., KERMINEN, V. M., KUPIAINEN, K., AARNIO, P., KOSKENTALO, T., TUCK, A. F. & VAIDA, V. 2002. New evidence of an organic layer on marine aerosols. *Journal of Geophysical Research-Atmospheres,* 107, 1-8.

THORNTON, D. C. O. 2012. Primary Production in the Ocean. *In:* NAJAFPOUR, M. M. (ed.) *Advances in Photosynthesis-Fundamental Aspects.* Rijeka, Croatia: Intech.

TRITSCHER, T., JURANYI, Z., MARTIN, M., CHIRICO, R., GYSEL, M., HERINGA, M. F., DECARLO, P. F., SIERAU, B., PREVOT, A. S. H., WEINGARTNER, E. & BALTENSPERGER, U. 2011. Changes of hygroscopicity and morphology during ageing of diesel soot. *Environmental Research Letters,* 6.

TWOHY, C. H. & ANDERSON, J. R. 2008. Droplet nuclei in non-precipitating clouds: composition and size matter. *Environmental Research Letters,* 3, 1-9.

VALLINA, S. M., SIMO, R. & GASSO, S. 2006. What controls CCN seasonality in the Southern Ocean? A statistical analysis based on satellite-derived chlorophyll and CCN and model-estimated OH radical and rainfall. *Global Biogeochemical Cycles,* 20, 1-13.

VALLINA, S. M. & SIMO, R. 2007. Strong relationship between DMS and the solar radiation dose over the global surface ocean. *Science,* 315**,** 506-508.

VAUGHAN, S., INGHAM, T., WHALLEY, L. K., STONE, D., EVANS, M. J., READ, K. A., LEE, J. D., MOLLER, S. J., CARPENTER, L. J., LEWIS, A. C., FLEMING, Z. L. & HEARD, D. E. 2012. Seasonal observations of OH and HO2 in the remote tropical marine boundary layer. *Atmospheric Chemistry and Physics,* 12**,** 2149-2172.

VERDUGO, P., ALLDREDGE, A. L., AZAM, F., KIRCHMAN, D. L., PASSOW, U. & SANTSCHI, P. H. 2004. The oceanic gel phase: a bridge in the DOM-POM continuum. *Marine Chemistry,* 92**,** 67-85.

VERDUGO, P. 2012. Marine microgels. *Annual Review of Marine Science*, 4, 375-400.

VIGNATI, E., FACCHINI, M. C., RINALDI, M., SCANNELL, C., CEBURNIS, D., SCIARE, J., KANAKIDOU, M., MYRIOKEFALITAKIS, S., DENTENER, F. & O'DOWD, C. D. 2010. Global scale emission and distribution of sea-spray aerosol: Sea-salt and organic enrichment. *Atmospheric Environment,* 44**,** 670-677.

WEBER, R. J., MCMURRY, P. H., MAULDIN, R. L., TANNER, D. J., EISELE, F. L., CLARKE, A. D. & KAPUSTIN, V. N. 1999. New particle formation in the remote troposphere: A comparison of observations at various sites. *Geophysical Research Letters,* 26**,** 307-310.

WEBER, R. J., MOORE, K., KAPUSTIN, V., CLARKE, A., MAULDIN, R. L., KOSCIUCH, E., CANTRELL, C., EISELE, F., ANDERSON, B. & THORNHILL, L. 2001. Nucleation in the equatorial Pacific during PEM-Tropics B: Enhanced boundary layer H2SO4 with no particle production. *Journal of Geophysical Research-Atmospheres,* 106**,** 32767-32776.

WESTERVELT, D. M., MOORE, R. H., NENES, A. & ADAMS, P. J. 2012. Effect of primary organic sea spray emissions on cloud condensation nuclei concentrations. *Atmospheric Chemistry and Physics,* 12**,** 89-101.

WEX, H., FUENTES, E., TSAGKOGEORGAS, G., VOIGTLAENDER, J., CLAUSS, T., KISELEV, A., GREEN, D. H., COE, H., MCFIGGANS, G. & STRATMANN, F. 2010a. The influence of algal exudate on the hygroscopicity of sea spray particles. *Advances in Meteorology*, 2010, 1-10.

WEX, H., MCFIGGANS, G., HENNING, S. & STRATMANN, F. 2010b. Influence of the external mixing state of atmospheric aerosol on derived CCN number concentrations. *Geophysical Research Letters,* 37, 1-4.

WHITBY, K. T. 1978. Physical characteristics of sulfur aerosols. *Atmospheric Environment,* 12**,** 135-159.

WOODHOUSE, M. T., CARSLAW, K. S., MANN, G. W., VALLINA, S. M., VOGT, M., HALLORAN, P. R. & BOUCHER, O. 2010. Low sensitivity of cloud condensation nuclei to changes in the sea-air flux of dimethyl-sulphide. *Atmospheric Chemistry and Physics,* 10**,** 7545-7559.

WU, J. 1982. Optimal power-law description of oceanic whitecap coverage dependence on wind-speed: Comments. *Journal of Physical Oceanography,* 12**,** 750-751.

WURL, O. & HOLMES, M. 2008. The gelatinous nature of the sea-surface microlayer. *Marine Chemistry,* 110**,** 89-97.

YOON, Y. J., CEBURNIS, D., CAVALLI, F., JOURDAN, O., PUTAUD, J. P., FACCHINI, M. C., DECESARI, S., FUZZI, S., SELLEGRI, K., JENNINGS, S. G. & O'DOWD, C. D. 2007. Seasonal characteristics of the physicochemical properties of North Atlantic marine atmospheric aerosols. *Journal of Geophysical Research-Atmospheres,* 112**,** 1-14.

YU, F. Q. & TURCO, R. P. 2000. Ultrafine aerosol formation via ion-mediated nucleation. *Geophysical Research Letters,* 27**,** 883-886.

ZAPPOLI, S., ANDRACCHIO, A., FUZZI, S., FACCHINI, M. C., GELENCSER, A., KISS, G., KRIVACSY, Z., MOLNAR, A., MESZAROS, E., HANSSON, H. C., ROSMAN, K. & ZEBUHR, Y. 1999. Inorganic, organic and macromolecular components of fine aerosol in different areas of Europe in relation to their water solubility. *Atmospheric Environment,* 33**,** 2733-2743.

ZHENG, J., HU, M., ZHANG, R., YUE, D., WANG, Z., GUO, S., LI, X., BOHN, B., SHAO, M., HE, L., HUANG, X., WIEDENSOHLER, A. & ZHU, T. 2011. Measurements of gaseous H2SO4 by AP-ID-CIMS during CAREBeijing 2008 Campaign. *Atmospheric Chemistry and Physics,* 11**,** 7755-7765.